Thermodynamics, Entropy, Information and the Efficiency of Solar Cells

By

Zeev R. Abrams

A dissertation submitted in partial satisfaction of the

requirements for the degree of

Doctor of Philosophy

in

Applied Science & Technology

in the

Graduate Division

of the

University of California, Berkeley

Committee in charge:

Professor Xiang Zhang, Chair
Professor Eli Yablonovitch
Professor Vivek Subramanian

Spring 2012

Thermodynamics, Entropy, Information and the Efficiency of Solar Cells

by Zeev R. Abrams

Abstract

Thermodynamics, Entropy, Information and the Efficiency of Solar Cells

By

Zeev R. Abrams

Doctor of Philosophy in Applied Science & Technology

University of California, Berkeley

Professor Xiang Zhang, Chair

For well over 50 years, the limits to photovoltaic energy conversion have been known and codified, and have played a vital role in the push for technological breakthroughs to reach – and even attempt to surpass – those limits. This limit, known as the Shockley-Queisser detailed-balance limit, was found by using only the most basic of thermodynamic assumptions, and therefore provides an upper bound that is difficult to contest without violating the laws of thermodynamics. Many different schemes have been devised to improve a solar cell's efficiency beyond this limit, with various benefits and drawbacks for each method.

Since the field of solar cell research has been analyzed and dissected for so long by a large variety of researchers, it is quite hard to say or discover anything new without repeating the work of the past. The approach taken in this work is to analyze solar cells from the joint perspective of thermodynamics and information theory. These two subjects have recently been appreciated to be highly interrelated, and using the formalism of Missing Information, we can differentiate between different novel technologies, as well as devise new limits for new and existing methodologies.

In this dissertation, the fundamentals of photovoltaic conversion are analyzed from the most basic of principles, emphasizing the thermodynamic parameters of the photovoltaic process. In particular, an emphasis is made on the voltage of the device, as opposed to the current. This emphasis is made since there is a direct relation between the open-circuit voltage of a solar cell and the fundamental equations of thermodynamics and the Free Energy of the system. Moreover, this relation extends to the *entropy* of the system, which subsequently relates to the field of Information Theory. By focusing on the voltage instead of the current, realizations are made that

are not obvious to the majority or researchers in the field, and in particular to efforts of surpassing the Shockley-Queisser limit, known as "3rd generation" concepts.

After analyzing the standard single-junction cell, other forms of surpassing the detailed-balance limit are presented and discussed, from the viewpoint of entropy and its relation to the amount of information lost or produced in the photovoltaic conversion process. In addition to the well-known 3rd generation methods: up- and down-conversion, carrier multiplication and intermediate band solar cells, other ideas are discussed such as using Feedback to shift the optimal bandgap of the cell, and the use of spectral splitting to completely utilize the solar spectrum. The focus on entropy (and the open-circuit voltage) as the primary variable of interest uncovers new limitations to these processes, and denotes preferences of certain technologies over others.

Using this parallel approach provides insights into the field that were either neglected or not realized. This work thus provides a new set of guidelines for searching for and analyzing innovative techniques to maximize the power conversion efficiency from solar cells.

Dedication Page

I would like to dedicate this work to a number of people who contributed to this work in both direct and indirect means.
First, to Prof. Xiang Zhang, for allowing me to pursue this work on solar cells in a completely different manner from what most others in the field – or group – are doing.
To the NDSEG Fellowship program, for funding most of my research.
To the "XREI" sub-group on energy at Xlab, who collaborated with me on some of the papers this thesis is based on: Chris Gladden, Majid Gharghi, Avi Niv, Sui Yang and Yuan Wang.
To Daniel Kimura and Thomas Zentgraf, for their technical advice (and who were otherwise never acknowledged).
To my collaborators in the LMI-EFRC, particularly Owen Miller, Matt Sheldon, Matt Lucas, Noah Bronstein and Carissa Eisler (for verifying my hair-brained theories).
To Profs. Eli Yablonovitch and Harry Atwater, for their helpful interactions.

Also of course, to Mikhal, who put up with me reading her copy of Cover's *Elements of Information Theory* while on the beaches of Tulum.

And to Ilai.

Table of Contents

Dedication Page i
List of Abbreviations and Acronyms iv
Preface v
I. Introduction 1
1. What is a Solar Cell? 1
2. The Solar Spectrum 2
3. Étendue and Sunlight 5
4. Semiconductors, Simplified 7
5. The Ultimate Efficiency 11
6. Detailed Balance 14
7. Concentrating the Sunlight and Efficiencies 17
8. Beyond the Shockley-Queisser Limit 22
II. Entropy, Transfer Functions and the Single Junction Solar Cell 26
1. The Detailed Balance Model Revisited 26
2. Entropy and the Reduction of Voltage 29
3. The Single Junction Transfer Function 33
III. Down-Conversion: A Detailed Analysis 37
1. Ideal DC Characteristics and Analysis 38
2. Down-Conversion Including Losses 45
IV. Carrier Multiplication and its Relation to Down-Conversion 50
1. The Original Carrier Multiplication Model(s) 51
2. A New Model for CM 54
3. Generalization to Multiple Splitting Systems 55
4. Comparison of Heat Generation 61
5. The Entropy Difference 63
V. Transfer Function Comparison between 3rd Generation Methods 66
1. TFs for Down-Conversion and Carrier Multiplication 66
2. Transfer Functions of Up-Conversion and Intermediate Band Cells 70
3. General Comparison between 3rd Generation Methods 75
VI. Feedback Method of Shifting the Optimal Bandgap 78
1. Optical Feedback Theory 78
2. High Carrier Concentration Limiting Factors 83
VII. The “Sliver of Energy” Cell 89

1. Using Spectral Splitting to Maximize Efficiency 89
2. Geometry Dependent Photon Management 91
3. Tandem Cell Analysis 93
4. Generalization to Multi-Junctions 96
5. Experimental Verification 97
VIII. A New Limit to Concentration? 99
1. Maximum Concentration Overview 99
2. Bandgap Dependence of the Maximal Concentration 101
IX. Summary & Future Work 106
References 110
Appendix: List of Formulas: 117

List of Abbreviations and Acronyms

AlGaAs Aluminum Gallium Arsenide
ARCs Anti-Reflection Coatings
B Geometric parameter
BM Burstein-Moss
BPF Band Pass Filter
c Speed of light in vacuum
CdTe Cadmium Telluride
CdSe Cadmium Selenide
CIGS Copper Indium Gallium Selenide
CM Carrier Multiplication
$\mathbf{C^{max}}$ Maximal concentration factor
DB Detailed Balance
dc Down-Conversion
E Energy (general term)
$\mathbf{E_g}$ Energy gap (bandgap)
e-h Electron-hole
eV Electron-Volts
$\mathbf{FeS_2}$ Iron disulfide (Pyrite)
FF Fill Factor
FWHM Full Width at Half Maximum
G Gibbs free energy
GaAs Gallium Arsenide
GaSb Gallium Antimonide
Ge Germanium
h Planck's constant
$\mathbf{H_{reg}/H_{int}}$ regular/Internal Transfer Functions
HPF High Pass Filter
IB Intermediate Band, or Impurity Band
$\mathbf{I_m}$ Maximal power point current
IR Infra-Red
$\mathbf{I_{sc}}$ Short-circuit current
I-V Current vs. voltage
k Boltzmann's constant
LED Light Emitting Diode
LPF Low Pass Filter
MEG Multiple Exciton Generation
N Photon flux (in numbers/second)
$\mathbf{n_c}$ Index of refraction of the solar cell
$\mathbf{n_S}$ Photon flux per energy interval
PbS Lead Sulfide
PV PhotoVoltaic
q Electric charge constant
QE Quantum Efficiency
$\mathbf{Q_{lost}}$ Heat loss due to thermalization
S entropy (thermodynamic)
Si Silicon
SiGe Silicon Germanium
SQ Shockley Queisser
SRH Shockley-Read-Hall
$\mathbf{T_c}$ Temperature of the cell (300° K)
TF Transfer Function
$\mathbf{T_o}$ Temperature of the ambient (300° K)
$\mathbf{T_S}$ Temperature of the sun (6000° K)
U Internal energy
u(E) Step function/Heaviside function
uc Up-Conversion
UE Ultimate Efficiency
UV Ultra-Violet
$\mathbf{V_m}$ Maximal power point voltage
$\mathbf{V_{oc}}$ Open-circuit voltage
vRS van Roosbroeck-Shockley relation
W Distribution of states
$\boldsymbol{\alpha}$ Correction terms (given different indices)
$\boldsymbol{\alpha_{abs}}$ Absorption coefficient
$\boldsymbol{\Delta}$ Bandwidth (used in different formats)
$\boldsymbol{\varepsilon_{emit}}$ Emission coefficient
$\boldsymbol{\eta_C}$ Carnot efficiency
$\boldsymbol{\eta_{eff}}$ Photovoltaic conversion efficiency
$\boldsymbol{\eta_{ext}}$ Extraction efficiency
$\boldsymbol{\kappa_{nr}}$ Non-radiative loss term
$\boldsymbol{\mu}$ Chemical potential

Preface

The following Dissertation is a compilation of my work as a PhD student at the University of California, Berkeley. It is based on a number of papers that I wrote during this period, most of which were published in peer-reviewed journals. Despite the variety of topics I addressed during this time, a central theme ran throughout my research: that of approaching the topic of Solar Cells on the broadest and most fundamental possible level. In particular, this work is primarily theoretical, and delves into the most basic of premises used to define the workings and efficiencies of photovoltaic power generation.

The title of the dissertation "*Thermodynamics, Entropy, Information and the Efficiency of Solar Cells*" concisely tackles the topics that will be covered in this work, with a focus on the generation of entropy and information lost in this process. The central theme of this work is a re-analysis of solar cell efficiencies using the most streamlined version of the equations that govern the calculations for the power conversion efficiency of solar cells. This approach utilizes equations and concepts that are known to most undergraduates in Physics and Electrical Engineering, and is relatively simple, compared to other approaches. For this reason, this dissertation was written under the assumption that it must be accessible enough for nearly anyone (with a scientific background) to read. As such, it has been written from "scratch", and does not use the original text from the cited papers written by myself in the lab of Prof. Xiang Zhang at UC Berkeley. I have taken special care to simplify all the preliminary Physics required to understand the workings of solar cells and photovoltaic power conversion to the barest of essentials. Furthermore, despite delving into topics of Information Theory and particularly "sticky" arguments regarding entropy generation in these systems, I have attempted to address these topics in such a way that nothing else is required to understand the arguments and results in this text. It is my hope that this work will be accessible to anyone in the sciences, despite the occasional foray into complex condensed-matter physics arguments.

As with any technology, an appreciation of the history of the development of solar cells is generally needed in order to distinguish between ideas and prevent ideas from being repeated. This point is crucial in the field of photovoltaics, since unlike most other fields of Physics or Engineering (e.g., "optics"), the field of solar cells has been around for quite a long time, and has been discussed, argued over and dissected by some of the most prominent scientists of the 20^{th} century. Therefore, before delving into the field of solar cells, it is sometimes worthwhile to read the basic textbooks on the field, some of which have been around for decades, in order to fully appreciate the plethora of ideas that have been generated, developed, disregarded, disbanded and even found to be incorrect, over the years. While the first working photovoltaic solar cells were produced by the 1950's, a great deal of research was poured into the field in the 1960's, in particular for use in extra-terrestrial satellites. Many of the pioneers in solar cell research were known from other fields, particularly the burgeoning field of solid-state physics and the nascent field of semiconductors. A great deal of research was implemented in the late 1970's, due to the worldwide energy crisis, and carried some momentum into the early 1980's. However, due to the fall in the price of oil in that period, much of the solar cell research was subsequently cut, and

many of these researchers then moved on to greener pastures. Many of the papers cited in this text come from that period, which was seen as almost a “golden era” of solar cell research.

While efforts continued worldwide to improve the quality of solar cells, particularly in Europe and Australia, the political and economic crises of the early 21st century have once again brought the concept of solar energy back into the forefront of technological research in universities and research labs all over the world. Moreover, the issues of “climate change” have focused on the production of renewable, sustainable, and otherwise “green” technologies, which solar power neatly falls into the category of. As a result, some of the best and brightest minds are currently being pulled into researching solar cells once again, attempting to find new ways of generating power from sunlight, using both traditional technologies, brute-force computational power, as well as integrating newer technologies such as Nanotechnology into solar cells in an attempt to overcome the limits imposed by the more traditional approaches to building solar cells.

In spite of the recent renewed interest in the field and concomitant increase in governmental funding, a basic question should be asked of anyone entering this field: Can we really think of anything that wasn’t thought of before? This question is not one of despair at arriving at new innovative ideas, but rather an identification of the severe limitations existing in the field: the limited scope and economic restrictions. In solar cell research, we are not looking for ways to produce power from artificial light sources such as a new-fandangle laser system, nor are we attempting to create a highly complex and expensive device to produce power. Instead, the goal is to create an economic (cheap) method of creating as much power as we possibly can out of our sun. The goal is to produce power at a reasonably cost-effective rate (grid parity).

The limitation in both material systems (what we have today), and the source of power (the sun) makes the challenge of innovating in the field of Solar Cells all the more interesting, since we are given a well-defined “box”, and we must do our utmost to break the boundaries of that box. However, the clichéd idea of “thinking outside the box” must also be done within the realm of the physical reality, and deriving results that violate fundamental laws of physics must not be endorsed. Many of the new researchers in this field fail to remember that fact, and assume that using new engineering techniques will allow us to violate these fundamental rules. These are not innovative insights, but rather sloppy work. Some of the chapters in this work address such grandiose schemes and dismantle them. A particular theme that will also be addressed is that of the solar cell producing *voltage* in addition to *current*.

The general approach of this work is thus to define the clichéd “box”, and find ways of thinking outside of that box. The approach I have taken is to attack the subject of solar cells not from the traditional viewpoint of semiconductors, diffusion and continuity equations, nor computational prowess, but rather by using a different mindset when thinking about the most fundamental aspects of what makes a solar cell work, and work *well*. I have used elements of basic thermodynamics and information theory to approach the problem of solar cell power generation with the fewest of possible equations and complications. It is my hope that this approach will be more widely used in the future when devising new (fandangle) ideas to make better use of our solar resources.

I. Introduction

1. What is a Solar Cell?

A solar cell is a device used for producing energy by absorbing sunlight. You can go out today, purchase a solar cell, have it installed on your roof, and quickly reap the benefits of generating power "for free" from the sun, thus offsetting your energy costs. In particular, a *photovoltaic* solar cell is one which produces electricity directly from the sunlight, and stands in contrast with *thermal-photo* devices that produce heat from the sunlight, which can then be used to heat water for residential use, or boil steam to rotate turbines for power generators. Since this work will focus on photovoltaic solar cells, there will be little discussion of thermal-solar (or, thermo-photo-voltaics), and the terms "solar cell" and "photovoltaics" (PV) will be used interchangeably. The ability to *directly* produce electricity from the sunlight, one of the most abundant and renewable of our natural resources, lies at the heart of photovoltaic research, and is viewed as becoming one of the primary sources of power in a "greener" future. Nevertheless, as a commodity, the questions regarding solar cell research today have less to do with the basic principles, and more to do with the *costs* of producing power.

The cost of a solar cell is related to a great many parameters including materials, labor and politics. However, from an ultimate power production viewpoint, the major limitation is the *efficiency* of the solar cell, with higher efficiencies offsetting higher production costs. Since the PV system directly produces power, the efficiency of the system will be related to the product of the two most basic of measures related to electricity, the current and the voltage, with $P=I\times V$. Since both of these cannot be maximized simultaneously, as will be shown in the following sections, an engineering trade-off will occur that provides a maximal efficiency, which cannot be surpassed.

To appreciate how a solar cell works, a great deal of physics is typically required in order to follow the equations, mechanisms and complications of the process of photovoltaic power generation. In particular, a basic understanding of the fundamentals of semiconductor physics is generally required to understand the mechanism of PV power generation whereby sunlight generates electron-hole (e-h) pairs, which are then drawn out as electricity using a p-n diode configuration. Since a great deal of equations would be required to explain this, from the basic semiconductor equations **[1,2]** to the workings of p-n junctions and solar cell models **[3]**. Instead, since this dissertation is not meant to be a textbook on the subject, a different approach will be taken that is more similar to the more basic direction used in thermodynamic approaches to solar energy conversion **[4-6]**.

This Introduction chapter will therefore include all that is necessary to understand the equations and arguments used in the subsequent chapters. Since the use of continuity and diffusion equations are never used within the text, physical explanations of these processes will not be included, in deference to the better textbooks on the subject. Instead, a focus on only the essential concepts needed for solar energy conversion using a bandgap-containing material will

be used. This chapter will therefore focus less on what a solar cell is, and instead on what an *ideal* solar cell is required to be. The chapter will describe the solar spectrum and its relation to terrestrial illumination, the basic requirements of a solar cell material – in terms of the generation of e-h pairs, which leads to the description of the "Ultimate Efficiency" by Shockley and Quiesser (SQ) **[7]**. This efficiency limit is the first of its kind to provide an upper physical limit to the amount of power conversion that can be generated in the most simplistic of solar cells, using only the basic thermodynamics of the system to determine this limit. The importance of a thermodynamic limit, as first described by SQ, is of primal importance since it sets an external limitation to the efficiency of a PV system using the field of thermodynamics, as opposed to traditional semiconductor equations. This thermodynamic limit is more general, and therefore harder to devise methods of overcoming. Moreover, the importance of the SQ limit is in the more complex and physically valid "detailed balance" model, whose significance will be explained at the end of this chapter. An understanding of these concepts will allow the subsequent chapters to be understood, without delving into any other sets of equations.

2. The Solar Spectrum

Understanding the nature of the solar spectrum irradiating the cell provides ~50% of the information required for understanding the ideal solar cell converter, as will be fully detailed in Chapter **II**.

Solar radiation is split into a spectrum of either energy (E) or wavelength (λ), both being the reciprocal of each other as described by the following equation:

$$E\,[\mathrm{eV}] = h\nu = \frac{hc}{\lambda} \cong \frac{1.24}{\lambda\,[\mu\mathrm{m}]} \qquad \textbf{I.1}$$

where h is Planck's constant (h=6.26×10^{-34} J/sec or h=4.13×10^{-15} eV/sec when using units of electron volts – eV – as will be used throughout the text), ν is the frequency of the photons, and c is the speed of light in vacuum (c=2.99×10^{8} m/sec). The relation between energy and wavelength as inversely proportional with a constant of 1.24 [μm/eV] is a good rule-of-thumb that is useable so long as the light remains in free-space, which includes both the vacuum of space, and to a good approximation, air.

The light emitted from the sun can be described as either individual photons or as an electromagnetic wave. Due to the wave-particle duality, we will use *only* the description of light as photons in this text. This usage has no loss in generality, since one can always view a single photon as a spatially isolated packet of electromagnetic radiation. However, using the photon description of light greatly simplifies the arguments to be used later in this text, and simplifies the reading, since it circumvents the usage of Maxwell's equations in the thermodynamic description. This will be further detailed when describing the boundaries of the thermodynamic model in the SQ detailed balance model. It also greatly simplifies the description of *flux* as being a measure of number of photons, as opposed to a description based on the Poynting vector.

There are two ways of understanding the nature of the spectrum of the solar radiation. The first is the data-driven, brute force approach of measuring and examining the solar spectrum using the best of detection techniques. From this perspective, we need to know the exact radiation pattern and spectrum at each point in earth to best match the absorption capabilities of the solar cell. This can be plotted as either the number of photons per unit of energy, or per unit of wavelength, depending on the preference of those involved. Since we will be dealing with the bandgap of semiconductors, the natural unit of measurement is energy, and therefore only it will be used and discussed here.

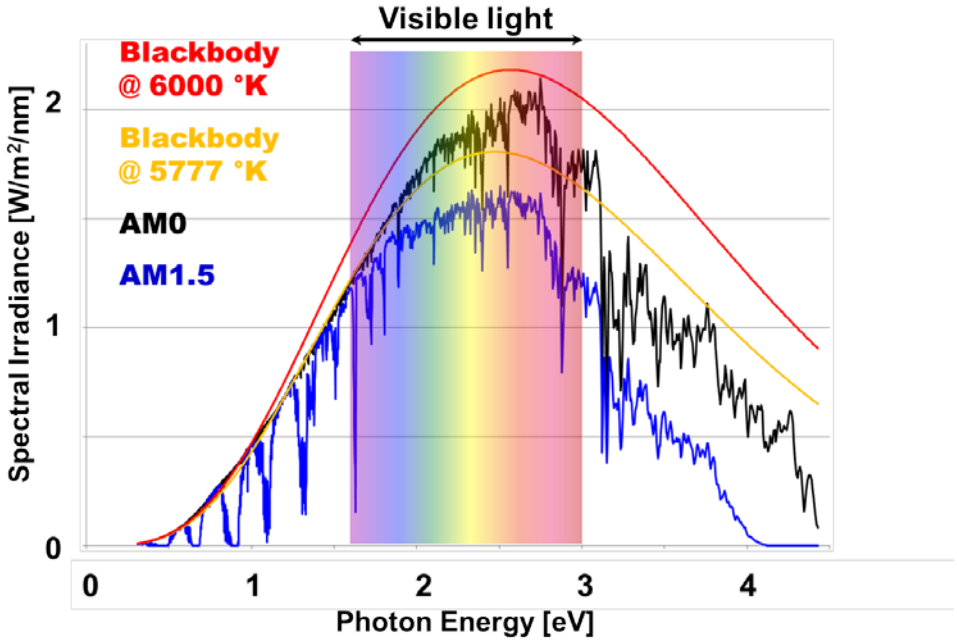

I-1: Solar Spectrum Irradiating the Earth. Displayed is the spectrum of light, irradiance as a function of energy of the photons, for various illumination patterns: AM1.5 and AM0, and the Blackbody spectrum of a source at 6000 and 5777 °K. the area under the 5777 °K curve matches the area under the AM0 curve.

The irradiation pattern on a solar cell is highly dependent upon the location of the cell. The solar illumination hitting a cell lying above the atmosphere will be higher than that lying beneath the cover of the atmosphere due to absorption of some of the photons by molecules in the atmosphere, and particularly resonant absorption peaks due to specific molecules in the atmosphere (such as H_2O). This can be seen in Fig. **I-1** in the difference between the AM0 spectrum (which is the extra-terrestrial one), and the AM1.5 spectrum, which is a calibrated measurement used by researchers worldwide and provided by the National Renewable Energy Lab **[8]** of the terrestrial radiation taken at an angle of the earth equivalent to the central United States (AM1.5 is at the angle of $1.5=1/\cos\theta$, where θ is the zenith angle between the location of the central United States and the equator). The AM0 spectrum contains more high-energy components, which correspond to Ultra-Violet (UV) light as compared against the AM1.5 spectrum, where much of this light is absorbed in the atmosphere. Furthermore, the absorption peaks of water, ozone and corbon dioxide can be seen in the AM1.5 spectrum, particularly in the low energy, Infra-Red (IR) regions (dips in the blue curve around an below 1 eV in Fig. **I-1**).

The radiation spectrum emanating from the sun closely resembles that of a pure blackbody radiator. The blackbody radiation spectrum was found by Planck as a function of the modes of energy within an enclosed black-body, and as a function of the thermal energy describing the system, at a temperature of T_S:

$$n_S = g \times \frac{E^2}{\exp[E / kT_S] - 1} \qquad \textbf{I.2}$$

where n_S is the flux of photons emanating from the blackbody per energy interval (in units of photons per second), k is the Boltzmann constant (k=1.38×10^{-23} J/K=8.62×10^{-5} eV/K) and g is a constant that will be used throughout the text:

$$g = \frac{2}{h^3 c^2} \qquad \textbf{I.3}$$

The units of the Boltzmann constant multiplied by the temperature (in degrees Kelvin) provide the energy metric of the system. For the sun, we can roughly estimate the temperature to be T_S=6000 °K (from hence forward, the degree symbol, °, will be dropped for simplicity), such that the solar thermal energy is kT_S=0.517 eV, or roughly half an eV.

The Planck distribution in Eq. **I.2** has very few variables and parameters, combining a few physical constants (h, c and k) as a function of the density of states of photons and the Bose-Einstein distribution of energy modes, which is the distribution that photons, which are Bosons, follows **[6]**. The temperature of the blackbody is the most significant parameter, with the peak in the blackbody radiation spectrum defined by Wien's law, and falls within the visible spectrum of light, which is why the human eye is designed to best visualize the yellow-green section of the spectrum, and why plants have green leaves to best match the peak solar intensity. It can be therefore stated that the source of the term "green energy" comes directly from the spectral maximum of the sun!

The blackbody spectrum of Eq. **I.2** is also displayed in Fig. **I-1**, and appears above that of the AM1.5 spectrum, and mostly matches the AM0 spectrum. The blackbody radiation pattern is therefore a fairly good estimate of the solar spectrum, although it does not include the contributions of absorption peaks due to molecular absorption resonances. The primary advantage of describing the solar spectrum in terms of the Planck distribution lies in the ability to produce analytical solutions to the models described throughout the text. It is therefore *this* spectrum which will be utilized throughout this text.

Understanding the relation between the parameters in Eq. **I.2** is a critical step in understanding the solar radiation characteristics. Although the actual AM0/AM1.5 spectra are the ones used to emulate and calculate the actual power conversion efficiencies, from the basic Physics perspective, the essential aspects of the solar radiation can be gleaned almost entirely from the formula for the blackbody radiation, as will be shown in the subsequent chapter. The maximum in the curve for the blackbody spectrum, as was displayed in Fig. I-1, can be explained by the interplay between the quadratic rise in modes of energy, signified by the "E^2" term in the numerator of Eq. **I.2**, in contrast to the Bose-Einstein distribution in the denominator, which is maximized at zero energy (degenerate state), where the distribution becomes a delta function (meaning a sharp peak at E=0). If we ignore the "-1" factor in the denominator, for large values of E, one can approach the Rayleigh-Jeans approximation for the blackbody spectrum, or,

assume that the distribution follows a Boltzmann distribution, instead of the Bose-Einstein distribution, and would be characterized by a factor of $exp[-E/kT_S]$. This latter approximation will be used extensively later in the text, however, it is only valid for values of the energy, E, that are larger than the thermal energy, kT_S, as stated above. Various attempts to develop the denominator of Eq. **I.2** can be used, including expanding it in Taylor series for low values of E, however the direct physical interpretation of these results become obfuscated, and with the computational abilities of today's computers, these are no longer required to help solve equations involving these formulas. These Taylor expansions are therefore not included here, however supply an interesting exercise for examining the numerical accuracy of the approximations used.

3. Étendue and Sunlight

The input solar spectrum is a function of the *étendue* of the incoming light, as well as its temperature. The concept of étendue **[9,10]** can be briefly explained using the analogue from the Brightness Theorem. Imagine a flashlight with a projection beam expanding outwards. We can imagine that each photon is a "ray" of light within this beam (this follows the Eikonal approximation for electromagnetic waves, which is the foundation of the ray approximation for geometric optics **[11]**). Since the number of photons (rays) must remain constant in this beam, there is a limitation to how bright the beam spot will become after expanding out from the initial beam area to the final one. This is shown pictorially in Fig. **I-2** for a beam going through an optical element (a lens, or any other translucent object), and expanded to a larger area. It is quite intuitive to understand that the final beam will be less "bright" due to "fewer photons". This intuitive understanding is quite close to the physical reality (so long as the ray approximation is used, and we are in the far-field of imaging). Furthermore, we can intuitively grasp the fact that the beam can be expanded no more than a 90° angle outward, since it will otherwise need to bend backwards.

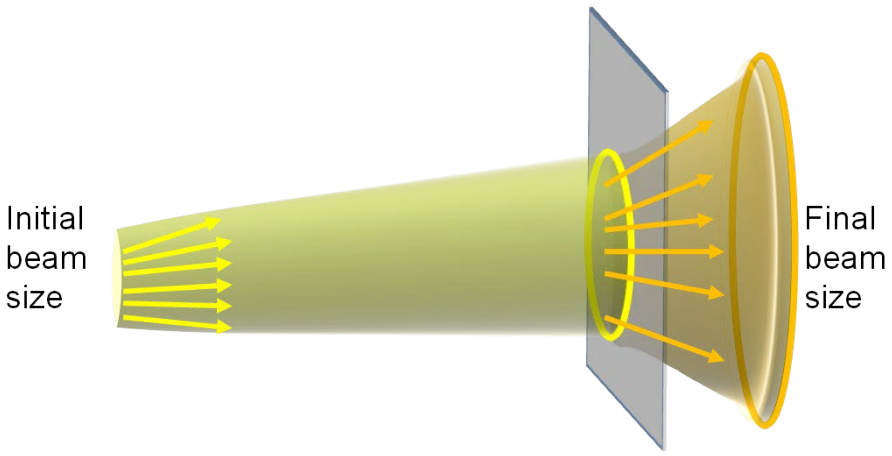

I-2: Generic Pictogram Demonstrating the Concept of Optical Étendue. Photons leaving the initial beam area will expand outward, but retain the same number of rays. If the beam passes through an optical element (grey plane), this conservation of "rays" must still be maintained, despite the increase in beam size area.

The optical étendue is therefore a geometrical factor that includes the area of the initial beam, A, the angle of the "cone" the beam initially began in, Ω, and the angle of propagation of the beam, $cos\theta$. These terms can all be found in the definition of the étendue, ε:

$$\delta\varepsilon = n^2 \cos\theta \delta\Omega \delta A \qquad \textbf{I.4}$$

where the "δ" symbol is used to signify that the equation is in the differential form. The index of refraction, n, also appears in the equation for the étendue, since the angle of the rays is dependent upon the material properties. The index can also be visualized in Fig. **I-2** if we imagine the plane as being the surface of (e.g.) water, with a higher index of refraction ($n \approx 1.5$), such that the rays expand outward. The étendue must remain constant regardless of the material system, be it air, glass, or a semiconductor. A change in étendue can always occur, however it will induce a change in entropy, as will be discussed in the next chapter.

The beam of light extending out from the sun follows the same principal of étendue conservation, with the light traveling through vacuum, and then traversing the atmosphere. While there is only a nominal change in index of refraction between the vacuum of space and the air that can be neglected, there is an additional scattering of light in the atmosphere from molecules known as Rayleigh scattering, which predominantly scatters the higher energy – blue and UV – light, making the sky appear "bluer". The absorption of the UV light also reduces the étendue term. This scattering of light distinguishes the solar radiation pattern between "direct" light, which only includes the component coming directly from the sun, and "diffuse", or "global", light, which includes the segment of light that is scattered in the atmosphere. The direct component of the sunlight will only comprise 70% of the light in clear sky areas, with the rest composed of the diffuse light **[12]**. For areas with large amounts of other scattering objects, such as clouds or haze, this variation can become even larger, emphasizing the diffuse light.

The predominant factor describing the étendue of light emanating from the sun is due to geometric considerations **[13]**. Since the sun is a giant sphere of diameter 1.4×10^9 m, sitting nearly 1.5×10^{11} m away from the earth, most of the light emitted radially outward is lost in space, and only a small fraction of it hits a square solar cell, with area A_{cell}. Since there is only one sun in the sky, the solar cell effectively sees a light source sitting above it, illuminating it with a beam of light at a solid angle of Ω_S, as is shown in Fig. **I-3**. This solid angle is uniquely defined by the distance between the sun and the earth (ignoring variations of the elliptical orbit), and is a constant of the solar illumination pattern. Since the sun traverses the sky during the day, it makes up a solid angle with an azimuth component. Considering the half-angle of the solar disk in the sky, with an angular radius of Δ_S=4.66 mrad, then the étendue of the light emitted from the sun is:

$$\Omega_S = \pi \sin^2 \Delta_S \cong 6.85\times10^{-5}\, sr \qquad \textbf{I.5}$$

since the solid angle is defined for the whole sky, the π term appears.

This geometric relation between the amount emitted from the sun, and that absorbed in earth on an area of 1 m^2 provides the solar constant, I_o=1372 W/m^2, which is the amount of power that can be obtained by the solar radiation. However, if we are interested in the *flux* of photons emitted from the sun, we must integrate over Eq. **I.2** to account for all the energies in interval dE. This provides the total number of photons absorbed.

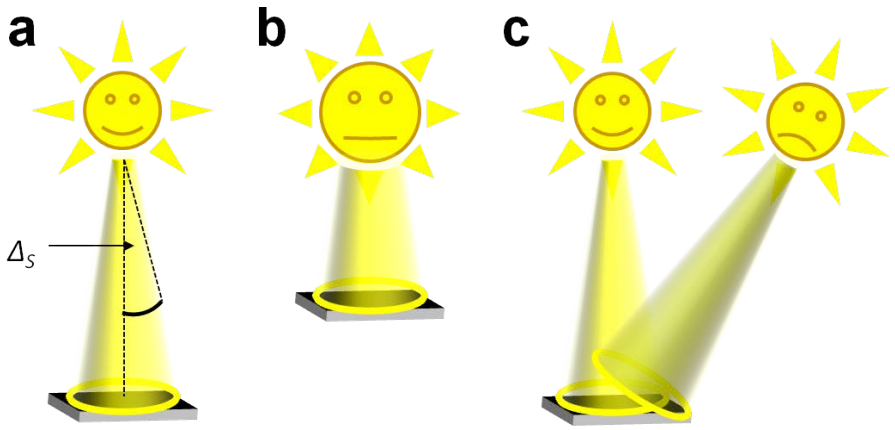

I-3: Geometric Relation Between the Sun and The Étendue. (a) A single sun in the sky emits light with an étendue of Ω_S, which is defined by the distance between the earth and the sun. (b) If the sun were closer, for example, on Mercury, the solid angle would be increased. (c) A second sun in the sky would increase the incoming étendue by a factor of 2, regardless of the angle between them.

Solar cells are typically made from materials with an internal threshold for absorption of photons (as will be explained in the next section). To obtain the total number of photons absorbed in the semiconductor, we integrate from the threshold value of E_{th} to infinity:

$$N_S = g \times \Omega_S \times \int_{E_{th}}^{\infty} \frac{E^2 dE}{\exp[E / kT_S] - 1} \qquad \textbf{I.6}$$

with N_S being the number of photons per unit area, flux, emitted from the sun, and counted from a threshold energy, E_{th} and up.

When the lower threshold is set to zero, we count all the photons absorbed. If we want to find the total *power* received (and thus, the solar constant), we replace the numerator in the integrand of Eq. **I.6** with the term E^3, and integrate from E_{th}=0, which results in the Stefan-Boltzmann constant, and the temperature, related by $P_S \approx \sigma T^4$.

4. Semiconductors, Simplified

This section will summarize the salient features of a semiconductor system used to absorb sunlight, and create a voltage on a per photon basis. Since the bulk of semiconductor formulas are not used in this text, they will not be presented here at all, and a simplified model of a semiconductor system will be used instead. While it is typically crucial to understand the internal workings of a semiconductor and a p-n diode to understand how a solar cell extracts the power from the sunlight, the purpose of this work is to simplify the concepts of solar cells down to the barest of assumptions and equations. It is in no means a replacement for the basic texts on semiconductors **[1,2]**.

We can simplify the workings of a solar cell as being a two level system (or, a two band system **[14, 15]**), with the levels being levels of energy within which electrons can exist. These two energy bands are the valence (lower) and conduction (upper) band, with a large surplus of electrons in the valence band, and a comparative dearth of electrons in the conduction band. This description is therefore more general, with the main distinction between a semiconductor and a conducting molecule (or quantum confined system) is that the former is comprised of bands of energy, whereas the latter has discreet levels (HOMO and LUMO), however, this distinction will not be described here **[14]**.

Fig. **I-4** displays the simplified version of such a system. Higher energy photons (dark blue) are absorbed since their energy exceeds the bandgap energy, E_g, which is the difference between the conduction and valence energy bands. The excess energy ($hv>E_g$) is imparted to the semiconductor material in the form of phonons, which produce heat. Note that in this two *band* model, photons can be absorbed in this range, whereas a two *level* system can only absorb discrete sets of photons, whose energy exactly matches the energy difference between the levels. The system will absorb all photons with energies above the threshold, which is the bandgap, E_g (cyan). However, photons with energy below this threshold are not absorbed, and the material is transparent to these photons. This means that these photons will almost completely be lost (ignoring intra-band absorption processes, known as free-carrier absorption **[1]**). It is therefore obvious that the lower the bandgap, the more photons there are to be utilized. The absorption of photons in the system creates e-h pairs by imparting the photon's energy to electrons in the valence band, thereby "bouncing" them up to the conduction band. These electrons can then be used in an external circuit (provided contacts are made at the edge of the bandgap energies to selectively extract them).

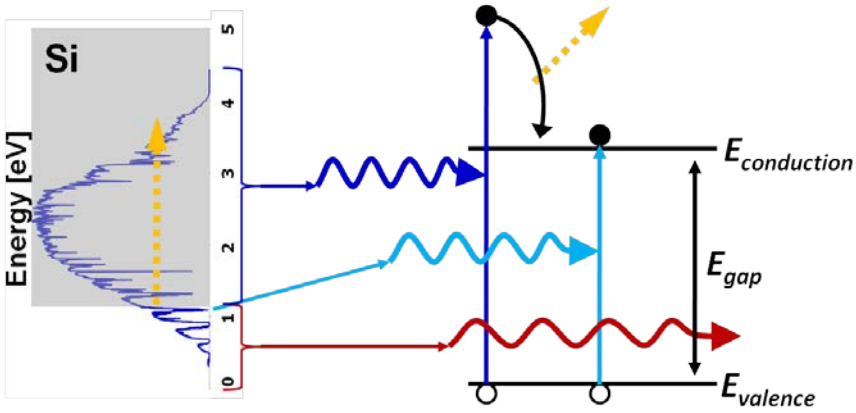

I-4: Simplified Version of the Absorption Capabilities of a Semiconductor. The left is a rotated version of Fig. I-1, plotting photon flux per energy, overlaid with a grey box signifying the absorption region of a Silicon solar cell, E_g= 1.1 eV. To the right is the simplified model of the semiconductor: two energy bands, conduction and valence, are separated by a bandgap, E_{gap}. This figure plots energy as a function of thickness. Higher energy photons (dark blue) are absorbed, and create an electron hole pair (full and empty circles), with the excess energy (yellow line) wasted as thermal energy (phonons). Photons that are matched to the bandgap (cyan) are the lowest threshold of photons absorbed, whereas lower energy photons (red) are completely transparent to the system.

This description vastly simplifies the material characteristics of the semiconductor. For example, in reality the absorption of photons is not unity or uniform, with a functional dependence of the absorption per thickness as a function of the energy of the photons, which is incorporated into the absorptions coefficient $\alpha_{abs}(E)$, which would be placed within the numerator of the integrand in Eq. **I.6**. As an example. Fig. **I-5a** shows the absorption coefficient for Gallium Arsenide (GaAs), one of the best semiconductors for use in PV. The absorption within this semiconductor would therefore be:

$$N_S = g \times \Omega_S \times \int_0^\infty \frac{\alpha_{abs}(E) \times E^2 dE}{\exp[E / kT_S] - 1} \qquad \textbf{I.7}$$

For the purpose of simplification, we can consider the optimal absorption as being a unity step function (or Heaviside function) **[7,15]**, $u(E)$, such that:

$$\alpha_{abs}(E) = u(E_g) = \begin{Bmatrix} 0 | & E < E_g \\ 1 | & E > E_g \end{Bmatrix} \qquad \textbf{I.8}$$

with E_g being the threshold for absorption. This approximation is good for many direct bandgap semiconductors (see below), such as GaAs. In this case, Eq. **I.8** becomes:

$$N_S = g \times \Omega_S \times \int_{E_g}^\infty \frac{E^2 dE}{\exp[E / kT_S] - 1} \qquad \textbf{I.9}$$

which is essentially Eq. **I.6**, with the lower threshold set to E_g. The appearance of the bandgap therefore transforms the equation into a "photon counter", counting the number of photons absorbed from the bandgap and up. The approximation of the bandgap threshold as being a unity step function, Eq. **I.8**, is comparable for materials such as GaAs, but not as much for many other materials. Various technologies can be used to better match the actual absorption coefficient with this step function approximation (the difference between them is portrayed in Fig. **I-5a**).

The appearance of the bandgap of the material within Eq. **I.9** thereby completes the required information for the input flux into a solar cell. It is a function of a few physical constants (h, c and k), as well as the étendue of the incoming light, the material's bandgap, and the nominal temperature of the source. These parameters, as well as the functional form of Eq. **I.9** thus provide all the information needed to calculate the input flux – with the emphasis on the *information*, since the change of information is essentially the *entropy* of the system **[16]** , as will be described in the next chapter.

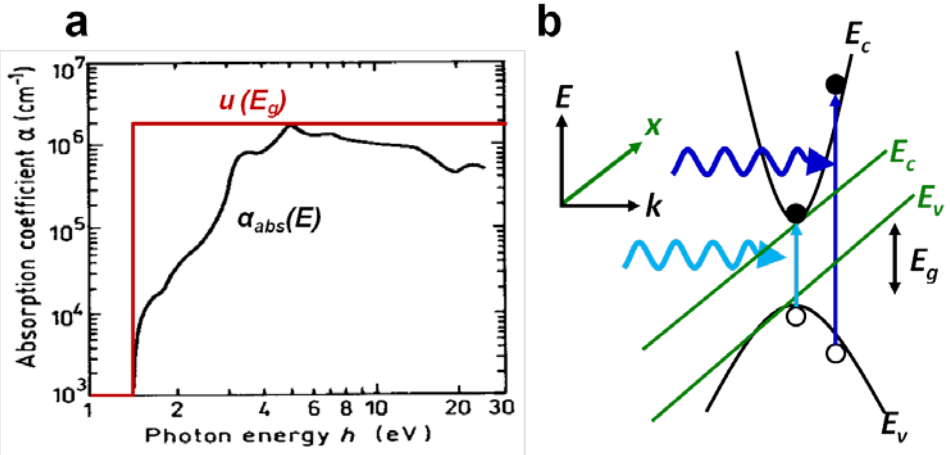

I-5: (a) Absorption coefficient of GaAs as a function of energy; overlaid is a step function at the bandgap of 1.4 eV [source: Ref. 17]. (b) E-k diagram of a semiconductor bandgap (in black), perpendicular to an E-x diagram (in green). The E-k description includes the parabolic bands common to most direct bandgap semiconductors, and plots the energy as a function of photon momentum.

This simplified description of the absorption of photons in a semiconductor is practically enough to describe all the other mechanisms within this text; however two essential properties of a semiconductor system must also be added to complete this simplified description. The first is that while the bandgap is the difference in energy levels between the conduction and valence bands: $E_g=E_c-E_v$, the actual energy level of importance is not the bandgap directly but rather the ensemble energy difference between electrons and holes. Since these are ensemble parameters, they are statistical and thus thermodynamic in nature, and depend heavily on the temperature, as well as the concentrations (number) of electrons and holes in each band. The variable of importance is therefore the *chemical potential*, μ, which is the difference between the two populations of electrons and holes **[4,6,7,15]**. This chemical potential is the difference in average chemical potentials of the electrons in the conduction band, and holes in the valence band. Since these populations are of Fermions (as opposed to photons, which are Bosons), their statistics follow the Fermi-Dirac distribution as opposed to the Bose-Einstein distribution, and the temperature of the lattice (i.e. the temperature of the solar cell itself) adds a 'width', or uncertainty, to the exact level of each of these bands. Therefore, the utilizable energy of e-h pairs, which is the voltage difference between the two populations, is the chemical potential difference between these two populations: $\mu=\mu_c-\mu_v$. From here on forward, only the single function, μ, will be used, despite its relation to the band populations, and it assumed that some method is available to separate the potentials of each population (essentially the reason why a p-n junction diode is used, as well as selective contacts).

An additional element that complicates the simplified band model used is the distinction between the *energy-space* description of a band, which is the *E-x* diagram shown on the left of Fig. **I-4**, as opposed to the more correct *energy-momentum* diagram, *E-k*, which plots the energy of the electron bands as a function of the momentum of the photons/electrons. This is plotted in Fig. **I-5b**, showing the traditional parabolic band diagram in *k*-space. In order for photons to be absorbed, and create e-h pairs, the momentum of the electron and hole (the "x-axis") must match.

This offsets the energy of the photons both above and below the bandgap edge. The two bands are not necessarily symmetric about the horizontal axis, with the valence band typically wider than the conduction band, which leads to "heavier" mass of the holes in the system (the effective mass of the electrons/holes is proportional to the inverse of the second derivate of the band diagram about the bandgap).

The parabolic band diagram of Fig. **I-5b** is that of a *direct bandgap* material, such as GaAs. However, *indirect bandgap* materials, such as Silicon (Si), will have the bottom tip of the conduction band offset from the top tip of the valence band. This offset prevents photons from being absorbed within these indirect bandgap materials, since the *k*-space momentum matching is harder to maintain, requiring carriers to already have momentum before absorbing photons. This feature of the bandgap, which distinguishes direct and indirect bandgap materials, is also the primary reason why certain materials are better for solar cells than others. In the indirect bandgap materials, more thickness must be used (viz. more material) to ensure the complete absorption of the photons within the semiconductor.

5. The Ultimate Efficiency

The Ultimate Efficiency (UE) is a concept coined by Shockley and Queisser **[7]** to describe the maximal efficiency of a hypothetically ideal solar cell. The assumptions used in calculating the ultimate efficiency are the most fundamental that can be made. The approach used by SQ was quite distinct from all others that preceded them: instead of attempting to calculate the efficiency of a solar cell by using the equations that govern a semiconductor, including the continuity equation that provides the relation between generated and recombining light, SQ decided to find the maximal efficiency achievable using *thermodynamic* arguments. The difference is that the thermodynamic limit is approachable from below, and cannot be surpassed, whereas the empirical models based on the equations for semiconductors were constantly improving and raising the maximal efficiency limit for power conversion in PV. In other words, the traditional method was a bottom-up approach, and provided incrementally increasing efficiency bounds, whereas the SQ approach was top-down, and provided a definitive upper bound to PV conversion for a semiconducting PV system.

The UE can be found by making a few assumptions **[7]**, delineated below. Each of these assumptions will be questioned and remarked upon in some form or other throughout this work. The assumptions are (in no particular order of importance):

a) The solar cell consists of a single junction semiconductor, being the ideal material to split e-h pairs via the absorption of photons.
b) The cell has no dimensions, acting as a thermodynamic body with no volume. The absorption within this body is infinite, following the step function of Eq. **I.8**. All photons below the threshold of E_g are not absorbed.
c) Photons absorbed with energy above the bandgap create e-h pairs with no detrimental loss involved in the heat loss due to the thermalization process.
d) A single e-h pair is created per absorbed photon.

e) Each e-h pair contributes to the short-circuit current of the solar cell. No absorbed photons are thus "lost".
f) The mobility of the carriers is infinite, resulting in a constant value of the chemical potential throughout the device, which has only two dimensions, with no thickness, as per assumption b).
g) No optics are used to help concentrate the light.

These assumptions are explicitly or implicitly noted in the original SQ paper, with some of the others, such as infinite mobility **[18]**, and the lack of thermalization loss **[15]** more explicitly stated in other works. Implicit in assumption e) is the assumption that the material is completely lossless, as will be emphasized later. This particular assumption was already questioned in the original model itself.

Under these assumptions, we can calculate the UE of a single junction solar cell (assumption a) using the formulas already mentioned above. For an ideal cell, we can imagine that the current of the cell is provided by the incoming flux of photons, each creating a single e-h pair per photon absorbed, and extracted at the bandgap, which would be the maximal achievable voltage. Considering the argument stated above regarding the difference between the bandgap and the chemical potential, we can recognize from the outset that if there is a difference between the bandgap energy (the threshold above which photons are absorbed) and the chemical potential (the maximal difference in potential/voltage between the electron and hole populations), this maximal voltage will not be achievable. Nevertheless, the *power* extracted under the UE assumptions is the product of the current and voltage of the device, which is the bandgap energy, E_g, multiplied by the photon flux, given in Eq. **I.9**. To calculate the efficiency, we must divide it by the incoming power flux, which is the Stephan-Boltzmann constant times the fourth power of the temperature (σT^4), as well as multiplied by the fraction of sunlight hitting the cell, which is the étendue (Ω_S). The étendue term thus cancels out, and if the integral is calculated in units of eV, we can simplify the formula for the UE efficiency as follows:

$$\eta_{UE} = g_2 \times E_g \times \int_{E_g}^{\infty} \frac{E^2 dE}{\exp[E/kT_S]-1} \qquad \textbf{I.10}$$

with the value of the pre-factor, g_2, given by:

$$g_2 = 15/(\pi k T_S)^4 \qquad \textbf{I.11}$$

The calculation of the UE given by Eq. **I.10** is presented in Fig. **I-6**, providing a maximal efficiency of 44% for an optimal bandgap of 1.17 eV. This maximum is a thermodynamic limit, defined solely on the photon flux emitted from the sun and absorbed by the cell, as well as the bandgap of the semiconductor, which is assumed to be an unchangeable parameter of the system.

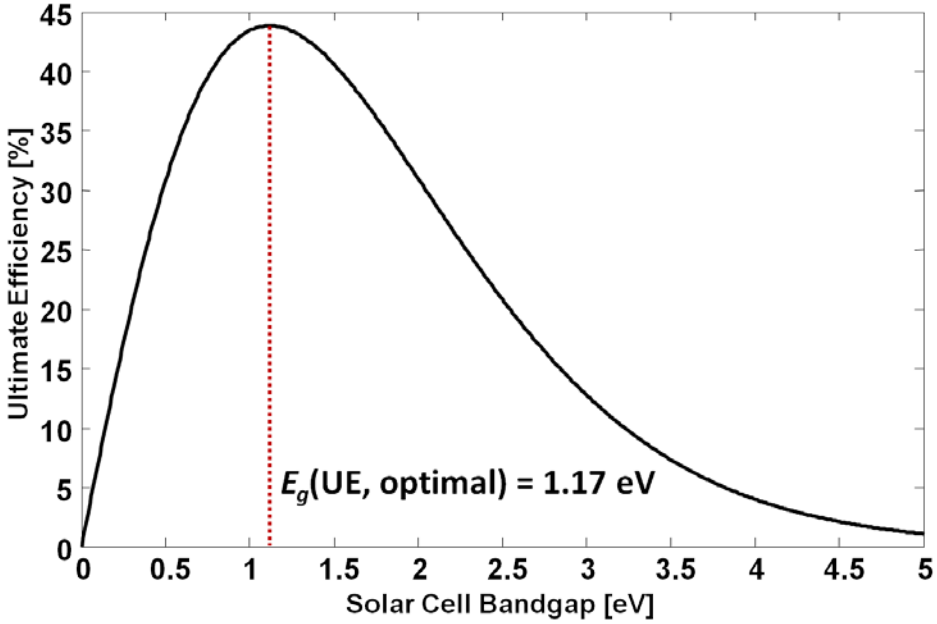

I-6: Ultimate Efficiency Calculation. The optimal bandgap, using these assumptions, is at 1.17 eV with 44% efficiency.

The reason there is a maxima in the UE is an interplay between the rising voltage obtained from the bandgap ($V \sim E_g$), multiplied by the solar spectrum current ($I \sim N_S$), which is the blackbody spectrum in Fig. **I-1**. It can also be explained using basic calculus as follows: at zero bandgap, the power out is zero ($V \sim E_g = 0$), and at infinite bandgap the current out is zero (since no photons are absorbed, $I \sim N_S = 0$). Since the function in Eq. **I.10** is nonzero, there must be a maximum, which can be found analytically using an approximation of the integral. This approximation, first used by SQ, and using an approximation of the integral already existing in the literature **[19]** is extremely useful, and is worth presenting here since it will be used extensively in the text. The approximation is as follows, where the "-1" in the denominator is neglected:

$$\int_{E'}^{\infty} \frac{E^2 dE}{\exp[E/kT]-1} \cong kTe^{E'/kT} E'^2 [1 + 2kT/E' + 2(kT/E')^2] \qquad \textbf{I.12}$$

where E' and T are used for general parameters, and generally is only valid if $E' >> kT$, however is relatively accurate to values approaching kT. This can be shown by expanding the denominator in a Taylor series (not shown here). For the solar flux, this means that the approximation is valid for all values of bandgap above ≈0.5 eV. Considering the UE value for a bandgap of E_g=0.5 eV, which is well below the maximal value, low bandgap materials are frequently ignored as being of less value for PV. This assumption is generally correct for a single junction cell, however we provide an example where this assumption is broken even for a single-junction cell in Chapter **VI**. Furthermore, it is no longer applicable for multi-junction cells, as will be addressed in Chapter **VII**.

6. Detailed Balance

The true SQ limit is known as the Detailed Balance (DB) limit, and is more complex than the UE limit, also defined by SQ in the same eponymous paper **[7]**. The UE limit, while easy to understand, fails to comply with the fundamental principal of *detailed balance*, which is a concept initially used in quantum physics to describe the reciprocity and/or time reversal phenomenon seen on a single quantum scale. The principal of DB states that in addition to the input flux of photons impinging upon the surface of the solar cell, we must also account for what happens to these photons within the confines of the cell, particularly, their possible re-emission.

Assuming a two band system, as described for a semiconductor above, we must be able to reverse the action of every photon, and state that if a photon can be absorbed within the cell, it must be able to be (re-)emitted as well. From rather basic arguments dating back to Einstein **[6,15]**, we know that there is a rate of emission due to three processes in any two level (band) system. These are shown pictorially in Fig. **I-7**. In Fig. **I-7a**, a photon is absorbed in the system, generating an excited electron (i.e. an electron in the conduction band, in an unstable state); this is known as *stimulated absorption*, and occurs at a rate of r_{abs}. Once the electron is excited, it prefers to lower its energy, and has two methods for doing so: the first is through *spontaneous emission*, at a rate of r_{spon}, and is portrayed in Fig. **I-7b**. This will occur 'spontaneously' after a specific lifetime that the electron stays in the excited (conduction band) state. The second process is more complicated, and is portrayed in Fig. **I-7c**. here, we must reverse the process of *stimulated emission* completely, and say that if an electron is already in the excited state, and another photon with energy matching (or above) the bandgap arrives, there is the possibility that this excess energy will induce the electron to immediately recombine with a hole (reduce its energy by "falling"), in a process known as *stimulated emission*. This rate of this process, r_{stim}, is dependent upon the concentration of electrons already in the excited (conduction) state, and therefore is not only dependent upon the input flux. In each of these processes, the conservation of energy, one of the most fundamental laws of physics, must apply. In spontaneous emission, or stimulated absorption, an exchange of energy between the photon and electron occur, such that $E_{photon}=h\nu_{photon}=E_g$. Any excess energy in the absorption process is transferred to thermal photons in the semiconductor lattice. In the stimulated emission process, the input energy is both the photon's energy, $h\nu$, as well as the excited electron's energy, at E_g; whereas the output process has *two* photons at $h\nu=E_g$ such that the total energy is conserved, however: *the total number of photons is <u>not</u> conserved!*

This final point is crucial to understanding the basic assumptions of the DB model. For any system at equilibrium (meaning that no other elements of energy are present), the rates of incoming and outgoing photons must match:

$$r_{abs} = r_{spon} + r_{stim} \qquad \textbf{I.13}$$

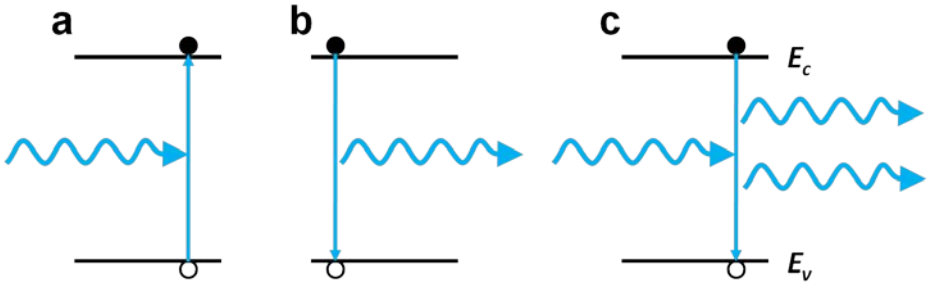

I-7: Absorption and Emission in a Two Level System. In all panels, the time axis starts on the left. (a) Stimulated absorption of a photon excites an electron to the conduction band, exchanging photon energy for bandgap energy. (b) Spontaneous emission of the excited electron, whereby the electron recombines with its hole, results in the emission of a single photon. (c) Stimulated emission occurs when an excited electron interacts with an incoming photon, resulting in an immediate recombination event and the emission of an extra photon to the field.

However, for PV, the assumption is that the rate of stimulated emission is less relevant, since the carrier concentration in the conduction band will result in a near negligible coefficient of stimulated emission **[6, 15]**. We can associate the rate of stimulated emission to be similar to the emission from a pumped laser; this essentially states that we are very far from the regime of laser operation, since we are not pumping enough electrons into the system. As we will show in Chapters **VI** and **VIII**, this may not be the case under certain conditions of operation. Therefore, for PV, the DB model states that for a standard semiconductor, the stimulated emission term is negligible, and we are only interested in the following reduced DB relation:

$$r_{abs} \cong r_{spon} \qquad \textbf{I.14}$$

Eq. **I.14** will be restated more effectively and in depth in the next chapter, however, the SQ DB model essentially assumes that the only emission process that must be dealt with is the re-emission of photons via the band-to-band (conduction-to-valence) recombination of e-h pairs.

The SQ DB model is a modification of the UE model, by including the physically required re-radiative loss as the essential loss mechanism of photons from the solar cell. The term for radiative recombination from the semiconductor follows the von Roosbroeck-Shockley (vRS) relation **[20, 21]**, which is quite similar to the Planck blackbody radiation, however accounts for the altered internal energy of the states as being a difference between the energy, E, and chemical potential, μ:

$$N_{out} = g \times \Omega_o \times n_c^2 \times \int_{E_g}^{\infty} \frac{E^2 dE}{\exp[(E-\mu)/kT_c]-1} \qquad \textbf{I.15}$$

where we have included the factor g as in Eq. **I.3**, the index of refraction of the material, n_c, as well as included the outgoing étendue of the emission, Ω_o. The temperature of the cell is denoted T_c, and is usually at ambient temperatures, T_c=300 K. Also assumed is that the emission follows the same step function dependence on the bandgap as the absorption, as in Eq. **I.8**, $\varepsilon_{emit}=\alpha_{abs}$. Eq. **I.15** appears nearly identical to Eq. **I.10**, except for the difference in étendue, and the addition of the chemical potential. However, the two equations are actually extremely different,

since the addition of the chemical potential reduces the exponent in the integrand of Eq. **I.15**, making the integrand function as a sharp, one-sided , delta function, about the bandgap energy. The emission line from the semiconductor is essentially the same as a Light Emitting Diode (LED), which radiates out a single color based on the bandgap of the semiconductor, however does not have nearly as sharp of a linewidth (meaning the amount of different colors/frequencies combined) as a laser. A laser, which utilizes stimulated emission, has a sharp linewidth that is more dependent upon the carrier concentration than the temperature.

For the DB model, we must reduce the incoming light impinging upon the solar cell by the outgoing light (re-)emitted from the solar cell itself, as a function of the chemical potential. The chemical potential is directly related to the voltage extracted from the solar cell, since:

$$V = \mu / q \qquad \textbf{I.16}$$

where q is the elementary electronic charge constant (q=1.6×10^{-19} C), and V is the voltage of the cell. This relation will be expounded upon in the next chapter. As stated above, the actual utilizable voltage of the cell will be *lower* than the bandgap, $V<E_g$, and will be reduced even further if a realistic load resistance is placed on it, which is essential for producing power from the cell. The SQ DB model therefore reduces the UE efficiency limit by a factor pertaining to the losses in re-emission, as well as finding the maximal power point of the product: $P=I\times V$, with the current, I, given by the input flux of photons (times q) minus the outgoing flux of photons.

To calculate the DB, we must also know the value of the étendue parameter, as well as the concentration factor, which will be covered in the next section. Losses in the radiative recombination can be added by multiplying the recombination emission rate in Eq. **I.15** by an efficiency factor, $0\leq\kappa_{nr}\leq1$, which can include nearly any loss process, such as non-radiative losses **[1,2,22,23]** (κ_{nr}=1 for a perfect material with no losses. Note that this term could equally have been defined as κ_{rad}, which is the inverse of κ_{nr}). This will transform the emission equation to:

$$N_{out} = \frac{g \times \Omega_o \times n_c^2}{\kappa_{nr}} \times \int_{E_g}^{\infty} \frac{E^2 dE}{\exp[(E-\mu)/kT_c]-1} \qquad \textbf{I.17}$$

The efficiency can then be calculated by subtracting Eq. **I.17** from Eq. **I.9**, and searching for a maximal value of μ (a more detailed description of the calculation appears in the following section). This calculation is shown in Fig. **I-8**, showing the maximum 30-31% efficiency expected from a PV system, assuming no losses other than radiative recombination. Adding losses will only reduce this maximal efficiency, which is what one would expect from a realistic system (see dashed line in Fig. **I-8**).

For most systems analyzed in this text, we will ignore the contribution of the index of refraction of the material, which leads to reflections off the surface of the solar cell, since anti-reflection coatings (ARCs) will reduce this factor. Furthermore, the inclusion of losses, as denoted by the κ_{nr} term, will only be included in certain sections of the text, and will be explicitly noted.

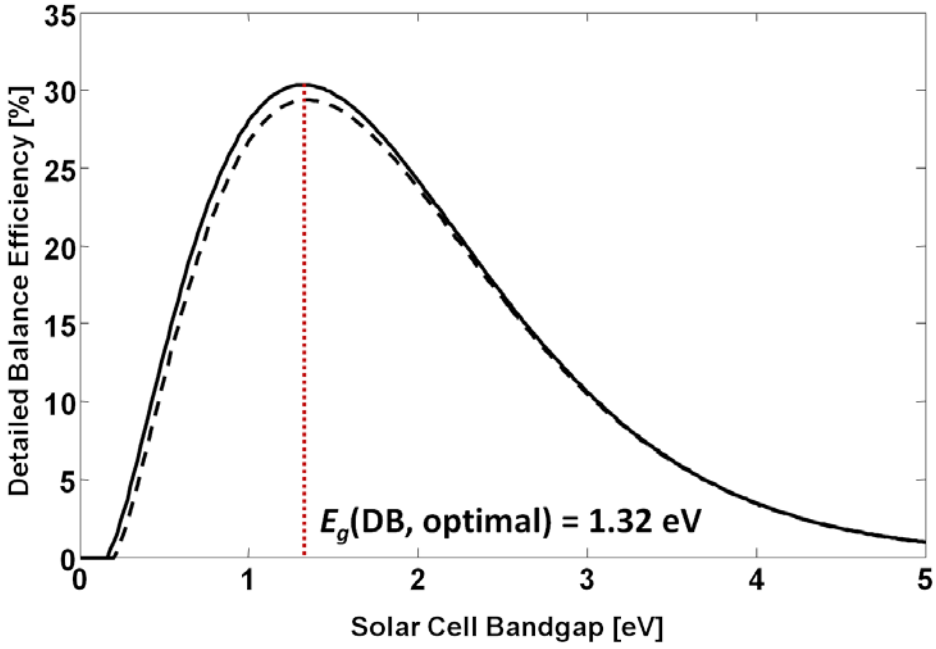

I-8: Detailed Balance Efficiency Calculation Per Bandgap. Compared with Fig. I-7, which is the Ultimate Efficiency, the maximal efficiency is reduced to ≈30.4%, at an optimal bandgap of 1.32 eV. The dashed line represents a lossy material that emits only 30% of the recombination light due to inefficiencies, lowering the maximal efficiency of the system.

Other models for maximal efficiency were developed concurrently with the SQ model, mostly based on semiconductor equations. In particular, a different set of upper-bounds was found by Wolf using semiconductor equations in conjunction with a thermodynamic approach **[24,25]**, and a convergence between the SQ thermodynamic model and the semiconducting models was found only more recently **[26,27]**. Regardless, the SQ model has stood the test of time, and remains the efficiency limit for a single junction solar cell, with no concentration or any other technique that violates the assumptions listed above. The addition of concentration for solar cells will now be described in brief.

7. Concentrating the Sunlight and Efficiencies

One of the assumptions in the SQ model was that the light was non-concentrated, and therefore there is a limiting factor matching the 'impedance' of the incoming sunlight absorbed from a solid angle of Ω_S, and subsequently emitted out at a solid angle of Ω_o from the cell. It is relatively easy to then deduce that using optics (such as a lens, or mirrors) to concentrate the light will improve the efficiency factor. We can also imagine that there is a limit to how much we can concentrate the sunlight, stemming simply from the Brightness Theorem as stated above, in which the rays of light cannot be 'bent backwards', and therefore they cannot be spread out by

more than an angle of 90°. This can be further proved via an implementation of the 2nd law of thermodynamics, as will be shown in Chapter **VIII [13,28]**.

The solar cell geometry described above was for a flat plate, which can emit light out (radiative recombination) at a solid angle of $\Omega_o=2\pi$ (a half angle of π, as well as emitting from both sides, adding a factor of two). However, it should be noted that the optimal geometry for a cell can in fact be spherical, in which case spherical coordinates should be used, and under this configuration, the cell can be illuminated by the entire spherical sky (as opposed to the hemisphere of the sky from above). The cell will then be able to absorb from a solid angle of 2π, as well as emit at a half angle of 4π (4π gives a spherical solid angle, which is then divided by two to provide the half angle, and then multiplied by two to account for radiation emitted in the negative *radial* coordinate).

To include the use of concentration, we must first define the *concentration fact*or, f_Ω, which provides information regarding how much the light was concentrated compared to the regular angular radius of the sun, with an incoming étendue of Ω_S. This leads to the definition of the f_Ω:

$$f_\Omega \equiv \frac{\Omega_o}{\Omega_S} \leq 1 \qquad \textbf{I.18}$$

which is simply the ratio of étendues. Any additional concentration will multiply this term, as will be shown below, in order to match the outgoing and incoming étendues. Since the tracking of the sun is essentially along a single axis, the solid angle, which is $\pi sin^2\theta$, it is only tracked along the θ angle of the azimuth. If we assume that the concentrator can only concentrate onto a flat plate, then the maximal outgoing étendue is π, which leads to the definition of the maximal concentration (f_Ω=1) as:

$$C^{\max} = \frac{1}{\sin^2 \Delta_S} \cong 46{,}000 \qquad \textbf{I.19}$$

where Δ_S was taken as ≈4.7 mrad, as above, and the value of C^{max} was rounded upward.

The concentrated sunlight can be viewed as multiplying the "number of suns" irradiating the solar cell, such as that portrayed in Fig. **I-3c**, or as increasing the incoming étendue of the sunlight, such as that portrayed in Fig. **I-3b**. Typically, the former usage is employed, such that a concentrating system is described as being (e.g.) "C=200 suns" or "C=1.2 suns". The merit of the physicality of the maximal concentration achievable, as described in Eq. **I.19** will be described in more detail in Chapter **VIII**. It should immediately be noted that adding a back reflector to the cell from below will create an effective concentration of C=2.

When including the concentration of sunlight into the efficiency calculations, we must also modify the incoming spectrum equation. Instead of simply using the photon flux of Eq. **I.9**, multiplied by the concentration, C, we must also include the ambient blackbody radiation, at a temperature of T_o – typically taken as T_o=300 K, which is the same as the cell's temperature. The ambient blackbody temperature adds an additional photon flux term:

$$N_{BB} = g(1 - Cf_\Omega)\Omega_o \int_{E_g}^{\infty} \frac{E^2 dE}{\exp[E/kT_o] - 1} \qquad \textbf{I.20}$$

where the concentration factor, f_Ω, is included, multiplied by the concentration itself, C.

Eq. **I.20** includes the portion of blackbody radiation from the ambient temperature and absorbed by the solar cell. The factor $(1\text{-}Cf_\Omega)$ appears since the portion of ambient blackbody étendue must not overlap that of the incoming sunlight étendue. This ignores the contribution of the diffuse light, although it can comprise a large portion of the incoming light angle, for simplicity. Fig **I-9a** displays the contribution of the ambient illumination for a system with no concentration. We must remove 1/46,000 of the hemisphere above the cell from the since that angle is taken up by the beam of incoming sunlight. For this system, the factor $(1\text{-}Cf_\Omega)$ is nearly unity, since C=1, and we can neglect the 1/46,000 term (with or without a back reflector). In contrast, when we begin increasing the concentration, effectively filling more of the sky with suns, we must reduce the contribution of the ambient blackbody, as show in Fig. **I-9b**.

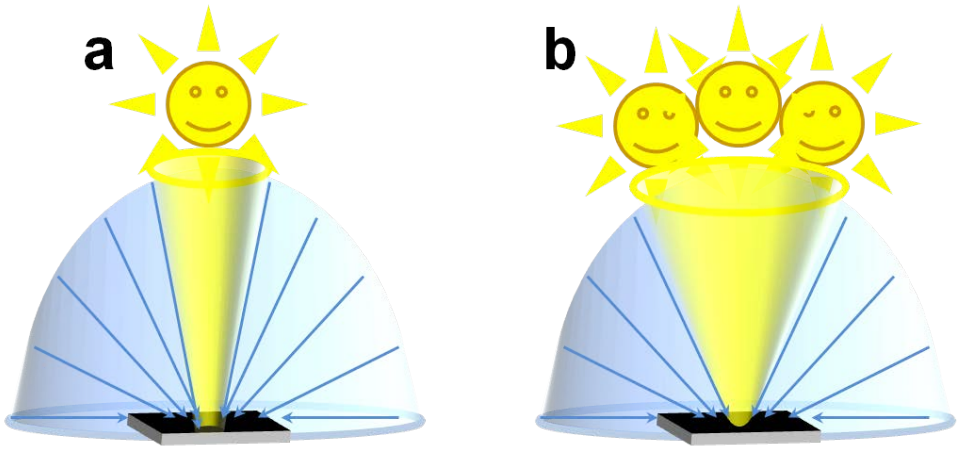

I-9: Concentrating Sunlight Versus the Ambient Blackbody Contribution. (a) For no concentration, the ambient blackbody fills the half angle of π-f_Ω, which accounts for everything other than the direct sunlight. (b) When increasing the concentration, the amount of ambient blackbody contribution is diminished.

The total input flux including the contribution from the ambient blackbody becomes:

$$N_{Total} = gC\Omega_S \int_{E_g}^{\infty} \frac{E^2 dE}{\exp[E/kT_S]-1} + g(1-Cf_\Omega)\Omega_o \int_{E_g}^{\infty} \frac{E^2 dE}{\exp[E/kT_o]-1} \qquad \textbf{I.21}$$

The difference between the two components is the étendue and the temperature. Since there is approximately a twenty-fold difference in temperatures between the solar and ambient blackbodies (T_S/T_o=6000/300), the contribution of the rightmost term is generally negligible in comparison to the stronger solar irradiation term. Since the short-circuit current is directly proportionate to Eq. **I.21** via a multiplication by q, the ambient blackbody produces some e-h pairs. However, even with no concentration (C=1), the rightmost term is five orders-of-magnitude lower the than the solar blackbody term, effectively making the contribution from the ambient negligible (this will be shown to be true for the open-circuit voltage as well in the next chapter). For this reason, the input flux that will be used throughout this text for *analytical* purposes will be Eq. **I.9**, whereas for *numerical* results, Eq. **I.25** is used.

The contribution of the ambient blackbody is important for finding the *dark current* of the solar cell, meaning the current that it provides when there is no solar input. In this case, the first integral in Eq. **I.21** is zero (C=0 suns), and the rightmost term is the only input term. This term is therefore important; otherwise there would be no definition for μ in this state **[29]**.

The effect of adding concentration can be seen as effectively reducing the radiative re-emission, in the same way that lowering the temperature, $T_c \rightarrow 0$ K would. In this sense, the UE is the same as the DB efficiency for a cell at 0 K, which is physically impossible to achieve, and thus provides a maximal upper limit for the energy conversion **[7]**. To find the maximal efficiency as a function of the concentration and voltage ($P=I\times V$), we must maximize the following equation as a function of $qV=\mu$:

$$\eta_{DB}(E_g, C) = g_2 \times V \times \left[\int_{E_g}^{\infty} \frac{E^2 dE}{\exp[E/kT_S]-1} - \frac{1}{C\Omega_S} \int_{E_g}^{\infty} \frac{E^2 dE}{\exp[(E-qV)/kT_c]-1} \right] \qquad \textbf{I.22}$$

where the first bracketed term comes from N_{Total} as in Eq. **I.9** (neglecting the ambient blackbody, for brevity), and the second bracketed term comes from N_{out} as in Eq. **I.17** above, and all other parameters are constants (T_S, T_c, T_o, Ω_S, Ω_o). For maximal efficiency, we ignore the effects of non-radiative losses (κ_{nr}=0), and refractive index mismatches (n_c=1). The division of the outgoing emission flux by the factor $C\Omega_S$ reduces the contribution of the second bracketed term in Eq. **I.22**. Therefore, we can see that an increase in concentration effectively nullifies the contribution of the second term, and Eq. **I.22** approaches the UE limit of Eq. **I.10**.

Fig. **I-10** displays both the current-vs.-voltage (I-V) curve for a solar cell with E_g=1 eV, and the efficiency for this cell with increasing concentration. The I-V curve, shown in black, is the bracketed term in Eq. **I.22**, and displays the most critical parameters of this curve: the open-circuit voltage, V_{oc}, and the short-circuit current, I_{sc}. The maximal output power is the maximum of the bracketed current term multiplied by the voltage, and provides the *maximal power point*, identified by the parameters I_m and V_m. There is no analytical solution to the maximum of Eq. **I.22**, being a transcendental equation, however these parameters are well defined.

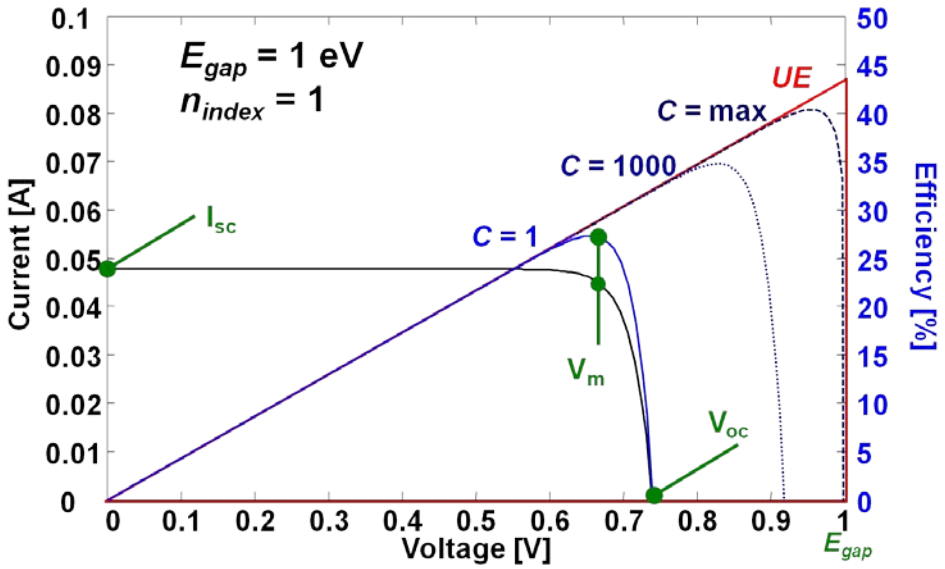

I-10: I-V Curve and Maximal Power Curves for a 1 eV Bandgap Cell. The left axis displays the black-curve I-V characteristic of a cell with no concentration, *C*=1. Displayed are the most important parameters of a solar cell, the short-circuit current, open-circuit voltage and maximal (voltage) power point: I_{sc}, V_{oc} and V_m, respectively. The curved right-hand corner of the I-V plot is a result of the diode-like characteristics of the two band model. In blue are the power point curves, $P=I\times V$, normalized to the input solar current (the efficiency). Adding concentration increases the efficiency of the system (I-V curves not shown), with maximal concentration approaching the Ultimate Efficiency limit, which is portrayed by the red triangle. The more "triangular" the power curve – or "square" the I-V curve – the higher the efficiency of the cell.

The difference between E_g and V_{oc} will be described in detail in the next chapter, however, it should be noted that this difference results here entirely due to thermodynamic principles of flux and not due to semiconductor equations of carrier concentration. The "square-ness" of the I-V curve is measured as the *Fill Factor*: *FF*, which is a measure of the maximal power point, to the easily measureable parameters of the solar cell: I_{sc} and V_{oc}, and is defined as:

$$FF \equiv \frac{I_m V_m}{I_{sc} V_{sc}} \le 1 \qquad \textbf{I.23}$$

with $FF\to 1$ for maximal concentration, and for $T_c\to 0$ K, i.e. the UE case. For C=1, the *FF* can be approximated to a near-analytical solution, given by **[30]**:

$$FF = \frac{v_{oc} - \ln[v_{oc} + 1 - \ln(v_{oc})]}{v_{oc} - \ln[v_{oc} + 1 - \ln(v_{oc})] + 1} \times \frac{v_{oc} - \ln\{v_{oc} - \ln[v_{oc} + 1 - \ln(v_{oc})] + 1\}}{v_{oc}\left[1 - \exp(-v_{oc})\right]} \qquad \textbf{I.24}$$

where $v_{oc}=V_{oc}/kT_c$. The *FF* is mostly dependent upon the V_{oc} of the system, as can be seen from Eq. **I.24**. This emphasis on the *voltage* of the solar cell, as opposed to the more intuitive grasp of the *current* of the solar cell is one of the main themes of this work; while most of the equations listed so far had a direct relation with the current, it is the voltage that supplies more information

(literally), and therefore plays an important role, if not more important, than the current. The emphasis on voltage can be seen in the simplified efficiency equation that makes use of the *FF*:

$$\eta_{eff} = FF \times I_{sc} \times V_{oc} \qquad \textbf{I.25}$$

In this equation, the efficiency is dependent upon three factors, two of which are voltage dependent, as a function of V_{oc}. This simplified equation, while always true, is useful for quick calculations of the efficiency using Eq. **I.24** for the *FF*. It is also important as it emphasizes the major measurable parameters of a solar cell, as can be seen from Fig. **I-10**. However, it belies the complexity needed to calculate the actual efficiency using the transcendental equations to find the maximum power point. The approximation of the *FF* given in Eq. **I.24** is fine for no concentration, however higher concentration result in higher *FF*s, and calculations using the *FF* method will not be used any more throughout the text.

The addition of concentration to the efficiency calculations is therefore seen as the first added level of complexity to the PV system. While one can theoretically use extremely high concentration values to improve the efficiency of an existing cell, the reality of the PV design and materials typically imposes a realistic limit of ~C=1000, beyond which losses (particularly serial resistance losses) begin to reduce the overall efficiency **[31,32]**. This will be detailed more fully in Chapter **VIII**.

8. Beyond the Shockley-Queisser Limit

The ≈31% efficiency limit for a single junction solar cell is one that is thermodynamically imposed, based on the assumptions listed in section 5. However, it was quickly noticed by many that this limit can be circumvented if any of the assumptions listed were violated in a manner that did not violate any physical principles. Each one of the assumptions listed has been questioned, using some combination of technology or another, in attempts to obtain higher efficiency PV systems, *beyond* the SQ DB limit. This is in addition to the general trend of the past 50 years of improving the efficiency of PV to approach the SQ upper limit *from below.*

There are many methods of improving the efficiency of PV beyond the SQ limit, while maintaining the laws of physics and not violating the laws of thermodynamics. Every one of the assumptions stated above can be questioned, and physical processes that counteract these limitations can be found. For example, the assumption that every photon will create a single e-h pair was known at the outset (in SQ's original paper **[7]**, in a footnote) to be false under certain circumstances. This possibility of creating more electrons from every photon is the foundation of the sub-field of Carrier Multiplication (CM) cells, as will be discussed in detail in Chapter **IV**. There are a number of methods such as this that have been described in the literature, and a description of these methods in terms of what they attempt to accomplish, and their drawbacks and advantages, will be covered in some of the next few chapters. In particular, Chapter **V**divides some of these methods in an easy to understand matrix.

The concept of surpassing the SQ limit was described and analyzed in detail by Green, and coined as "3rd Generation Photovoltaics" **[4,33]**. The concept of 3rd generation PV is to go

beyond the SQ limit while simultaneously reducing the cost of the system. The 1st generation was described as simple, single junction cells, which were designed to improve up to the SQ limit. The 2nd generation was assumed to encompass the field of thin-film PV, where the same efficiencies could be gained while reducing the material usage and cost. The 3rd generation concept is to maintain the low cost, while exceeding the SQ limit for a single junction cell. This was summarized in a well-publicized graph showing the cost of the cell, in dollars per square meter, versus the efficiency, and is reproduced here in Fig. **I-11**.

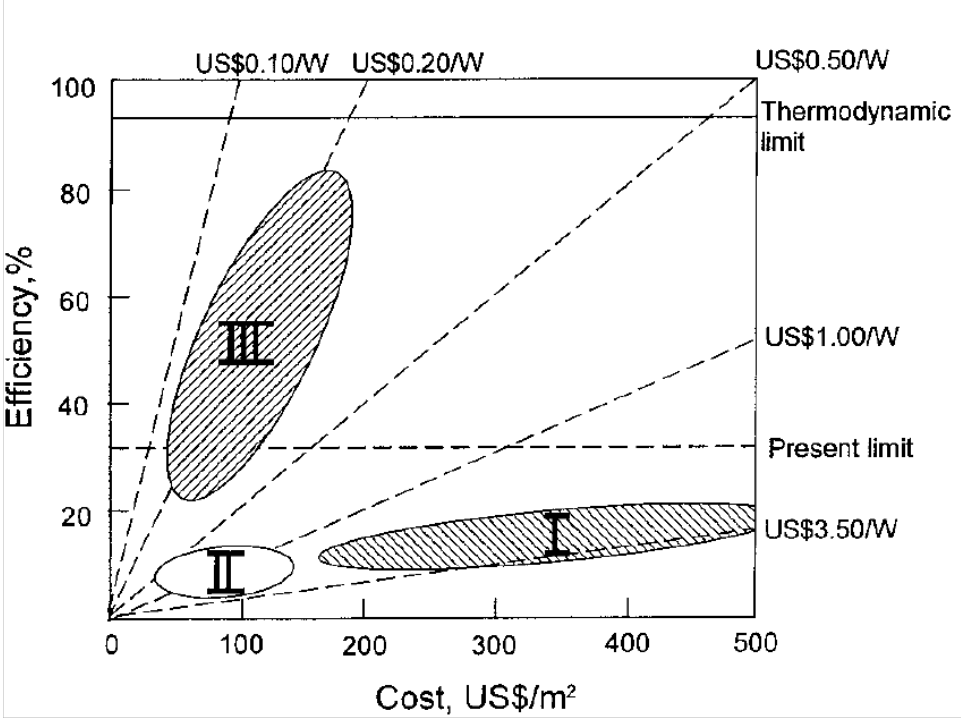

I-11 3rd Generation Photovoltaics, as a Function of Cost and Efficiency. The 'Present Limit' is the SQ limit for a single junction cell, and the 'Thermodynamic Limit' is the maximal possible efficiency achievable if concentration is used as well. Reproduced from Ref. [33].

The goal of surpassing the SQ limit was immediately recognized to be possible if more than a single semiconducting junction was used **[24]**. Since each junction would be limited by the similar equations used to derive the SQ limit, by adding them together, one could increase the overall efficiency of the system. Since the SQ limit for a single junction cell has a maxima per bandgap, it is obvious that not every bandgap is can achieve the optimal efficiency; however, if we imagine each junction as an independent voltage supply, with a current running through it generated by the solar irradiation, we can connect these power supplies together to create a larger, more efficient power supply. How to connect these cells together is a different question, but for the existing architecture of multi-junction cells today, they are connected in series, such that the current is matched in each cell, by selecting the bandgaps of each junction to absorb the same number of photons (assuming each segment of absorbed photons produces the equivalent number of e-h pairs, and thus an equivalent current). This type of device architecture, known as a multi-junction cell will be analyzed more thoroughly in Chapter **VII**. Regardless of the

architecture itself, the overall efficiency of such a multi-junction system can approach the thermodynamic limits of solar energy conversion **[4,6,34-39]**.

The number of materials used for PV has expanded over the years, as well as the device architectures and methods. In addition to the mainstream use of Si as the semiconductor material of the solar cell, the use of GaAs has recently become feasible due to scalable manufacturing techniques, and compound materials such as CIGS (Copper-Indium-Gallium-Selenide) are also being used by some manufacturers due to its ease of manufacturing as well. Each material system has its merits and drawbacks in terms of material abundance, costs and other issues. While Si currently controls most of the PV material market, the fact that it is an indirect bandgap material makes it less suitable than others; however its mature development in the information technology landscape has given it the largest head-start. Regardless, for a single junction cell, the material's bandgap must be chosen so as to sit near the top of the efficiency curve of the DB limit in Fig. **I-8**, which severely limits the number of materials available. This limitation will be addressed in Chapter **VII**.

The use of multi-junction cells allows the use of more materials, however is generally limited by other material-science related issues of combining these materials together, without inducing losses. For a stack of multi-junction materials, the major constraint is the lattice growth of different materials upon one another, which if improperly matched, induce defects in the semiconductor crystal and make each segment of cell less efficient. The materials used for these multi-junction cells typically include a base of either Germanium (Ge) or Gallium Antimonide (GaSb), which have low bandgaps (0.67 and 0.73 eV, respectively), followed by layers of growth of GaAs and Aluminum Gallium Arsenide (AlGaAs) derivatives, which can tune the bandgap of the layer, depending on the amount of materials interchanged. Typically, concentration is used to improve the efficiency of these devices, since the high cost of manufacturing can only be offset by the high *efficiency* made possible through the use of these multi-junction materials.

The efficiency of each design can be confirmed at a few internationally recognized locations, and the 'champion cell' efficiency of each design is released in a multi-variable graph on an annual basis by NREL, as is reproduced in Fig. **I-12** for the period up to mid-2011. Additional techniques exist to make solar cells, as referenced in the graph, and many companies, designs and materials are mentioned.

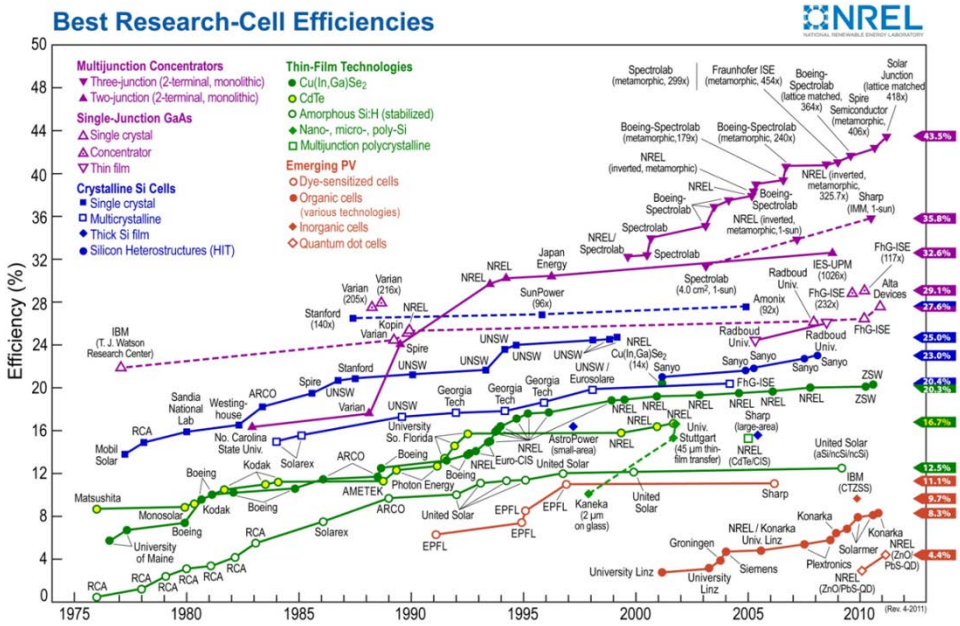

I-12 Validated Solar Cell Efficiency Data from NREL. All data points show the peak efficiency of a specific solar cell design. Graph reproduced from NREL.

The remaining chapters of this text will focus on certain aspects of solar cell efficiency calculations, based entirely on the thermodynamic approach. In particular, the emphasis on the open-circuit voltage, and its relation to the entropy of the photons will be discussed in the following chapter. The relation between the maximal voltage and information will be the main topic discussed throughout all the following chapters.

II. Entropy, Transfer Functions and the Single Junction Solar Cell

**Publication note*[1]

1. The Detailed Balance Model Revisited

The following chapter delves into the concept of entropy, and how it relates to the thermodynamic description of a solar cell. To account for the entropy, the most simplified version of the SQ DB limit is constructed, as first devised by Ruppel and Würfel **[15]**. The entropy arguments follow many other works in the field **[35,41-43]**, with the entropy of photons described in many different variations **[44,45]**.

While the original SQ paper **[7]** described the DB limit as a function of the UE limit, multiplied by loss terms such as the 'impedance mismatch' and 'voltage correction', as well as using the diode approximation to described the outgoing flux of photons, the most simplified version of the DB limit can be described simply by the current flow in at short-circuit, and the voltage at open-circuit. This description was used in the preceding chapter to provide the equation for the DB limit, however, it was *not* the form used by SQ in their original paper. Part of this difference stemmed from the use of approximations by SQ to simplify their calculation in a time when computers were not available to calculate the maximal power point. While we use numerical techniques to find the maximal power point, the thermodynamically important parameters of the PV system were described as being I_{sc} and V_{oc}, as portrayed in Fig. **I-10**. The I_{sc} was described as being directly related to knowledge of the input flux:

$$\begin{aligned} I_{sc}^{reg} &= qgC\Omega_S \int_{E_g}^{\infty} \frac{E^2 dE}{\exp[E/kT_S]-1} - qg\Omega_o \int_{E_g}^{\infty} \frac{E^2 dE}{\exp[(E-0)/kT_c]-1} \\ &\approx qgC\Omega_S \int_{E_g}^{\infty} \frac{E^2 dE}{\exp[E/kT_S]-1} \end{aligned} \qquad \textbf{II.1}$$

where we have neglected the ambient blackbody contribution, and the chemical potential $\mu=qV$ was set at zero, which is the voltage at short-circuit. The I_{sc} for a 'regular' single junction cell can therefore be taken as the input solar flux alone.

In contrast, the V_{oc} of the system is not directly inferable, but can be found using the *flux equilibrium method* **[15]**. At open-circuit, the current must be zero, and therefore we can equate the incoming and outgoing light, since the *flux* of photons, meaning the number of photons impinging upon the surface, as well as emitted from the surface, must be *equal* at steady-state equilibrium. This statement is in fact a re-phrasing of Kirchhoff's law of radiation, in which a

[1] The following chapter includes material from all of my publications, but in particular the description of the single junction transfer function was defined in Ref. **40**. That publication, however adds more detail to the discussion, as well as includes the transfer functions of other 3rd generation techniques, which will be dealt with in Chapter **V**.

material's emissivity, ε_{emit}, is equal to its absorptivity, α_{abs}, assuming no losses are incurred **[6,15]**. For the simplified model, we take both absorptivity and emissivity as unit step functions:

$$\alpha_{abs} = \varepsilon_{emit} = u(E_g) \qquad \textbf{II.2}$$

just as was done in Eq. **I.8**. The difference between the regular description of Kirchhoff's law of radiation, and the one used here for the flux equilibrium method, is that here we are describing an equation of total photon number, whereas the original law was stated for total energy flow. The flow of *energy* from the sun to the cell at open-circuit is *not* equal **[6]**. Furthermore, the emissivity and absorptivity are typically functions of the energy as well as the solid angle of flux, and we are here assuming that $\alpha_{abs}=\varepsilon_{emit}$ under all angles and energies. These terms are therefore more correctly written in their form: $\alpha_{abs}=\alpha_{abs}(E,\Omega)$, including both the angular and energy terms. The idea of limiting the input and output emission will be discussed again in Chapter **VI**.

At open-circuit, the cloud of photons emanating from the sun interacts with the solar cell, and generates electron hole pairs. While the chemical potential of *blackbody* photons is ill-defined (essentially zero), after the interaction with the solar cell (or matter in general), the photons can have a chemical potential ascribed to them. This non-intuitive fact has been noted by several authors **[15,46,47]**, and can truly be defined only at open-circuit, where the chemical potential of the electrons, $\mu_{oc}(electrons)$, is wholly imparted to the outgoing recombination photons, $\mu_{oc}(photons)$. If we zero I_{sc} in Eq. **II.1**, and leave the chemical potential equal to the open-circuit voltage, $\mu=qV_{oc,}$ we obtain the following flux equilibrium relation:

$$C\Omega_S \int_{E_g}^{\infty} \frac{E^2 dE}{\exp[E/kT_S]-1} = \Omega_o \int_{E_g}^{\infty} \frac{E^2 dE}{\exp[(E-qV_{oc})/kT_c]-1} \qquad \textbf{II.3}$$

Examining Eq. **II.3**, it is obvious that the major differences preventing the two sides of being equal are the mismatch in étendues (Ω), as well as the variation in the exponent, as a function of temperatures. Since the concentration amount, C, can counter the étendue mismatch, the equivalence of the exponents relates the temperature and chemical potential of light:

$$\frac{E}{kT_S} = \frac{E-\mu_{oc}}{kT_c} \qquad \textbf{II.4}$$

However, this relation is deceptive, since Eq. **II.3** does not relate the integrands, but rather the full integral (the area below the integrands), as will be displayed below. Nevertheless, at maximal concentration ($C\Omega_S=\Omega_o$), we can use Eq. II.4 to find the *maximal* value of the open-circuit voltage under normal operation:

$$qV_{oc}^{\max} = \mu_{oc}\big|_{C=C^{\max}} = E_g\left(1-\frac{T_c}{T_S}\right) \equiv E_g\eta_C \qquad \textbf{II.5}$$

where η_C is the Carnot efficiency between two sources of different temperature ($\eta_C\approx95\%$ for the temperatures used here) **[48,49]**, and the replacement of E with E_g can be found by a finding the maximal value of Eq. **II.3** in terms of the energy as a function of a constant chemical potential **[29]**. This appearance of the Carnot efficiency signifies the thermodynamic relevance of the open-circuit voltage, as will be discussed in the next section.

To find the value of V_{oc} for all other values of C, we must solve Eq. **II.3** for V_{oc}. This can be done numerically, for an exact solution, however the physical meaning of this solution can also be found by using the approximation of the integral from Eq. **I.12**, for both sides of the equation. This approximation only holds under the following assumptions: $E>>kT_S$ and $E-qV_{oc}>>kT_c$. The approximation actually holds fairly well for values of E approaching these limits as well (as can be shown using a Taylor expansion). Using this approximation, V_{oc} can be found as:

$$qV_{oc}^{reg} = E_g\left(1-\frac{T_c}{T_S}\right)+kT_c\times\ln\left[\left(\frac{C\Omega_S}{\Omega_o}\right)\left(\frac{T_S}{T_c}\right)\left(\frac{\alpha_{S1}}{\alpha_{c1}}\right)\right]+kT_c\times\ln(\kappa_{nr}) \qquad \textbf{II.6}$$

Where we have included the possible losses, and neglected the n^2_{sc} term which can provide a total $4n^2_{sc}$ enhancement **[50]**. The α terms are correction terms of the form:

$$\alpha_{S1} = 1+2kT_S/E_g+2(kT_S/E_g)^2 \qquad \textbf{II.7}$$

which is due the integral expansion, and can be non-negligible for moderate bandgaps (e.g. $\alpha_{S1}\approx 2.5$ for $E_g=1$ eV), and:

$$\alpha_{c1} = 1+2kT_c/E_g+2(kT_c/E_g)^2 \approx 1 \qquad \textbf{II.8}$$

Which is typically negligible (unity) due to the small thermal energy: $kT_c|_{300\ K}=25.8$ meV. If we ignore the losses, and the α terms, we can simplify Eq. **II.6** to:

$$qV_{oc}^{reg} = E_g\left(1-\frac{T_c}{T_S}\right)+kT_c\times\ln\left[\left(\frac{C\Omega_S}{\Omega_o}\right)\left(\frac{T_S}{T_c}\right)\right] \qquad \textbf{II.9}$$

This equation of the open-circuit voltage provides a closed form equation that relates this crucial parameter of a solar cell to the constants of the material and architecture. Furthermore, it will be shown in the next section that it has important ramifications regarding the thermodynamic state variables of the system. Plotted in Fig. **II-1** are I_{sc} and V_{oc} following the equations above. The approximate solution is nearly identical to the numerical solution.

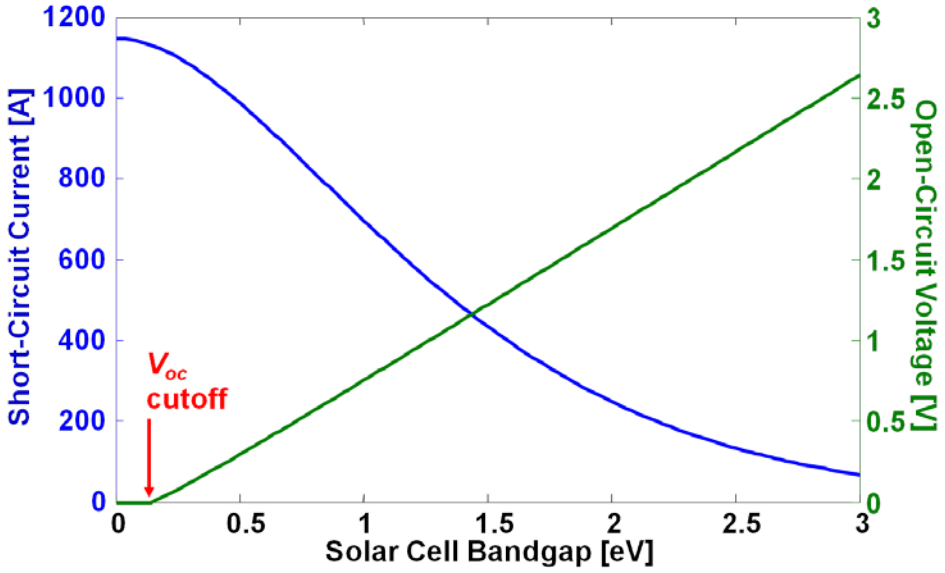

II-1 Short-Circuit Current and Open-Circuit Voltage of a Solar Cell. The V_{oc} has a cutoff for low bandgaps due to the logarithmic term.

Due to the logarithmic term in the open-circuit voltage, there is a cutoff (or cut-on) for small bandgaps, below which the voltage is zero. This cutoff is highly dependent upon the parameters of the system, and becomes higher with losses, reflections (non-unity index) and different étendues; for these calculations, $\Omega_o=2\pi$ and $C=1$. It should be noted that for $C=C^{max}$, $V_{oc}\rightarrow E_g$, and not $E_g\times\eta_C$; this discrepancy is discussed in Chapter **VIII**.

2. Entropy and the Reduction of Voltage

The chemical potential, and thus the voltage, at open circuit is a thermodynamic variable. At open-circuit equilibrium (with no current extracted), all the photons are absorbed and re-emitted, and the semiconductor solar cell has transformed the total energy of the photons in the most efficient manner. This is the essence of the DB model. From the fundamental equations of thermodynamics, we can relate the chemical potential to the Gibbs free energy of the system, *G*, which is related to the other thermodynamic variables by:

$$G = U - T \times S = \mu \qquad \textbf{II.10}$$

where *U* is the internal energy and *S* is the entropy. Generally speaking, the Gibbs free energy also includes the pressure-volume product, which is what differentiates the Gibbs and Helmholtz free energies. While we will not associate any volume with the photon cloud, the étendue can be taken as a thermodynamic replacement for the volume expansion **[10]**.

The use of the term 'entropy' can better be explained if we interpret entropy as meaning a measure of the *Missing Information* of a system **[16]**. This measure is just as fundamental a property of the system as its temperature and internal energy, and is not arbitrary. The entropy is therefore a measure of *information* in the system, where the information is a measure of the distribution functions, *W*, of all the relevant parameters of the system **[16,51,52]**:

$$S = k \times \ln(W) \qquad \textbf{II.11}$$

where the natural logarithm, *ln*, is used in place of the base-two logarithm, log_2, typically used in information theory for binary variables, and the Boltzmann constant is taken as the units of physical entropy. Conversely, we can view the entropy as unit-less, and associate the temperature in units of energy, as *kT*, which is a factor that appears in all thermodynamic equations. The connection between the thermodynamic entropy and the entropy of information theory has been dealt with by many recent authors, and despite the common claim that the two are nominally unrelated, they are in fact one and the same **[16]**.

We can recognize from Eq. **II.9** that the formula for V_{oc} contains an entropic term of the form $k\times ln[]$. The bracketed terms contain ratios of distributions, which we assume to simply be constants. As such, we can ascribe an entropic meaning to each of these terms, as has been done before **[10,43]**. The first of these terms relates the étendues:

$$S_{\Omega} = k \ln(\Omega_o / C\Omega_S) \qquad \textbf{II.12}$$

where the logarithm has been inverted due to the minus sign of the entropy in Eq. **II.10**. This term therefore tells us that in the PV conversion process using a semiconductor, entropy is created from the emission of isotropic recombination from the semiconductor at an angle of Ω_o, as compared with the small angular incoming irradiation at Ω_S. From an information perspective, there is a loss of information when take a small solid angle cone of "ray" distributions, and convert it into a larger hemispherical radiation distribution. The Concentration factor is appended here to the incoming radiation étendue, Ω_S, since it is a factor that can "match" the radiation distributions, and therefore nullify the entropy generation. At maximal concentration, this term is zero, since the term in the parentheses is unity, signifying that there is no loss of information when the incoming radiation distribution is the same as the outgoing one. For all other values of concentration, $C<C^{max}$, this entropy term is *positive*, and in units of voltage produce a *negative* voltage. In particular, there is a ≈220 mV loss of open-circuit voltage for C=1 due to this term with Ω_o=2π. The relation of the distribution of étendues to the probabilities stated in Shannon's interpretation of the entropy is that we will here assume that the probability of finding any photon (or ray in the beam) is distributed uniformly over the entire solid angle, such that the probability, p, of a photon being at an angle of $d\Omega_S$ is $p_{d\Omega}=1/\Omega_S$. This probability distribution is valid as long as there is no dispersion relation between the energy of each photon and its position within the angular radius (i.e. p is not a function of E). It will not hold if there is any non-uniformity in the beam, such as when the "blue" light is scattered more in the atmosphere due to Raleigh scattering. Nevertheless, the approximation is quite good even for regular diffuse sunlight.

The second entropic term is due to the temperature difference between the sun and the cell:

$$S_T = k \ln(T_c / T_S) \qquad \textbf{II.13}$$

This term is *negative*, producing a *positive* voltage gain. From an information perspective, the temperature is a measure of kinetic energy, which provides *uncertainty* (i.e. lack of information) of the location of the rays/electrons (since at open-circuit, the chemical potential of the photons is equal to that of the electrons, as stated above). Therefore, lowering the effective temperature of the photons, as per Eq. **II.4**, provides us with *more* information, and thus lowers the uncertainty (missing information).

Both entropic terms described above relate to a ratio of distributions, and a sense of relative information loss in the conversion process. Since entropy is a measure of information, as per Shannon's description of Information Theory, this ratio difference between the entropy of the photon gas after and before the conversion process provides us with a measure of the *divergence* of information between the two distributions. This is known as the *Kullback-Liebler Distance* in Information Theory, and is always related by a ratio of distributions **[52]**. This measure of missing information between two distributions will be used to compare other methods of PV in the other chapters.

The relation between the Information Theory use of entropy as a form of missing information, or uncertainty, and the traditional use of the second law of thermodynamics as describing the heat loss as a generator of entropy can be reconciled by taking a more exact form of the entropy from Eq. **II.6**. Instead of simply "associating" the entropy term with that of the $k\times ln[]$ term, we

will use a more precise description of the entropy that stems from the use of the Gibbs free energy, as described in Eq. **II.10**. In this relation, the exact form of the entropy is given by the partial differentiation of the Gibbs free energy, as a function of the temperature of the cell:

$$S = -\frac{\partial G}{\partial T_c} = -\frac{\partial \mu}{\partial T_c} \qquad \textbf{II.14}$$

where we replaced G with μ using Eq. **II.10**. For this calculation, we assume that $T_c \neq T_S$, as well as $T_c \neq T_o$, meaning that the temperature of the cell is not necessarily related to the temperature of the ambient atmosphere. Using this formula to derive the entropy provides:

$$S = \frac{E_g}{T_S} + k\left(\frac{\alpha_{c2}}{\alpha_{c1}}\right) + k \times \ln\left[\left(\frac{\Omega_o}{C\Omega_S}\right)\left(\frac{T_c}{T_S}\right)\left(\frac{\alpha_{c1}}{\alpha_{S1}}\right)\right] \qquad \textbf{II.15}$$

Where α_{S1} and α_{c1} are as defined in Eqs. **II.7** and **II.8**, respectively, and α_{c2} is a constant that occurs due to the internal partial derivative:

$$\alpha_{c2} = \frac{\partial(T_c \alpha_{c1})}{\partial T_c} = 1 + \frac{4kT_c}{E_g} + 6\left(\frac{kT_c}{E_g}\right)^2 \qquad \textbf{II.16}$$

Since kT_c=25.8 meV, one can generally assume that both α_{c1} and α_{c2} are negligible and unity; however in Chapter **VIII** we examine the case for low bandgaps, where this approximation does not necessarily hold. It should also be reminded that these approximations were a result of the approximation of the integral, as in Eq. **I.12**, where it was assumed that $E >> kT_S$ and $E+\mu >> kT_c$. With these assumptions, we will simplify the writing of Eq. **II.15** to:

$$\frac{S}{k} \cong \frac{E_g}{kT_S} + 1 + \ln\left[\left(\frac{\Omega_o}{C\Omega_S}\right)\left(\frac{T_c}{T_S}\right)\right] \qquad \textbf{II.17}$$

in unit-less entropy values of S/k. The production of entropy in the PV conversion process must follow the second law of thermodynamics, which is $\Delta S \geq 0$, and can be seen to hold for Eq. **II.17** since the terms are almost always positive; Chapter **VIII** deals with the extreme case where this no longer holds. The terms in Eq. **II.17** can be described using Information Theory for the rightmost term involving the $k \times ln[]$ components, as well as using the more classical description of entropy as the heat loss energy for the leftmost term, E_g/kT_S. This form of the entropy includes all the relevant parameters of the system: T_S, T_c, Ω_S, Ω_o, as well as the variables and E_g and C.

The information balance involved in the input and output of the PV conversion process can be described, at open-circuit equilibrium, as involving the change in distributions of the photon cloud before and after interaction with the solar cell. Fig. **II-2** contains all of the relevant information, in a graphical depiction. The incoming photon cloud has a wide distribution in energies, as shown in Fig. **II-2a**, which is the integrand of the solar blackbody spectrum, Eq. **II.1**. This wide dispersion of energies of photons can be considered as an uncertainty of the *energy-per-photon* of the incoming beam (after being absorbed by a material with E_g), and can be compared to the uncertainty of measuring any spectrum as a function of the Full Width at Half Maximum (FWHM) of the peak. Every photon absorbed by the cell has a wide array of possible energy levels to have been emitted from (as a function of the blackbody distribution), which is a function of the temperature of the source as well. In contrast, the incoming beam has a

low distribution of angles of absorption (neglecting the diffuse light contribution), as described above concerning the solar étendue, and as depicted in Fig. **II-2c**.

During the PV conversion, the electrons generated by photons with energy exceeding the bandgap, $E_{ph}>E_g$, thermalize down to the bandgap generating heat loss, Q_{lost}, as depicted in Fig. **II-2c**. The photons are then emitted with the narrow vRS distribution, as a function of $\mu_{oc}<E_g$, and with a large solid angle. The FWHM of the vRS distribution for a given μ, as displayed in Fig. **II-2b**, and is showed to closely resemble a one-sided delta function, with a very narrow linewidth. This narrow linewidth is associated with a very small uncertainty for the energy-per-photon distribution, since we can reliably say that the majority of the photons are emitted at the energy of the bandgap, with a tail of $\approx kT_c$ (or 3 to 4 kT_c).

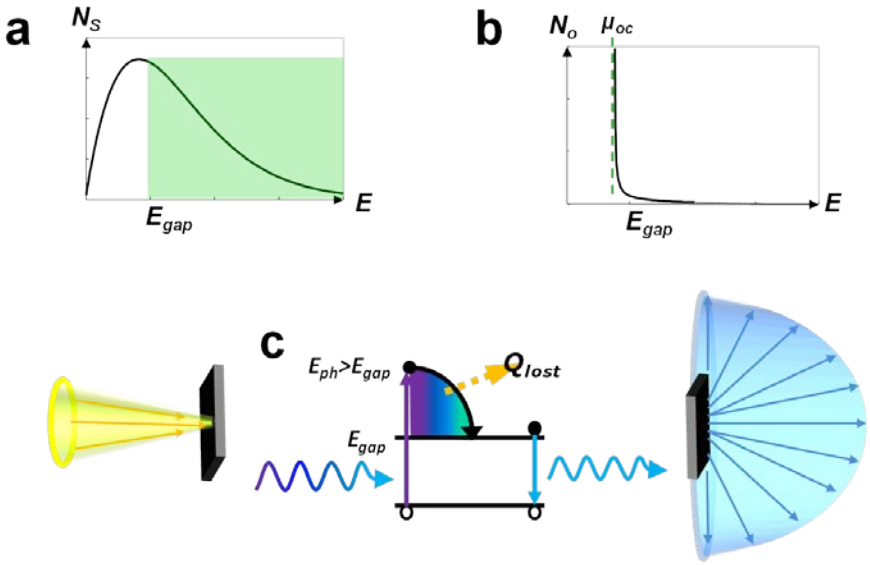

II-2 Graphical Representation of the Entropy Production in Photovoltaic Conversion. (a) The incoming solar spectrum follows the blackbody emission, which has a broadband distribution of energies. (b) The outgoing spectrum is similar to the emission from an LED, with a very narrow distribution of energies, following the vRS relation. (c) Pictorial representation of the process, showing the angular dispersion of the incoming and outgoing beams, as well as the production of heat loss, Q_{lost}, due to the thermalization of energy from electrons generated above the bandgap.

The heat loss described in the entropy of Eq. **II.17** was not taken into account in the original Ruppel-Würfel description of the DB model, yet we can associate the term $E_g/kT_S \approx Q_{lost}$, using the traditional description of the second law of thermodynamics. Furthermore, it should be stated once again that the entropy described here relates to the *relative* entropy of the process, and other additional entropy terms can be added to contain parameters that were not measured here. For example, we can include the polarization of the light as another parameter that can be analyzed as a source of (missing) information. The incoming solar flux is non-polarized, with an equal distribution of both polarizations; this can be attributed to the factor of "2" appearing in the blackbody distribution and here taken as a constant in the g term of Eq. **I.3**. If we design a solar cell that only makes use of one of the polarization modes, or emits only one of the polarizations,

then a certain degree of information will be gained/lost, and will appear as an entropic term such as Eq. **II.11**.

Finally, to complete this description of the entropy of a single junction cell, we will demonstrate that the effect of adding the ambient blackbody input contribution has a negligible effect on the entropy production, and therefore the V_{oc}. Taking the full input flux as Eq. **I.21**, and re-writing it as a function of the solar flux:

$$N_{Total} = gC\Omega_S \int_{E_g}^{\infty} \frac{E^2 dE}{\exp[E/kT_S]-1} \times \left[1 + \Omega_o \int_{E_g}^{\infty} \frac{E^2 dE}{\exp[E/kT_o]-1} \Big/ \Omega_S \int_{E_g}^{\infty} \frac{E^2 dE}{\exp[E/kT_S]-1} \right] \quad \textbf{II.18}$$

where we assume for generality that $T_c \neq T_o$, and use $C=1$ as the case where the contribution from $(1-Cf_{\Omega}) \approx 1$ is maximized, we can then use the approximation of the integrals to simplify to:

$$N_{Total} = gC\Omega_S \int_{E_g}^{\infty} \frac{E^2 dE}{\exp[E/kT_S]-1} \times [1+\beta_o] \quad \textbf{II.19}$$

Where the term β_o is:

$$\beta_o = \frac{\Omega_o}{\Omega_S} \frac{\alpha_o}{\alpha_{S1}} \times \exp[-E_g \times \eta_C / kT_o] \quad \textbf{II.20}$$

The Carnot efficiency term appears here, as well as another small correction term:

$$\alpha_o = 1 + 2kT_o/E_g + 2(kT_o/E_g)^2 \cong \alpha_{c1} \cong 1 \quad \textbf{II.21}$$

is similar to the α terms appearing above, and will be approximately equal to α_{c1} if $T_c = T_o$.

The overall effect on V_{oc} will be:

$$V_{oc}^{reg}\,\textbf{(with ambient)} = V_{oc}^{reg} + kT_c \times \ln[1+\beta_o] \cong V_{oc}^{reg} \quad \textbf{II.22}$$

with V_{oc}^{reg} being that of Eq. **II.6**. The contribution of this added term is on the order of *micro*-volts, and is therefore negligible. The ambient blackbody contribution is therefore shown to produce little important effect on both the short-circuit current, as well as the open-circuit voltage.

3. The Single Junction Transfer Function

The flux equilibrium method described in section 1 of this chapter provided the most abridged version of the DB limit, being a simplification of the original SQ limit to include only the thermodynamic variables, and removing the diode model. In this section, an even more simplified version of the DB limit will be devised that places all of the thermodynamic equations within a "black box" – meaning, a box whose internal processes are unknown, and which can be measured strictly as a ratio of the input and output. In engineering terms, this form of black box is known as a *Transfer Function* (TF).

If we were to attempt to simplify the entire workings of the solar cell as a TF, it would probably measure the outgoing photon flux, N_o, as a function of V, assuming a fixed solar photon flux, N_S. The internal workings of the solar cell would be hidden inside the TF, but we would not need to know what occurs inside. A graphical representation of this TF, which will be called H_{int}, appears in Fig. **II-3a**. The advantage of this TF is that it provides the internal workings of the cell, as well as a description of the DB process: we expect the ideal solar cell to act almost as an ideal LED, such that at open circuit ($V=V_{oc}$) the outgoing flux is equal to the incoming one. Furthermore, it provides us with an understanding of the boundaries of the solar cell's thermodynamic system (dashed line in Fig. **II-3**), which is where me must be measuring the input and output flux. It should be recalled that the ideal solar cell, according to the SQ model, has no thickness dimension, and therefore is wholly defined by its surface **[27]**. However, it is not very helpful in directly calculating the parameters that we have defined as useful: I_{sc} and V_{oc}, which can only be indirectly calculated from these fluxes; the current is found by subtracting the two fluxes and multiplying by q. Nevertheless, we will return to this form of TF in Chapter **V**, where the internal workings of the solar cell are to be modified.

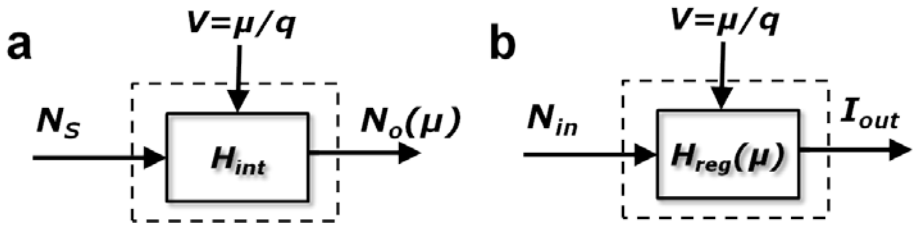

II-3 Transfer Functions for a Single Junction Solar Cell. (a) This TF displays the internal and external fluxes of the cell, without knowledge of what occurs within the TF itself. (b) This TF, which will be used later in the text, assumes that all that is needed to understand the thermodynamic equations of the cell are defined by the input flux, and the measured current, with the TF defined in the text in Eq. II.23.

An alternative form of the TF attempts to unify the internal action of the cell as a function of its input and output fluxes alone. This is the form of TF that will be utilized in the majority of the rest of this work. We do not need to know how the solar cell works, other than to make the following assumptions:

a) The current is maximal at $V=0$.
b) The current is zero at $V=V_{oc}$.
c) The only emission channel available for the semiconductor (two band system) follows the vRS relation.

These assumptions lead to the following definition of a TF, displayed in Fig. **II-3b**:

$$H_{reg}(\mu)/q = 1 - \frac{g\Omega_o \int_{E_g}^{\infty} \frac{E^2 dE}{\exp[(E-\mu)/kT_c]-1}}{N_{in}} \qquad \textbf{II.23}$$

where N_{in} is the incoming flux, and can be taken as N_S, N_{total} or any other input flux. Note that the factor q divides the transfer function, to retain the units of flux. This input flux can be completely

changed, for example to model the flux from a white dwarf sun, or the AM0 spectrum, but the TF will remain the same. The TF should supply the information for the output as a function of the input:

$$\boldsymbol{I_{out} = N_{in} \times H_{reg}(qV)} \qquad \textbf{II.24}$$

This definition, while seemingly circuitous, provides the needed parameters, I_{sc} and V_{oc}, using the following simple procedure: At short-circuit, to find the output current, we need to solve the equation for $H_{reg}(0)$; for open-circuit, we need to solve the equation $H_{reg}(\mu)=0$. These two simple procedures provide the necessary parameters. In particular, the equation $H_{reg}(\mu)=0$ is the definition of the flux equilibrium.

The advantage of the TF method is that it simplifies the conceptual thermodynamic argument for what makes an ideal solar cell, and what the important parameters are. All that we are required to know is what the input flux is *at the surface of the cell*, and we should be able to obtain the important current and voltage characteristics from this information. This is assuming that the emission follows the vRS relation, as was stated above, and that no other complex physical processes occur inside the "black box", other than internal losses. The other advantage of the TF is that we can replace the entire cell by a circuit, which can be connected to other circuits in a straightforward manner. Finally, non-idealities in the cell can be added by placing the non-radiative loss term, κ_{nr}, within the numerator of fraction in H_{reg}.

The TF method, with its emphasis on a simplified, graphic form, allows us to concentrate on the two most important elements controlling the efficiency of a PV system, the current and the voltage, which must be optimized almost independently while also being intrinsically linked. Maximizing the short-circuit current will only solve ~50% of the problem, since the open-circuit voltage is shown to be as important, if not more so. The TF method also allows a methodological viewpoint to view any PV system: we need to ascertain the incoming and outgoing fluxes, as a function of their surface (thermodynamic boundary) as well as their relevant parameters.

The TF is usually a useful element in *linear system* analysis. The definition of a linear system is that it follows the following relation:

$$\boldsymbol{L(a \times x + b \times y) = a \times L(x) + b \times L(y)} \qquad \textbf{II.25}$$

where L is a generic linear operator, such as a TF. The definition states that a linear system must obey the laws of superposition (adding two different inputs, x and y), as well as scaling (a multiplication by a constant). For H_{reg} to be linear, it must follow this definition, yet it does not strictly do so. If we consider the output of the TF as being only the *number* of photons/electrons, then this definition holds. For example, if we double the number of incoming photons, then at open-circuit the outgoing photon flux must also be doubled. Or if we add a flashlight to the incoming flux, the outgoing flux should equal it. However, since H_{reg} contains the input inside the denominator it is almost by definition non-linear. This can be seen at short-circuit conditions: For any degree of concentration, C (which is similar to a multiplication scaling), the I_{sc} increases only the flux input, but does *not* affect the outgoing emission, which follows the vRS relation (with μ_{sc}=0). Although we generally neglected the outgoing emission term at short-circuit, as in Eq. **II.1**, it fails the scaling law for linear systems. If the approximation is made, then the scaling law holds. At open-circuit, H_{reg} is zero, regardless of the scaling law (by definition of the μ_{oc} cut-off), however, if we insert a voltage slightly less than V_{oc}, at $V=V_{oc}-\delta$, then the TF is nearly zero.

If we then increase the concentration, V_{oc} must increase as well (by a factor of $kT_c ln[C]$), so the output current will be reduced, but not as much as when the voltage V_{oc}- δ. The results of this argument once again show that H_{reg} does not strictly follow linear system theory. We can therefore call this TF a *pseudo*-linear system.

The conclusion of this section is that the TF method, while not strictly linear, allows a simplification of the thermodynamic parameters of the system to within a simplified "black box". The major advantages of this method are that it allows the identification of the vRS relation as an unchangeable and internal specification of the PV system, as well the identification of the importance of the total input spectrum as being measured upon the (front) surface of the cell. Modifications to the spectrum must be viewed in the same way as the scaling or superposition of inputs, with the shifting of the V_{oc} cutoff as a function of the inputs. This modification will be shown in the following chapter, where down-conversion is viewed as a modification of the input spectrum.

III. Down-Conversion: A Detailed Analysis

**Publication note*[2]

One of the methods of improving the efficiency of a single material solace cell is to make use of the excess energy imparted by photons with energies higher than the bandgap. Since we need at least $1E_g$ of energy per photon to create an e-h pair, we can imagine that any photon with $h\nu > 2E_g$ of energy will be able to produce more than a single e-h pair if it were split into two photons. This resulting two photons would conserve energy, as required by the 1st law of thermodynamics, such that $h\nu_{original} = h\nu_1 + h\nu_2$. The photons with energy above $2E_g$ would then be used in a more efficient manner, and not produce the thermalization energy and heat loss typically associated with these higher energy photons. We can imagine an imaginary material that would split these photons before they reach the solar cell, such that the spectrum that the cell eventually sees (as per the argument of the preceding chapter), is better matched to the bandgap of the single junction cell. Such a configuration appears in Fig. **III-1**, with the higher energy (blue) photons split into two lower energy (red) photons each, and then proceeding on to the cell.

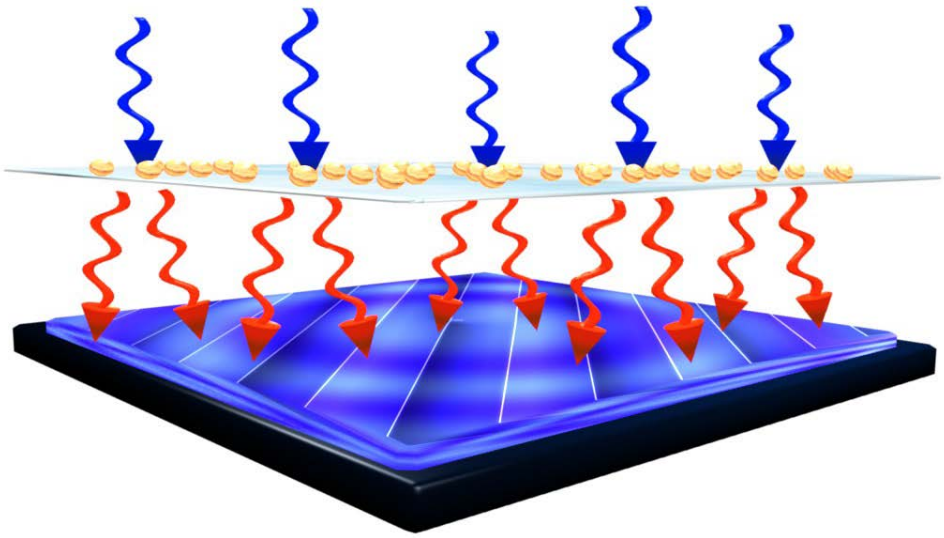

III-1 Down-Conversion scheme. Higher energy photons (blue) are absorbed by a down-converting layer that splits the photons into two lower energy photons each (red). This depicts the ideal down converting scheme.

The Down-Conversion (dc) process is designed to make use of a material whose properties are only to split, or *quantum cut*, the photons with energies $h\nu > 2E_g$ into two photons of energy E_g each, as depicted in Fig. **III-2a** for imaginary particles (gold dots) placed on a transparent film. This scheme was first analyzed in 2002 **[55,54]**, with some basic of assumptions used, and resulting in a ≈9% efficiency increase over the SQ limit. This result does not violate any physical laws since it modifies the assumption that the solar radiation is constant, and is here modified by

[2] The following chapter follows the paper published in Ref. **[53]**. Nearly all of the figures were redone to correct minor errors in the original code, as well as plotting the figures for $\Omega_o = 2\pi$ instead of 4π.

the dc layer, as is demonstrated in Fig. **III-2b**. The dc photons are essentially folded onto the bandgap, such that they appear as a spike in the *number* of photons impinging upon the solar cell, and better matched to the bandgap of the cell. This modification of the spectrum is an essential aspect of the dc process. As was described in the previous chapter, as far as the solar cell is concerned, it is only interested in the makeup of the spectrum impinging upon it, as given by the TF, H_{int}. Since the dc process concerns a layer that is placed above the cell, the spectrum that the cell sees is *different* from the one it would have seen without this layer, which has an effect upon both I_{sc} as well as V_{oc} as will be shown in this chapter.

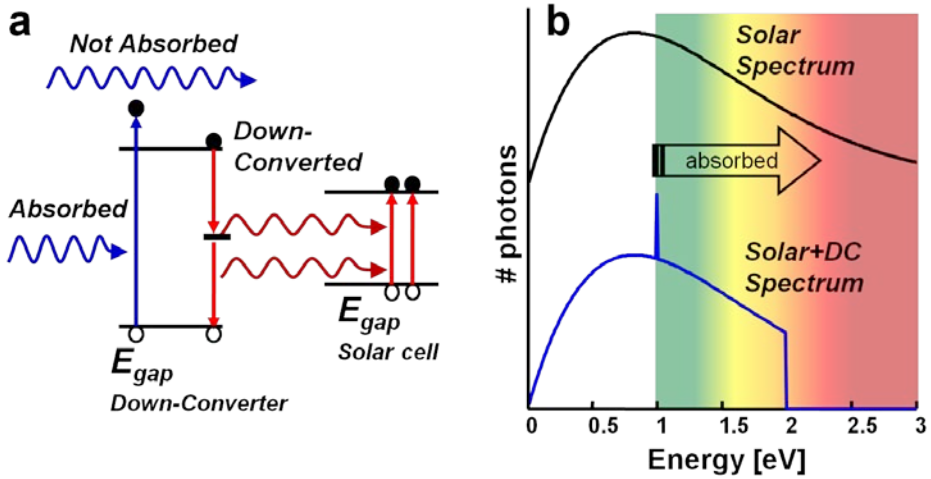

III-2 Down-Conversion process band diagram and spectrum shift. (a) The dc layer is modeled as a semiconductor with a bandgap of $E_{g,dc}=2E_g$ of the underlying cell. A "trap state" on the output end of the dc layer allows the transition of electrons first to the mid-level state, emitting the first photon with energy of E_g, and then a second radiative transition to the valence band, emitting the second photon. Depicted are the photons that can be absorbed by the dc layer, as well as those that may perhaps not be absorbed by it. (b) A graphical representation of the shift in the spectrum emitted from the dc layer, in comparison with the original blackbody spectrum emitted from the sun. The higher energy photons are folded over into a single spike at the bandgap (here taken as E_g=1 eV).

1. Ideal DC Characteristics and Analysis

The original analysis of the dc process assumed that the dc layer was ideal, with no internal losses, and absorbed all photons with energy above $2E_g$. In order to prevent double counting of the incoming photons, the model also assumed that the solar cell was a unique material that would only absorb from E_g to $2E_g$, and would therefore be perfectly matched to the dc material. This type of semiconductor does not exist, and was used merely as a way for the authors to simplify their modeling. This model **[54]**, as well as later improvements to the model that included the effect of the index of refraction on the impedance matching between the dc and solar cell layer **[55,56]**, also understood that there was a severe limitation of placing the dc layer

above the cell: that the photons could be backscattered away from the cell. Therefore, the conclusion of these previous authors was that the ideal placement if the dc layer was *behind* the cell, and then backed up by a rear reflector to reflect all photons back at the cell. This result counters the effect of the dc layer, since upon passing through the cell, the majority of higher energy photons are absorbed before reaching the underlying dc layer. This is a result of the Beer-Lambert law for absorption in a material with an absorption coefficient α_{abs}:

$$N_S(x) = N_S \times \exp(-a_{abs}\, x) \qquad \textbf{III.1}$$

where x is the direction of propagation of light into the cell, in a simplified one-dimensional model. This absorption is even more critical for the higher energy photons, which are typically absorbed at the top surface of the material, since the absorption coefficient is energy (frequency) dependent, and is typically quite high for the higher energy photons [$\alpha_{abs}=\alpha_{abs}(E)$].

The problem of re-emission of the photons from the dc layer can be encapsulated into a *geometric factor*: B_{dc}, which accounts for the percentage of photons emitted towards the cell. This is shown in Fig. **III-3a**, demonstrating the range of values for B_{dc}. Note that we define B_{dc} as being a function of *both* photons, so that B_{dc}=1 implies that both photons are emitted down towards the cell, B_{dc}=½ implies that only one photon is directed at the cell with the other being backscattered away, and B_{dc}=0 implying that both photons are backscattered. It is obvious that this latter case is not interesting, since this would result in the *loss* of photons impinging upon the cell.

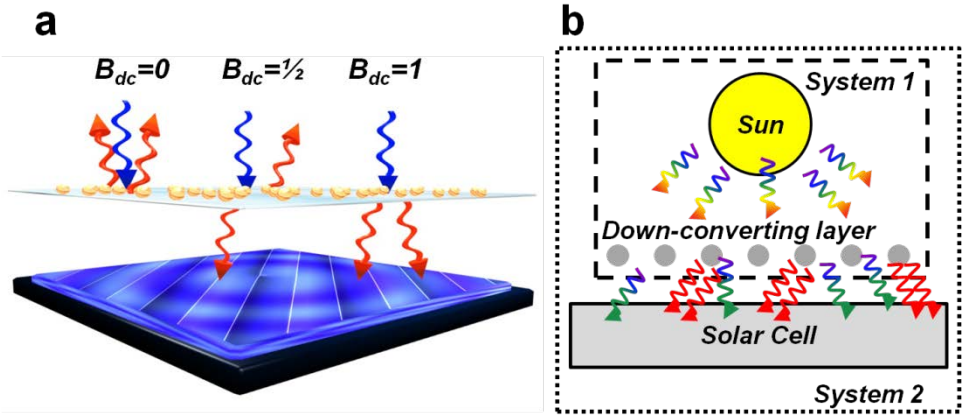

III-3 Geometric Factor and System Diagram for a Down-Conversion cell design. (a) The scattering dc layer can either forward- or backward-scatter the down-converted photons, with a fraction B_{dc} defined in the figure. (b) The system diagram of a dc cell can be split into the sun-dc layer, and then use the output of System 1 as the input of System 2, which includes the solar cell.

Using the formalism of system diagrams, as we did with the TFs, we can split the problem of solving the equations of a dc system by first recognizing that the sun and the dc layer are in flux equilibrium with each other, and that the combined output of this layer is the input to the cell itself. This is shown in Fig. **III-3b**, where the sun and the dc layer are in System 1, and the solar

cell in System 2 uses the output of System 1 as its input. For System 1, we can write the flux equilibrium for the dc layer as:

$$f_{abs}\Omega_S \int_{2E_g}^{\infty} \frac{E^2 dE}{\exp[E/kT_S]-1} = \frac{1}{2} f_{dc}\Omega_{dc} \int_{E_g}^{\infty} \frac{E^2 dE}{\exp[(E-\mu_{dc})/kT_{dc}]-1} \qquad \textbf{III.2}$$

Here, we have neglected the index of the dc layer **[55,56]**, and modeled the dc layer as emitting at twice the rate of the incoming flux, to accommodate the splitting of the photons, as well as assuming that the dc layer has an internal temperature, T_{dc} and chemical potential, μ_{dc}. Furthermore, in this analysis, we will account for the fact that some of the photons may go through the dc layer without being absorbed, as depicted in Fig. **III-2a**, with a fraction f_{NA}, with the complementary number of absorbed photons, $f_{abs}=(1-f_{NA})$. In addition, of those photons absorbed, not all of them may be down-converted, with some of the electrons recombining directly to the valence band and emitting a photons with energy $2E_g$; therefore, we include another fraction, f_{dc} to account for this. The étendue of the dc layer, Ω_{dc}, does not include the geometric factor at this point, and is assumed to be isotropic, with $\Omega_{dc}=2\pi$.

Crossing to the solar cell system (System 2), we use the flux equilibrium again on the front surface of the solar cell. Once again, we are reminded that the solar cell is not interested in anything other than the input flux, as described by the TF, and ignoring near-field effects that may alter the directionality of flow of the fluxes. At equilibrium:

$$\begin{aligned}&\Omega_S \int_{E_g}^{2E_g} \frac{E^2 dE}{\exp[E/kT_S]-1} + f_{NA}\Omega_S \int_{2E_g}^{\infty} \frac{E^2 dE}{\exp[E/kT_S]-1} \\ &+ B_{dc} \times f_{dc}\Omega_{dc} \int_{E_g}^{\infty} \frac{E^2 dE}{\exp[(E-\mu_{dc})/kT_{dc})]-1} = \Omega_o \int_{E_g}^{\infty} \frac{E^2 dE}{\exp[(E-\mu_{oc})/kT_c]-1}\end{aligned} \qquad \textbf{III.3}$$

This equation is made up of several parts: the leftmost segment consists of photons that are entirely unaffected by the dc layer and are transparent to it, and the second term contains the photons not absorbed by the dc layer. These first two terms therefore constitute a fraction of photons from the original spectrum that remain unchanged. The next term includes the fraction of dc photons, where we have included the geometric factor, B_{dc}. Finally, the emission from the solar cell remains the same, on the right hand side, following the vRS relation. We have neglected the ambient blackbody contribution. Since Eq. **III.3** is quite large, we will condense it. First, we can replace the dc term with that of Eq. **III.2**, since the dc system is in flux equilibrium at all times. Next, we can make use of the following relation for integrals:

$$\int_a^b dx = \int_a^{\infty} dx - \int_b^{\infty} dx \qquad \textbf{III.4}$$

Finally, we will simplify the temperature relations, and assume that the dc layer is in thermal equilibrium with the cell, such that $T_{dc}=T_c$, as well as ignore the possible directional emission from the dc layer **[55,56]**, such that $\Omega_{dc}=\Omega_o$. This results in:

$$\Omega_S \int_{E_g}^{\infty} \frac{E^2 dE}{\exp[E/kT_S]-1} + f_{dc}(2B_{dc}-1)\Omega_S \int_{2E_g}^{\infty} \frac{E^2 dE}{\exp[E/kT_S]-1} = \Omega_o \int_{E_g}^{\infty} \frac{E^2 dx}{\exp[(E-\mu_{oc})/kT_c]-1} \quad \textbf{III.5}$$

Here, we have assumed that all those photons absorbed in the dc layer were converted, such that $f_{dc}=f_{abs}=(1-f_{NA})$. The dc fraction is therefore a measure of those photons absorbed by the dc layer, and no non-idealities are assumed in this layer. The next section will include such losses. To simplify Eq. **III.5** even further, we will write the integrals as a function of the photon flux, *N*, and simplify the parameters into the parentheses:

$$N_S\{E_g \to \infty\} + f_{dc}(2B_{dc}-1)N\{2E_g \to \infty\} = N_o\{E_g, \mu_{oc}\} \quad \textbf{III.6}$$

Using this notation, we can also write this as:

$$N_S\{E_g \to \infty\} \times \left[1 + f_{dc}(2B_{dc}-1)N\{2E_g \to \infty\}/N\{E_g \to \infty\}\right] = N_o\{E_g, \mu_{oc}\} \quad \textbf{III.7}$$

Using the approximation of the integrals as was done in the previous chapters, we can obtain a closed-form equation for $qV_{oc}=\mu_{oc}$:

$$qV_{oc}^{dc} = E_g\left(1-\frac{T_c}{T_S}\right) + kT_c \ln\left[\left(\frac{\Omega_S}{\Omega_o}\right)\left(\frac{T_S}{T_o}\right)\left(\frac{\alpha_{S1}}{\alpha_{c1}}\right)\right] + kT_c \ln(1+\beta_1) \quad \textbf{III.8}$$

where:

$$\beta_1 = f_{dc}(2B_{dc}-1) \times 4\left(\frac{\alpha_{S2}}{\alpha_{S1}}\right)\exp(-E_g/kT_S) \quad \textbf{III.9}$$

and:

$$\alpha_2 = 1 + \frac{kT_S}{E_g} + \frac{(kT_S)^2}{2E_g^{\,2}} \quad \textbf{III.10}$$

with α_{S1} defined as before, in Eq. **II.7**. Once again, the index of refraction of the cell has not been included, nor have any other losses, which would appear as an additional $kT_c ln[\kappa_{nr}]$ term. We could have additionally written the term β_1 as:

$$\beta_1 = f_{dc}(2B_{dc}-1) \times \frac{N_S\{2E_g \to \infty\}}{N_S\{E_g \to \infty\}} \quad \textbf{III.11}$$

We can now examine these formulas. For the ideal case, where all the photons are dc, and they are all emitted directionally towards the solar cell, we have f_{dc}=1 and B_{dc}=1. In this case, the term β_1 in Eq. **III.8** and **III.11** is simply the ratio of photons above $2E_g$ to the photons above E_g, and counts the number of photons converted. If there is no dc layer, then f_{dc}=0, and β_1=0,

reverting Eq. **III.8** back to the open-circuit of a regular solar cell, as given in Eq. **II.6**. If all the photons are backscattered, then B_{dc}=0 and β_1 is *negative*, creating a voltage *loss* due to the $kT_c ln[1+\beta_1]$ term.

From the point of view of entropy, the voltage *gain* is due to an *increase* in information in the ideal dc process (for which f_{dc}=B_{dc}=1). The information gain can be seen in the comparison between the two spectral distributions in Fig. **III-2**, with the peak in the spectra at E_g corresponding to more information regarding the energy-per-photon, or the FWHM. Pictorially, we can describe this voltage gain to be:

$$qV_{oc}^{\ dc} = qV_{oc}^{\ reg} + kT_c \ln$$

The voltage gain is quite small, and is highly dependent upon the fraction of dc photons, f_{dc}. Fig. **III-4a** displays the V_{oc} for the dc system, in comparison with the regular V_{oc} for a standard solar cell. The gain in voltage, up to a few tens of mV, is only visible if the dc fraction is unity, and the photons are emitted directionally. For higher bandgaps, this gain becomes negligible as the ratio of photons down-converted drops significantly.

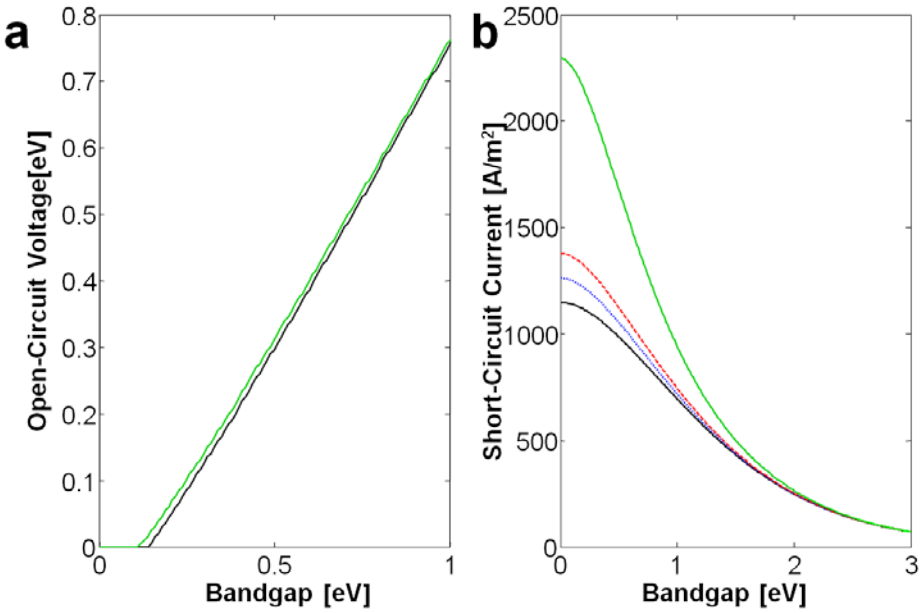

III-4 Open-Circuit Voltage and Short-Circuit Current for a Down-Converting system. (a) V_{oc} for the dc system, assuming that all the photons are directionally emitted towards the cell (B_{dc}=1 and f_{dc}=1, in green), and compared with the V_{oc} of a regular solar cell (black). (b) I_{sc} for varying fractions of dc efficiency, f_{dc}, including 0, 0.1, 0.2 and 1 (black, blue, red and green, respectively). The black line (f_{dc}=0) signifies the current of a regular cell.

The short-circuit current uses the same formalism as the above equations, and can be written as:

$$I_{sc} = qgN_S\{E_g \to \infty\} \times \left[1 + f_{dc}(2B_{dc} - 1)\frac{N_S\{2E_g \to \infty\}}{N_S\{E_g \to \infty\}}\right] - qgN_o\{E_g, \mu = 0\} \quad \textbf{III.12}$$

The I_{sc} does *not* simply "double" due to the dc layer, but increases as a function of the fraction of photons above $2E_g$ over the fraction of photons from E_g. In theory, the current would be doubled for a material with a bandgap $E_g \to 0$, as shown in Fig. **III-4b**, but that material would also produce zero power, since the voltage would also be zero. The increase in current is the major improvement of a dc system, which is a function of the fraction converted, f_{dc}, as well.

The overall efficiency increase can be calculated by finding the maximum $P=I\times V$, and is calculated from the following equation:

$$\eta_{dc} = g_2 V_m \times \left(N_S\{E_g \to \infty\} \times [1 + \beta_1] - qgN_o\{E_g, \mu = qV_m\}\right) \quad \textbf{III.13}$$

Using the formalism above, or calculated using the input N_{total} instead of N_S. The efficiency is a function of both the geometric factor, B_{dc}, as well as the dc fraction, f_{dc}, making this equation a multi-variable equation. Since we are not interested in the backscattering case, B_{dc}=0, Fig. **III-5** displays the overall efficiency for the ideal dc system, using these parameters. The absolute ideal case holds $f_{dc}=B_{dc}=1$, which is approximately the case originally analyzed in 2002 **[54]**, and did not account for fractional dc efficiencies, or geometrical constraints.

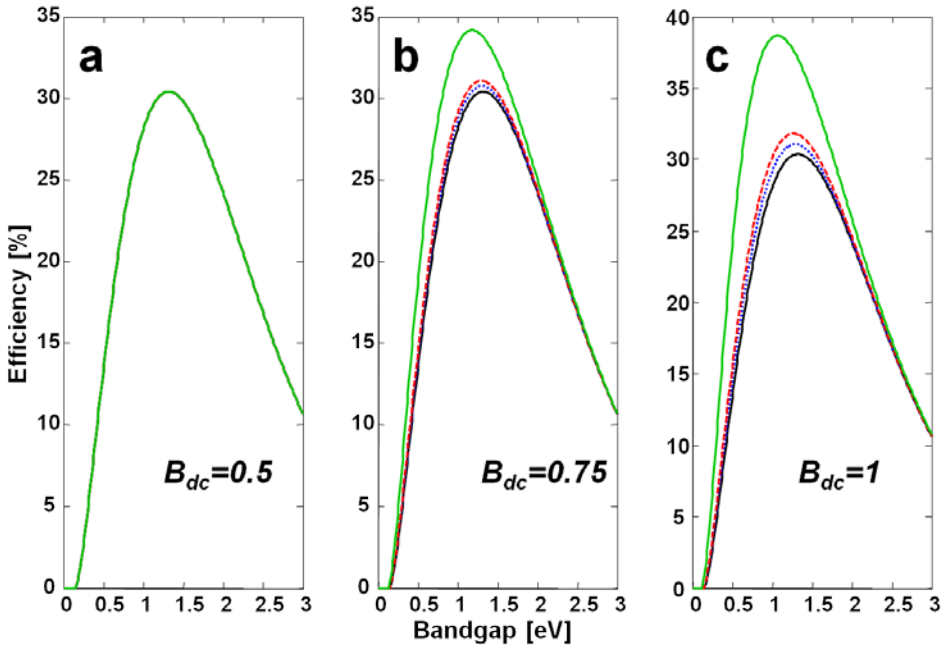

III-5 Efficiency of the Down-Converting System, with No Losses. The efficiency is plotted for increasing degree of directive photon emission (B_{dc}, from panel a to c), as well as increasing down-conversion fraction, f_{dc}: 0, 0.1, 0.2 and 1 (black, blue, red and green, respectively). Maximal efficiency increase is 8.3%, from the black to green curves in panel (c).

The maximal efficiency of the dc system, assuming that all photons are both directionally emitted towards the cell, and all the photons above $2E_g$ are absorbed and down-converted (i.e. $f_{dc}=B_{dc}=1$), is 38.7%, rising from 30.4% for a regular cell, being an 8.3% overall rise in efficiency. Realistic systems would have lower overall efficiency, since not all the photons would necessarily be down-converted, or received at the cell's surface, as displayed in the various curves in Fig. **III-5**. Furthermore, the difference between the results presented here, and those calculated in Ref. **[53]**, is that here the calculation assumed no losses of reflection ($n_{sc}=1$), whereas there, we assumed an index of $n_{sc}=4$. This index would reduce the efficiency due to reflective losses, unless light-trapping techniques are used **[50]**. Also, here $\Omega_o=2\pi$ and not 4π.

If we focus on the maximal efficiency only, then we can plot the maximum efficiency as a function of the down-conversion fraction, f_{dc}, as well as the optimal bandgap for this efficiency, as shown in Fig. **III-6**. The optimal bandgap is reduced from the regular DB calculation of 1.3 eV down to nearly 1 eV, if the dc process is completely efficient. This range still remains within the region of material properties typically used for PV materials, including Si, GaAs and CIGS, so the addition of the dc layer would not alter the material choice for a solar cell. Furthermore, the 8.3% efficiency gain is seen to be strongly related to both f_{dc} and B_{dc}, which are assumed to be ideal. If the photons are emitted isotropically, $B_{dc}=0.5$, then no gain will be seen, since the dc process does not produce any additional e-h pairs.

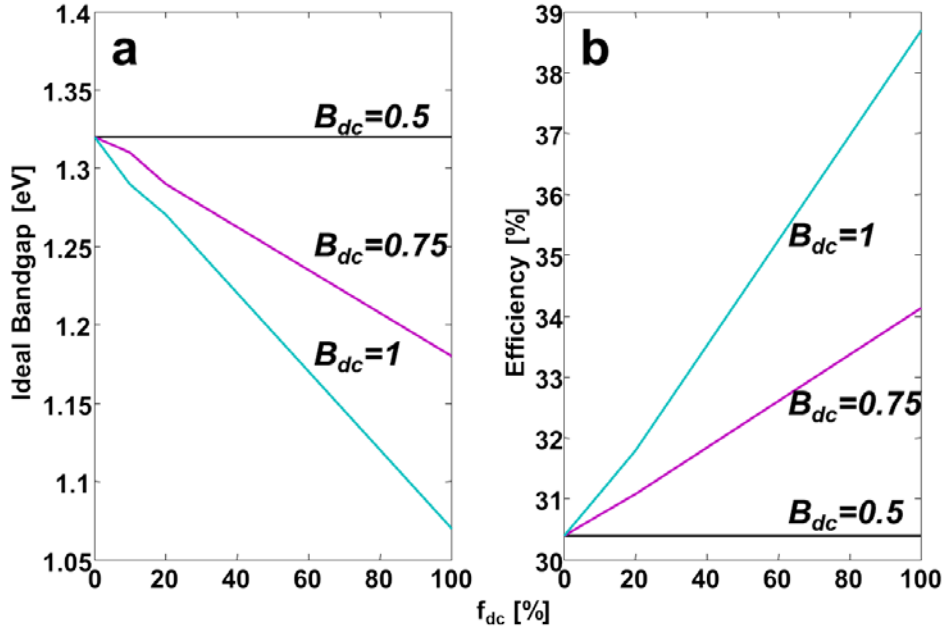

III-6 Optimal Bandgap and Efficiency for the Down-Converting System, as a Function of Fraction Down-Converted. (a) Optimal bandgap per f_{dc} fraction, as calculated by the bandgap for which the optimal efficiency appears. (b) Optimal efficiency per f_{dc} fraction. Both graphs were calculated for directional photons, with varying degrees of directional emission.

The preceding set of calculations and graphs considered only the lossless case, where all the photons absorbed were down-converted. The ratio f_{dc} therefore could be considered a measure of

how dilute the dc particles are on the film depicted in Fig. **III-1**, such that if it covers the entire surface, and is thick enough, the layer would absorb all the higher energy photons and down-convert them. The next section will include more realistic material systems.

2. Down-Conversion Including Losses

Adding losses to the dc layer is a simple process, comparable to the regular solar cell analysis, introducing an efficiency of dc:

$$\kappa_{dc} = \frac{f_{dc}}{f_{abs}} = \frac{f_{dc}}{f_{dc} + f_L} \qquad \textbf{III.14}$$

where we have included another factor, f_L, which is a loss factor, and counts the fraction absorbed by the dc layer and *not* emitting any photons, due to a non-radiative (thermalized) physical process. We must place this factor within the first use of the flux equilibrium between Systems 1 and 2, being the sun and dc layer:

$$f_{abs}\Omega_S \int_{2E_g}^{\infty} \frac{E^2 dE}{\exp[E/kT_S]-1} = \frac{1}{2\kappa_{dc}}\Omega_{dc} \int_{E_g}^{\infty} \frac{E^2 dE}{\exp[(E-\mu_{dc})/kT_{dc}]-1} \qquad \textbf{III.15}$$

If f_L=0, we revert back to Eq. **III.2** above. Using this equation, we can re-write the V_{oc} and I_{sc} in their abbreviated form:

$$qV_{oc} = qV_{oc}^{reg} + kT_c \ln(1+\beta_2) \qquad \textbf{III.16}$$

and:

$$I_{sc} = qgN_S\{E_g \to \infty\} \times [1+\beta_2] - qgN_o\{E_g, \mu = 0\} \qquad \textbf{III.17}$$

where:

$$\beta_2 = (f_{dc} + f_L) \times (2\kappa_{dc} B_{dc} - 1) \times 4\left(\frac{\alpha_{S2}}{\alpha_{S1}}\right) \exp[-E_g / kT_S] \qquad \textbf{III.18}$$

The difference between β_1 and β_2 terms is the introduction of the loss term, as well as the use of $f_{abs}=1-f_{NA}=f_{dc}+f_L$. (Note: there is an error in Ref. **[53]** in this formula).

The introduction of losses via the κ term **[22,23]** simplifies the equations, however, it adds another variable to the calculations such that the efficiency is now a function of f_{dc}, f_L and B_{dc}, with κ_{dc} uniquely defined by the choice of f_{dc} and f_L. Calculating the peak efficiency as a function of these two factors, as well as separately for different geometrical factors, is shown in Fig. **III-7** for value of B_{dc}=0.75 and B_{dc}=1, with the isotropic (B_{dc}=0.5, as well as the backscattering, B_{dc}=0) cases being of less interest.

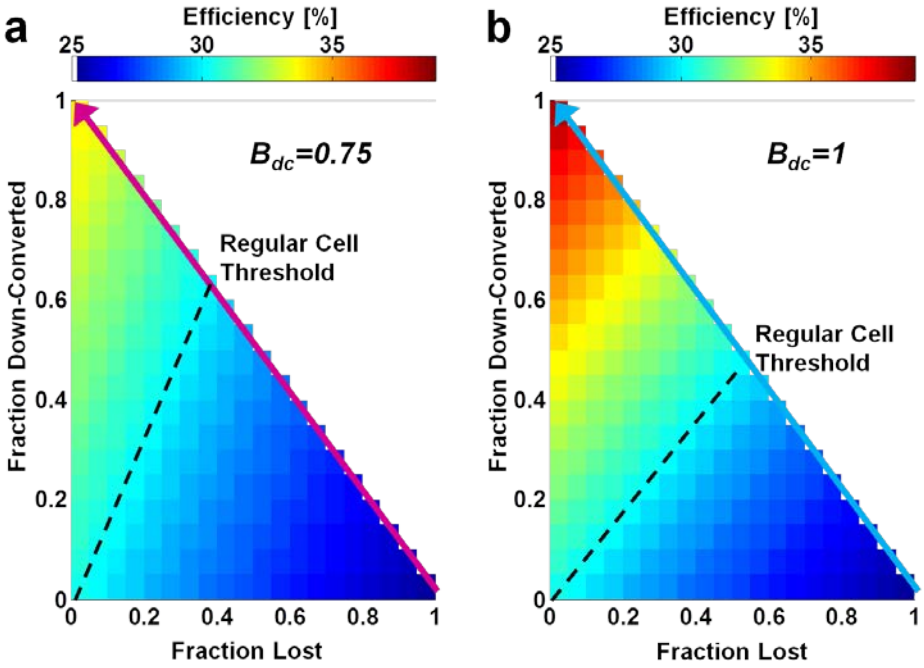

III-7 Peak Efficiency for the Down-Conversion Process, Including Losses. The calculation is done for all values of loss fraction, f_L, and down-conversion fraction, f_{dc}, for two value of geometrical factors, (a) B_{dc}=0.75 and (b) B_{dc}=1. The threshold for the efficiency of a regular solar cell, at 30.4%, is plotted in dashed black lines. Arrows relate to the quantum efficiency, *QE*, shown in the next figure.

The efficiency of the cell is intrinsically linked to the efficiency of the dc layer to emit in a radiative manner, such that $\kappa_{dc} \rightarrow 1$. For this to occur, we need not only for the photons to be absorbed in the dc material (f_{abs}=1 or alternatively, f_{NA}=0), but also that the layer itself have no losses (f_L=0). Assuming such a material is found, we can externally measure the efficiency of the dc process in this material using a spectrometer. However, this measurement will ignore the fraction of photons not absorbed, f_{NA}, so that what would be measured is the *quantum efficiency* (QE) of the material. We can relate the QE of the material with the losses as:

$$QE = \{\kappa_{dc} \mid f_{dc} + f_L = f_{abs} = 1\} \qquad \textbf{III.19}$$

meaning that no photons are not absorbed. This can be measured in Fig. **III-7** as the hypotenuse of the triangles of efficiency, as depicted by the arrows in **III-7a** and **b**. Plotting these arrows as a function of the QE, we can measure the expected peak efficiency of a given material, as presented in Fig. **III-8**.

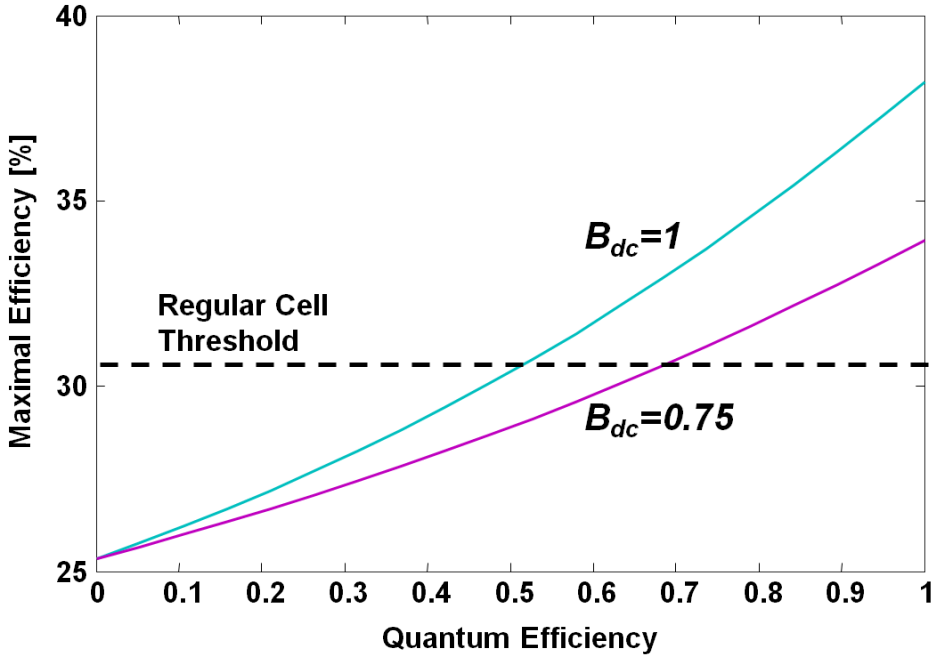

III-8 Efficiency as a Function of the Quantum Efficiency of the Down-Converting Material. The QE neglects the not-absorbed light (f_{NA}=0), and is plotted for two different values of the geometrical factor, B_{dc}. Also plotted is the threshold of a regular single junction cell, without a dc layer. Below this threshold, there will be a net *loss* of efficiency.

The dc layer is required to be highly efficient at the dc process itself, as well as almost entirely lossless in order for the dc process to produce any benefit. As demonstrated by the dashed line in Fig. **III-8**, the QE of the dc layer must be quite high in order for the overall system to achieve any efficiency gain, as well as not to *lose* efficiency, when compared with the same cell that doesn't have a dc layer. Anything below the dashed line in Fig. **III-8**, or to the right of the dashed lines in Fig. **III-7** will display a net loss, and therefore would be better off without the dc layer. This high degree of QE required for the DC layer is in addition to the requirement that the photons be emitted directionally towards the cell ($B_{dc}\rightarrow 1$).

The major two difficulties in employing a dc layer to improve the efficiency of a solar cell lie in the material science question of finding a highly efficiency dc system, as well as the geometric problem having the down-converted photons preferentially emit towards the cell. The only existing dc materials currently have very low internal dc conversion efficiency values, and have focused on using Lanthanide materials **[57,58]**. Until a dc material is found with very high internal efficiency, the possible use of dc as an improvement method for solar cells will remain in theory alone.

A possible avenue for research of a dc material would be in using newer physical concepts to modify the properties of the band structure of materials. The major problem with finding a dc material is that if it were to follow the band structure of Fig. **III-2**, it would require that the "trap" state allow the radiative transition of electrons and photons in two distinct, radiative steps. If the process is wholly non-radiative, then the material is just an absorber, and is not a useful dc layer. If only one of the transitions is radiative, then effectively the material acts as a fluorescent

material, with the single outgoing photons exhibiting a Stokes shift, which is a characteristic feature of fluorescence. This form of transition is known as down-*shifting*, and is quite separate from dc, since only one photon is re-emitted. There is an advantage to be had from this down-shifting, and that is that the absorption inside the solar cell can be better tuned for these lower energy photons **[59-63]**. This can be seen from the relation between the absorption coefficient and the depth absorption of Eq. **III.1**, with the higher energy photons typically absorbed at the surface, and therefore not usually reaching the extraction depth required for most solar cell designs (as a function of the depletion width of a diode, or of the surface recombination rate). Nevertheless, down-shifting cannot achieve the same type of efficiency *gain* that dc can theoretically create, and is limited to improving the efficiency of cells to approach the SQ limit from *below*. One way to possibly obtain a doubly-radiative transition from a "trap" state is to create so many traps that their quantum states begin to coalesce into a single radiative state **[64]**. This has been theorized to be the case for the creation of Intermediate Band, or Impurity Band (IB) devices **[64,65]** – which will be described in Chapter **V**. This condition uses the reverse intuition of regular trap-state physics: typically these trap states induce non-radiative transitions, however, the theory predicts that when the number of these individually isolated trap states exceed a certain threshold (of concentration), then they will form a single radiative band.

Using the reverse concept of inducing *more* trap states in a semiconductor in order to create this form of doubly-radiative band, we can imagine that a material with a large number of surface trap states can achieve such a state. When a semiconducting particle's dimensions are reduced to the nanometer (nm) level, the surface area of the material – which is typically where these surface trap states occur – may exceed the threshold of traps needed to create such a band. One can therefore hypothesize that creating nanoparticles covered in mid-level trap states will be the preferred material choice for a dc layer, as was depicted in the gold spheroids in Fig. **III-1**. The concentration of these nanoparticles is also important, since it will directly relate to the amount of light absorbed, f_{abs}, and will also need to be controlled.

The use of nanoparticles for the dc layer can also help solve the geometric issue of preferred emission towards the solar cell. Instead of thinking only in terms of planar structures, as was shown schematically in the previous figures, we can envision a three-dimensional solar cell that would make use of these nanoparticles. Three examples of such a design are depicted in Fig. **III-9**. The first design would simply have the dc nanoparticles embedded within the matrix of the cell. They could also be embedded within a transparent film above the cell, such that the total-internal-reflection will force the dc photons towards the underlying solar cell. A second type of design would make use of 3D solar cell designs such as micro- or nano-pillar arrays. In these designs, the light is absorbed in the direction normal to the sun's rays, but then extracted in the orthogonal, horizontal, axis **[66,67]**. For the micro-pillar designs, nanoparticles are already used to help scatter the light between the pillars, and achieve an isotropic emission rate within the pillar array. Instead of using non-functional scatterers, the dc nanoparticles could act as both functional roles, both scattering the light, as well as more efficiently converting it.

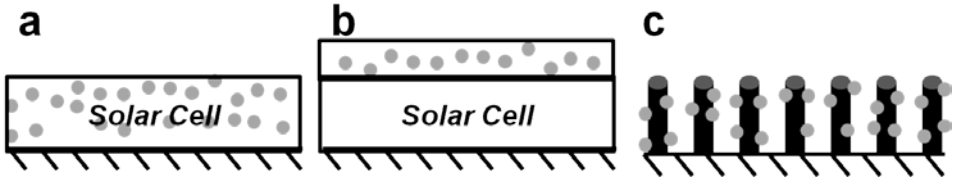

III-9 Three-Dimensional Designs of Solar Cells Incorporating Down-Converting Nanoparticles. (a) Nanoparticles embedded within the cell itself, or (b) in a transparent layer above the cell. (c) Nanoparticles embedded within a pillar array of cells, acting as both light scattering objects, and a dc layer.

Both designs depicted above make use of the isotropic scattering from the nanoparticles to solve the issue of B_{dc} depicted in Fig. **III-3**. This form of solution will allow the dc layer to be placed above, or within the cell, and not below the cell, as was needed in the original dc calculations **[54-56]**. The model used here is both simpler, and more rigorous than the original calculation, since the original model included a solar cell that only absorbed light from $E_g \rightarrow 2E_g$, which is *not* what a regular solar cell does. The model described here therefore better mimics the effect of adding a dc layer to an existing cell. It also is the first to describe the possible entropic gain to be had if the dc layer emits preferentially towards the cell, with high internal efficiency.

IV. Carrier Multiplication and its Relation to Down-Conversion

**Publication note*[3]

Carrier Multiplication (CM) is another conceived method of improving the efficiency of solar cells beyond the SQ limit. Like other 3rd generation techniques, it too changes one of the assumptions of the original DB model. For CM, the assumption that each photon can generate a single e-h pair is violated, since in certain materials, high energy photons can generate more than one e-h pairs **[69-71]**. As in dc, the conservation of energy must be upheld, so in order for the CM process to work, these higher energy photons must have at least twice the bandgap energy to produce two e-h pairs. This process was known at the time of the original SQ paper, but was only seen in rare occasions in some crystalline materials under high energy illumination. A schematic of the CM process is shown in Fig. **IV-1**. Recent advances in nanotechnology, specifically, in the development of colloidal quantum dot crystals, have improved the efficiency of some of these CM processes. In these types of material systems, the e-h pair is highly bound due to Coulomb interactions, and is known as an *exciton*; therefore, the CM process in these materials is also called the Multiple Exciton Generation (MEG) process **[72]**. Many quantum dot crystal systems have been found that can create MEGs, including SiGe **[73]**, CdTe/CdSe **[74]** and PbS **[75]**. However, typically energies of up to 10 eV – which is far outside the range of the solar spectrum – are needed in order to efficiently generate these MEGs. This limitation is just one of the many that have been found for the MEG system, leading many recent authors to question the validity of the MEG concept for solar cell use **[76]**. Nevertheless, since the issues appear to be primarily a materials science question of finding the suitable material, some of which have been found **[77]**, it is still an interesting opportunity to increase the efficiency of a single junction cell beyond the SQ limit.

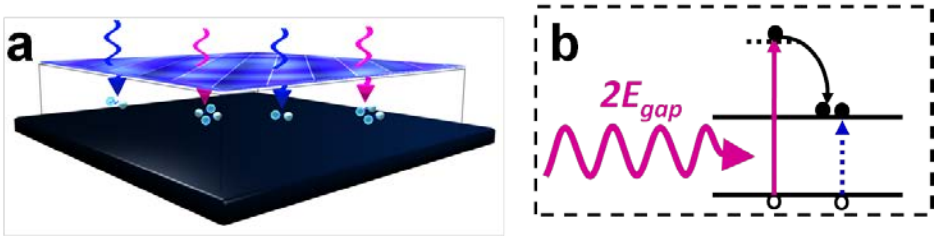

IV-1 Schematic of the Carrier Multiplication Process. (a) Multiple e-h pairs can be created *within* the semiconductor by high energy photons (magenta), whereas lower energy photons generate a single e-h pair (blue). (b) Band diagram of the CM process: a high energy photon excites an electron to above $2E_g$, which then transfers its excess energy to another electron excited to the bandgap. The dashed border indicates that the process occurs internally within the solar cell.

[3] The following chapter is a condensed version of the paper in Ref. **[68]**. The order has been changed in order to match the information of the previous chapters.

Modeling the CM process using the thermodynamic method, where only the current and voltage are important, has produced a standard model for the MEG process. Since the MEG system is supposed to create a higher current from the higher energy photons, in the same way that the dc system does, it has been assumed that the two processes are equivalent **[4]**. In this chapter, the original model will be presented, followed by a newer model devised by us **[68]**. The model will then be compared against the dc system of the previous chapter, demonstrating the differences between the two.

1. The Original Carrier Multiplication Model(s)

The CM process is expected to produce an increase in current due to the increase in the e-h pair generation rate. This process occurs internally within the semiconductor crystal, and is therefore a direct process. Since most models focus only on the *current* aspect of the solar cell, instead of also focusing on the *voltage* aspect, the first model to describe the CM process simply defined the current expected from an ideal CM system, and then maximized the power as a function of $P=I\times V$ **[73,78]**. The current was modeled as:

$$I = g\Omega_S\left(\int_{E_g}^{2E_g}\frac{E^2dE}{\exp[E/kT_S]-1}+2\times\int_{2E_g}^{\infty}\frac{E^2dE}{\exp[E/kT_S]-1}-f_\Omega\int_{E_g}^{\infty}\frac{E^2dE}{\exp[(E-\mu)/kT_c]-1}\right) \quad \textbf{IV.1}$$

The first term in Eq. **IV.1** includes the incoming spectrum that is below the $2E_g$ threshold for CM generation, and is therefore unaffected. The second term is the generation of 2 e-h pairs, at a rate proportionate to the quantity of photons above the $2E_g$ threshold. The last term is the standard vRS relation for the output emission of a semiconductor. We note that this equation for the current is *exactly* that of the current for a dc system, in Eq. **III.12** above, if we ignore the non-idealities, setting $f_{dc}=B_{dc}=1$. Although this was not done in the original models, we can simplify the first two terms by using the integral rule of Eq. **III.4** above, and obtain:

$$I = qg\Omega_S N_S\{E_g\to\infty\}\times\left[1+\frac{N_S\{2E_g\to\infty\}}{N_S\{E_g\to\infty\}}\right]-qg\Omega_o N_o\{E_g,\mu\} \quad \textbf{IV.2}$$

This form is once again, *exactly* that of the dc system, if we take the term $f_{dc}(2B_{dc}-1)\to 1$. The efficiency of the CM system was then modeled as taking the product of $I\times V$, maximized for V_m.

The relation between the dc and CM models was not pointed out in any of the original papers, since the first dc model was published 8 years later **[54]**. However, the authors of the original CM model paper understood that they may have a difficulty in their model, since it assumed that the CM process was not a reversible one: If the photons could be absorbed at discrete levels above the bandgap, they should perhaps be able to emit at these levels too **[79,80]**. This process is also known as the inverse of Auger recombination. Auger recombination is a process that is disadvantageous for PV; in Auger recombination, an excited electron at the conduction band will *non-radiatively* recombine with a hole in the valence band and transfer its excess energy to another electron in the conduction band, which will then be excited even higher within the

conduction band. According to the inverse-Auger theory, if the electron is excited to the threshold state in a CM material, instead of merely thermalizing back down to the conduction band again, it will emit a photon at $2E_g$. This process also conserves the energy of the system, as shown in Fig. **IV-2b**. The inverse-Auger process is therefore assumed to be a form of time-reversal process for the CM process.

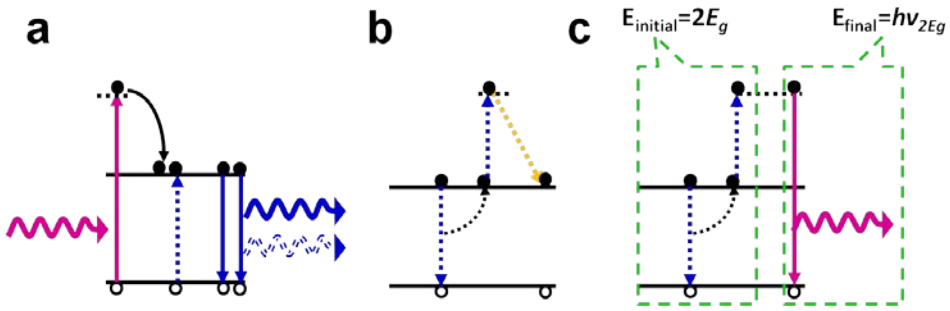

IV-2 Recombination in a Carrier Multiplication System. (a) The original CM model posited that there would be only a single photon at the output end of the CM process, instead of the required 2 photons – second photon is in outline (in equilibrium, when no current is extracted). (b) The Auger recombination process: an electron recombines with a hole, and transfers its energy in a non-radiative manner to a second electron, which is excited higher into the conduction band, and then thermalizes back down to the conduction band edge. No photon is emitted. (c) The modified CM emission process, being the inverse of CM: the excited electron recombines directly with a hole from the threshold state, and emits a high energy photon. The green boxes denote the energy of the system both before and after the event, which is shown to be conserved.

The need for this inverse-Auger process was realized immediately after the publication of the original model, by essentially the same authors, and was explained in terms of a violation of detailed-balance: If the original model included 1 photons out for every 1 high energy photon in, as in Fig. **IV-2a**, then there is a violation of the conservation of energy. Therefore, to account for the extra photon, they added a recombination term to the outgoing flux of the CM system, which was modeled as an inverse-Auger process, emitted from an extra energy level of the system, at 2μ **[79,80]**. The flux equilibrium at open-circuit then becomes:

$$\Omega_S \int_{E_g}^{\infty} \frac{E^2 dE}{\exp[E/kT_S]-1} \times (1+\theta) = \Omega_o \int_{E_g}^{\infty} \frac{E^2 dE}{\exp[(E-\mu)/kT_c]-1} + \Omega_o \int_{2E_g}^{\infty} \frac{E^2 dE}{\exp[(E-2\mu)/kT_c]-1} \qquad \textbf{IV.3}$$

Here, the first two terms are the same, and the last term includes the emission from the excited state, at $2E_g$, and which is supposed to be at a separate chemical potential of 2μ. The term θ is the fraction of photons above $2E_g$, and will be used from now on, and is defined as:

$$\theta \equiv \frac{\int_{2E_g}^{\infty} \frac{E^2 dE}{\exp[E/kT_S]-1}}{\int_{E_g}^{\infty} \frac{E^2 dE}{\exp[E/kT_S]-1}} = \frac{N_S\{2E_g \to \infty\}}{N_S\{E_g \to \infty\}} \leq 1 \qquad \textbf{IV.4}$$

The parameter θ=1 only at E_g=0. This process is depicted in Fig. **IV-2c**. Note that the last two terms cannot be combined in any way, since the integrands are different, with only the first emission term following the vRS formulation. Note that the term θ is equivalent to the gain term we found for the dc process, when the efficiencies were taken as optimal:

$$\theta = \{\beta_1 \mid f_{dc} = B_{dc} = 1\} \qquad \textbf{IV.5}$$

With β_1 given by Eq. **III.9**. One can isolate the chemical potential for this model, which will be:

$$qV_{oc}^{CM}(old) = qV_{oc}^{dc} - kT_c \ln\left\{1 + 4\exp[-E_g/kT_c] \times \left(\exp[qV_{oc}^{CM}/kT_c] - 1\right)\right\} \qquad \textbf{IV.6}$$

With V_{oc}^{dc} given previously in Eq. **III.8**. However, this equation is not very useful, since it remains a transcendental equation for V_{oc}^{CM}, and is thus unsolvable analytically.

Under Eq. **IV.3**, the flux equilibrium of photons is now conserved, however, in addition to violating the DB assumption that only one e-h pair is generated per incoming photon (which is known to occur), another assumption is violated in that the chemical potential is no longer constant in the system, with two levels, μ and 2μ. This violation of a non-uniform chemical potential, which is a critical assumption in the SQ DB model, did not appear to be an issue for any of the earlier authors, who also assume that the emission from a CM material will follow the inverse-Auger spectrum **[81]**.

The major issue of the original model for CM, as opposed to the modified one of Eq. **IV.3** was that it was shown that the original model violated the second law of thermodynamics under maximal concentration, since it produced negative entropy **[45,82]**. This can be explained in a hand-waving argument as being due to the violation of Kirchhoff's law of radiation (flux equilibrium) in the original model, as described above. However, by the same argument, it could be argued that the inclusion of a second chemical potential in the cell at 2μ is both arbitrary [i.e. why should the level be at 2μ, and not $2E_g$ or $2(\mu+\delta)$?], as well as lacking in thermodynamic meaning, since the Gibbs Free Energy, G, is a uniquely defined variable of the system, and is equivalent to the (single) chemical potential. We have already associated the chemical potential with the entropy of the photon cloud in a well-defined manner in the proceeding chapters, yet by adding another chemical potential at 2μ, we must then assume that the amount of entropy for the threshold level is somehow related to the properties of the étendue, temperature, and energy dispersion. Furthermore, we showed quite clearly that the original CM model was, in fact, the correct model for a dc system, and there is no thermodynamic problem associated with the dc entropy creation, as was described in depth in the previous chapter. Therefore, there must be a distinction between these two models that was not taken into account.

2. A New Model for CM

Due to the issues described above, a new model for the CM process was created by us **[68]** in order to account for both the thermodynamic description of the system, as well as account for Kirchhoff's law of radiation at the surface of the cell. This newer model accounts for the flux equilibrium in a direct manner, without the introduction of an artificial second chemical potential in the system.

The CM system, at open-circuit, can be split into two distinct systems: The first describes all the photons with energies from E_g to $2E_g$, and are absorbed and emitted on a one-to-one fashion, according to Kirchhoff's law of radiation. In this regime of energies, the material is a *linear* system (pseudo-linear, as defined in Chapter 3**,** Eq. **II.25**). The second system consists of all the higher energy photons, above $2E_g$, which undergo the CM process, in this system, the material should absorb a photon, create two electrons, which then recombine to create *two* photons, and thus the flux equilibrium is broken. In this regime of energies, the system acts as a *nonlinear* system! We would expect to get *photon doubling* if we shone a $2E_g$ energy laser at this kind of material (assuming that the CM process is 100% efficient), receiving twice the number of photons that we input. This does *not* violate the conservation of energy, and non-linear optical materials are quite often used in many applications; however it *does* appear to violate Kirchhoff's law of radiation! The reason this is not truly a violation, is that Kirchhoff's law of radiation *explicitly* only relates to *linear* materials, and is known to be violated in any nonlinear material. A CM material is obviously such a nonlinear material, as is easily demonstrable using the laser experiment just described.

The new model for CM therefore relates the flux at open-circuit for both segments of the energy regime simultaneously, and we assume that the chemical potential is *uniform* throughout the semiconductor. However, since we have shown that the flux-equilibrium is nonlinear, we do not equate the *flux*, but rather the *current*, just as we did with the TF, where the input was the current in photons, and the output was the current in electrons. Using this terminology, the *electron* current increases by a factor of $(1+\theta)$, and therefore the output *photon* current must increase by that same amount:

$$\Omega_S \int_{E_g}^{\infty} \frac{E^2 dE}{\exp[E/kT_S]-1} \times (1+\theta) = (1+\theta) \times \Omega_o \int_{E_g}^{\infty} \frac{E^2 dE}{\exp[(E-\mu)/kT_c]-1} \qquad \textbf{IV.7}$$

Combining the linear and nonlinear terms in Eq. **IV.7** allows us to equate the number of photons in to the number of electrons created, and is therefore the closest one can get to achieving Kirchhoff's law of radiation for this nonlinear material. However, we see that using this formalism, and extracting the V_{oc}, we obtain for the CM system:

$$qV_{oc}^{CM} = qV_{oc}^{reg} + kT_c \ln[1+\theta] - kT_c \ln[1+\theta] = qV_{oc}^{reg} \qquad \textbf{IV.8}$$

For the CM system, following this model, the open-circuit voltage remains the *same* as for a regular solar cell, since the gain in entropy of the process (the term $kT_c ln[1+\theta]$) is then lost at the emission end. This difference will be described in section 5 of this chapter.

While the V_{oc} of the CM system may not have any gain, the efficiency gain expected from the CM system – like the dc system – is in the rise in current due to the increase in electrons generated. The efficiency is once again a function of the product $P=I\times V$, which will be linearly proportional to the additive term: $(1+\theta)$. We will first generalize the equations to include multiple splitting processes.

3. Generalization to Multiple Splitting Systems

The formula for the CM process, as well as those for the DC process, can be generalized for multiple splitting levels, using the formalism described here, as a function of the fraction of photons above each threshold level. Fig. **IV-3** displays the simplified band diagrams for a CM and DC system with 2 splitting levels. For the CM system, this would mean that a photon with $3E_g$ units of energy will produce 3 electrons, and that a dc system will split the photons twice, eventually producing 3 electrons as well.

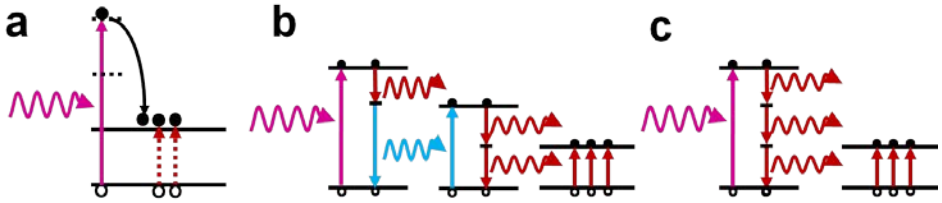

IV-3 Multiple Splitting Processes for Carrier Multiplication and Down-Conversion. In all three processes shown here, a photon with energy of at least $3E_g$ is incident on the device. (a) A three-electron generating process, whereby the higher energy photon surpasses two threshold levels, and non-radiatively transfers the excess energy to excite another two electrons. (b) A dc process with two different splitting materials, such that the incident photon is first split into two photons, with different energies, and the higher-energy photon is then split again by a second dc layer, ultimately generating three electrons. (c) A dc process where the dc layer splits the high energy photon three times via two radiative trap states.

The splitting process for both of these systems can be continued indefinitely, providing the photons have enough energy to be split. In particular, provided that they have enough *free energy* to be split, since the lower energy photons have less free energy associated with them, due to the entropic losses of the photon cloud after the PV process. We will show below that this can modified using concentration. Since the left hand side of the flux equilibrium method is the same for both the CM and dc processes (though describing different things, the former described the electron generation, and the latter the photon flux), we can write the *input* side of the equations for a level of splitting multiplicity, M, as follows:

$$N_{in}^{CM,dc}(M) = gC\Omega_S\left(\sum_{m=1}^{M} m\int_{m\times E_g}^{(m+1)\times E_g}\frac{E^2dE}{\exp[E/kT_S]-1} + f_m M\times\int_{M\times E_g}^{\infty}\frac{E^2dE}{\exp[E/kT_S]-1}\right) \quad \textbf{IV.9}$$

where the concentration factor, C, has been included as well. Note that M=1 provides the regular solar cell case, so that a single dc or CM system will be from M=2 and up using this formalism. Also included is an internal efficiency factor for each stage in the splitting, $0\le f_m\le 1$, which is similar to the term f_{dc} from the previous chapter.

Eq. **IV.9** can be simplified if we collect each overlapping segment of the integrals, we can simplify the summation to:

$$N_{in}^{CM,dc}(M) = gC\Omega_S\sum_{m=1}^{M} f_m\int_{m\times E_g}^{\infty}\frac{E^2dE}{\exp[E/kT_S]-1} \quad \textbf{IV.10}$$

Using the formalism used for defining the term θ, we can simplify this formula to account for the major segment of the spectrum (as defined by the bandgap of the cell), from $E_g\rightarrow\infty$, and write this as:

$$N_{in}^{CM,dc}(M) = gC\Omega_S\times\left(\sum_{m=1}^{M} f_m\theta_m\right)\times\int_{E_g}^{\infty}\frac{E^2dE}{\exp[E/kT_S]-1} \quad \textbf{IV.11}$$

Where each θ_m is defined by the relation:

$$\theta_m \equiv \int_{m\times E_g}^{\infty}\frac{E^2dE}{\exp[E/kT_S]-1}\Bigg/\int_{E_g}^{\infty}\frac{E^2dE}{\exp[E/kT_S]-1} \quad \textbf{IV.12}$$

Note that the term θ described in Eq. **IV.4** is for a multiplicity of M=2 ($\theta_{m=2}=\theta$), and $\theta_{m=1}$=1.

The emission from the CM and dc systems, however, differ considerably; while the CM system increases the number of vRS emitted photons, by a fraction proportionate to $\Sigma\theta_m$, the dc system retains the single vRS emission factor, since there is nothing internally modified in the dc cell. It must be remembered that the dc system applies to an existing cell, which follows the vRS relation, and does not have any internal threshold levels from which to emit from. As a result, when calculating the total efficiency from the cell, the dc and CM system will consist of slightly different equations. For the dc system, it will be

$$\eta_{eff}^{dc} = g_2\times V_m\times\left[\int_{E_g}^{\infty}\frac{E^2dE}{\exp[E/kT_S]-1}\times\sum_{m=1}^{M} f_m\theta_m - \frac{f_\Omega}{C}\int_{E_g}^{\infty}\frac{E^2dE}{\exp[(E-qV_m)/kT_c]-1}\right] \quad \textbf{IV.13}$$

whereas the CM system will be:

$$\eta_{eff}^{CM} = g_2 \times V_m \times \sum_{m=1}^{M} f_m \theta_m \times \left[\int_{E_g}^{\infty} \frac{E^2 dE}{\exp[E/kT_S]-1} - \frac{f_\Omega}{C} \int_{E_g}^{\infty} \frac{E^2 dE}{\exp[(E-qV_m)/kT_c]-1} \right] \quad \text{IV.14}$$

For both of these sets of equations, we have included the term f_m as an efficiency term, however, it should be noted that this term for the dc system will also include the geometric factor [$f_m = f_{dc} \times (2B_{dc}-1)$]. The difference between the two sets of equations is that the dc system includes the term $\Sigma f_m \theta_m$ within the brackets, and therefore will affect the calculated value of V_m, whereas the CM system has the $\Sigma f_m \theta_m$ term outside the brackets, and will be ignored when maximizing the efficiency for V_m. This difference also appears in the generalized relation for the V_{oc}, which can easily be seen to simplify to:

$$\begin{aligned} qV_{oc}^{dc} &= qV_{oc}^{reg} + kT_c \ln\left[\sum_{m=1}^{M} f_m \theta_m\right] \\ qV_{oc}^{CM} &= qV_{oc}^{reg} \end{aligned} \quad \text{IV.15}$$

These equations demonstrate the slight advantage of the dc system over the CM system, so long as the efficiency factor, f_m is positive – which may not be the case if $B_{dc}<0.5$.

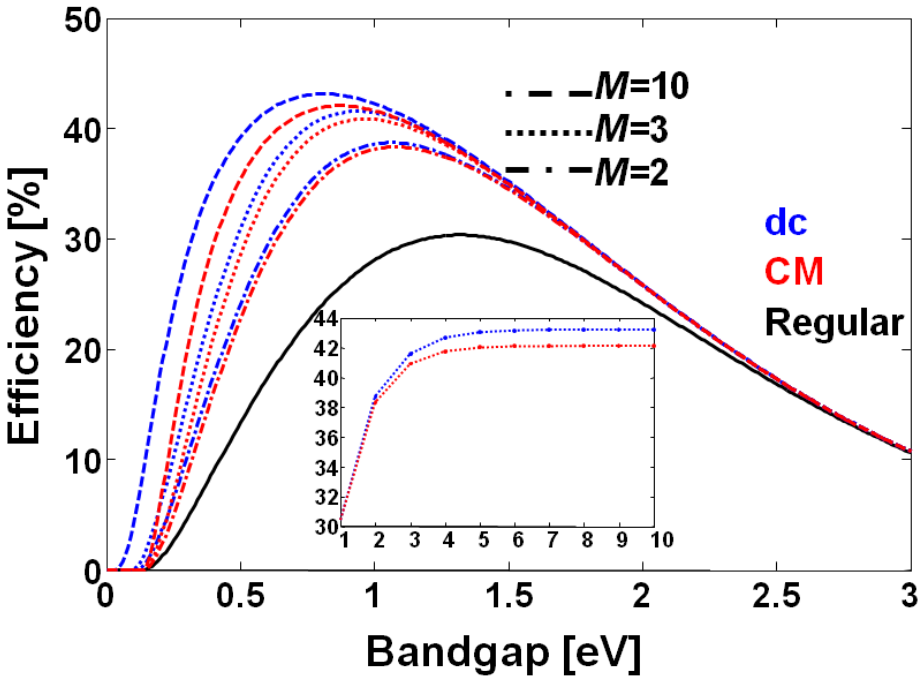

IV-4 Efficiency Comparison between the Down-Converting and Carrier Multiplication Systems. The efficiency is plotted for multiple splitting levels, as described in Fig. IV-3. A single splitting level starts with M=2. After M=3, the peak efficiency begins to converge. For this calculation the outgoing étendue was taken as $\Omega_o = 2\pi$. Inset: The peak efficiency as a function of multiplicity for both systems. Compare this inset with Fig. IV-7 below.

Fig. **IV-4** displays the efficiency for the CM and dc systems, as a function of increasing multiplicity levels, $M \rightarrow 10$, and no concentration, $C=1$. These curves were calculated assuming that the dc and CM conversion efficiencies were unity, with absolutely no losses included: $f_m=1$. Due to the small advantage of the dc process, primarily visible in the open-circuit voltage gain, the dc system outperforms the CM system for all values of multiplicity, by a small amount. The peak efficiency can be up to 1% more efficient for the dc system than the CM system using these models. The overall efficiency saturates after a few multiplicity levels, as shown in the inset of Fig. **IV-4**, since the number of photons in the spectrum segment $m \times E_g$ is constantly reduced, and is limited from above by the drop in the number of photons above 4-5 eV. This saturation suggests that it is only worthwhile to produce a single, or perhaps double, splitting layer, as will also be shown below.

Including losses in the dc/CM conversion efficiency f_m factor will also reduce the efficiency of each method, relative to the ideal case. As in the previous chapter, we can assume that not all of the higher energy photons will be converted via the dc or CM process, with some of them absorbed directly in the direct semiconductor bandgap. The reduction of converted photons will reduce the overall efficiency; however an efficiency increase is still achievable. This is plotted in Fig. **IV-5** for the dc/CM systems under no concentration, $C=1$, a single splitting multiplicity, $M=2$, and including a fraction $f_m=0.5$ for both methods. The I_{sc} is reduced for each method, which leads to an overall efficiency loss. There is essentially no difference between the plots in Fig. **IV-4** and **IV-5** since the factor f_m appears directly in association with the multiplicity factor, M, so that the two factors play a nearly identical role.

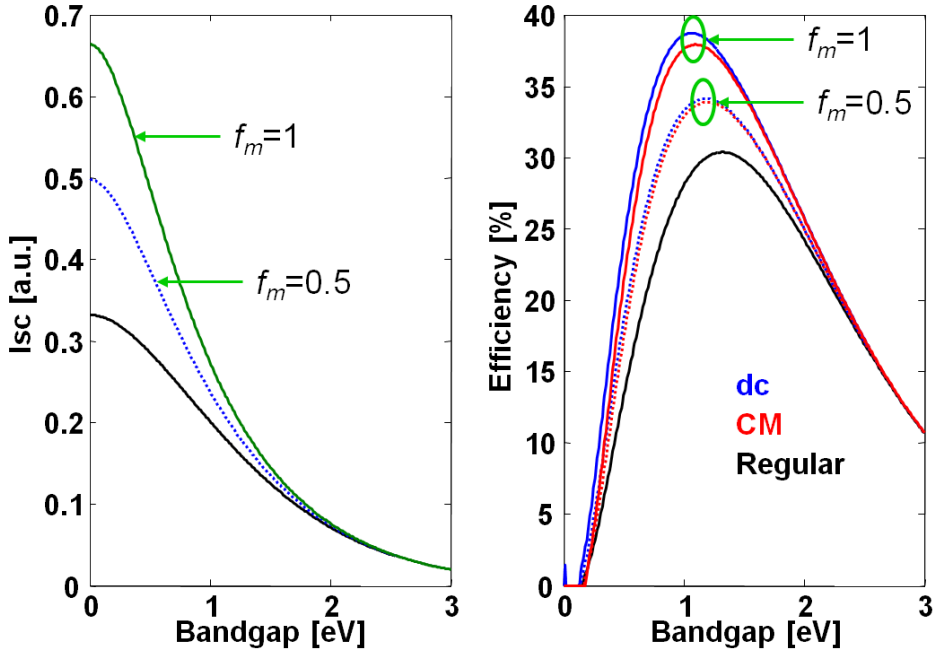

IV-5 Characteristics of a Non-Ideal Converter. Plotted are the short-circuit current and efficiency for a dc and CM system assuming no concentration, and a single splitting level, with a conversion efficiency of f_m. The short circuit current is reduced at lower conversion factors, as well as the efficiency, with the same trend as in the previous figure.

The peak efficiency can be tracked for each method, as a function of the multiplicity level, as well as when adding concentration. The original models predicted a maximal efficiency of ≈86% for infinite multiplicity levels and maximal concentration **[78,83,84]**. In addition, the optimal bandgap for such a device for CM was predicted to drop to zero. Since a zero bandgap device will proved no power, an optimal, minimal bandgap was found to be $E_g(min)$=0.048 eV **[79,83,84]**. This low bandgap is well below the $3kT_c$≈75 meV limit typically used by electronic device engineers as a rule of thumb for when the device properties will fail due to thermal effects. Furthermore, it assumes that the bandgap of the device is physically existent at that range. The models for dc and CM described here uphold the same prediction for large multiplicity levels, as shown in Fig. **IV-6a**. The same rise in efficiency is seen, with an advantage for the dc system over the CM system, as described above. The high peak efficiencies at extremely low bandgaps, approaching kT_c=25.8 mV were found using the models here as well, but without resorting to any approximations of the integrals, as was done in earlier works **[83.84]**. Since multiplicity levels beyond M=3 are probably physically difficult to create, plotted in Fig. **IV-6b** are only the optimal bandgap values up to M=10. The formulas tend to break-down at the limit of high concentration and low bandgaps, such that the numerical results are affected by the choice of starting point and variable distributions in the code. This variability occurs once the energies are of the order of kT_c, and particularly when E-μ≈kT_c.

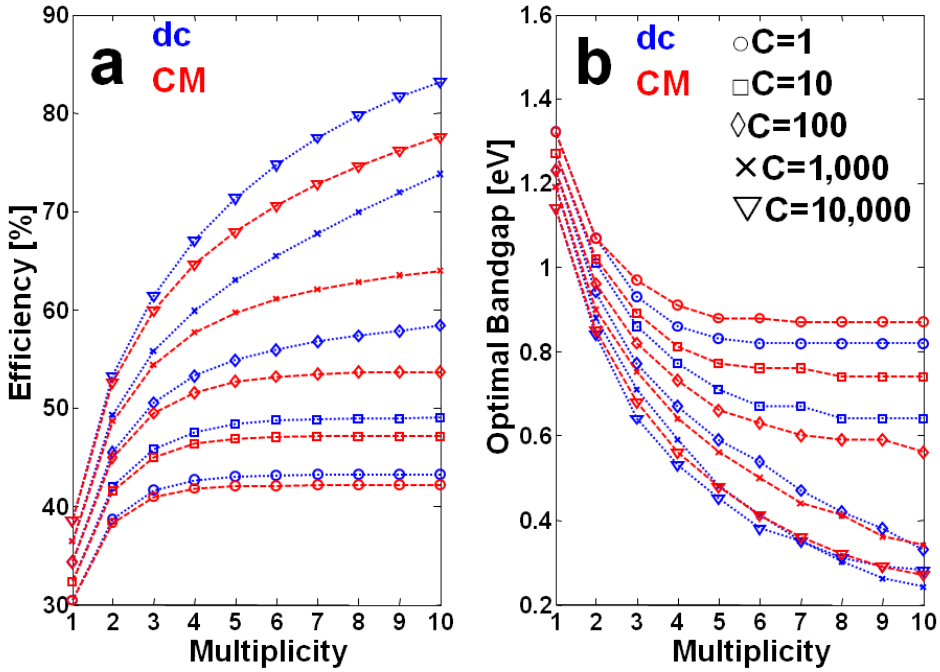

IV-6 Peak Efficiency as a Function of the Levels of Multiplicity. (a) Peak efficiency as a function of multiplicity, and (b) optimal bandgap as a function of multiplicity. Both dc and CM are plotted, with a slight efficiency advantage for the dc system, regardless of the multiplicity level, or concentration. The curves begin to diverge at high concentration levels due to the disappearing of the entropy completely. Concentration levels are as marked in panel (b).

The exponential growth of the peak efficiency cannot be found using strict analytical tools, since the equations that must be solved for the peak efficiency are transcendental. However, we can approximate the curves to follow the following empirical relation:

$$\eta_{peak}(\mathrm{m}) = \eta_{\mathrm{m}\to\infty}\left[1-\exp(-m/X)\right]+\eta_{m=0} \qquad \textbf{IV.16}$$

where m is the multiplicity variable and X is the average of the peak bandgap for m=1 to $m\to\infty$, divided by kT_S (0.517 eV). The value of X can be approximated assuming that the summations in the formulas for the current given in Eq. **IV.9** can be approximated by a geometric series. If the common ratio of the series is assumed to be *exp(-m/X)*, where this ratio can be evaluated using the Fundamental Theorem of Calculus when finding the derivative of the efficiency as a function of bandgap, such that:

$$e^{-m/X} = \sum_{M}^{\infty} \frac{E^4 m^3 dE}{\exp[E/kT_S]-1} \Bigg/ \sum_{1}^{\infty} \frac{E^4 m^3 dE}{\exp[E/kT_S]-1} \qquad \textbf{IV.17}$$

This approximation of the curve is quite accurate, despite its course assumptions, yet is still only an approximation, whose importance is of empirical value alone.

As shown in Fig. **IV-6**, the peak efficiency for dc converges to a higher level than the traditionally held limits for thermodynamic conversion! The breakdown in the efficiency limits for dc and CM models at maximal concentration can be seen using our knowledge of entropy that stated that at maximal concentration, the DB limit of a solar cell should approach the UE limit. This statement is true for 3rd generation ideas as well, with higher UE efficiencies possible. The UE efficiency for a CM system was thought to approach the Carnot efficiency, which is traditionally held as the highest thermodynamically possible efficiency limit **[85]**. However, if we push the models for the UE of a CM or dc system – which are identical since the input term is the same for both, and the UE model ignores the output – we find that at increasing multiplicity, the efficiency actually hits 100%. This is shown in Fig. **IV-7**, with the peak UE approaching 100% for extremely high levels of multiplicity, as demonstrated in the inset. The near unity efficiency at near zero bandgap is a clear signal of a breakdown in the thermodynamic assumptions, however, if the UE maximum value is taken as the limit for when $T_c\to 0$, then the Carnot efficiency also approaches unity. The carriers are then extracted regardless of their temperature.

The possibility of having a material with 300, or even 1000 internal splitting bands borders on being non-physical. If 1000 bands are considered, the UE reaches 99.64% (not shown) at the very first interval of bandgap considered (e.g., 0.01 eV, which is a function of the discretization choice used in the numerical calculation); this would also require meaningless 10 eV photons to be present, and is therefore irrelevant to the solar spectrum. Moreover, since it is assumed that photons can only be absorbed from the valence band up to the multiplicity level, and no internal absorption process (say, from $5E_g$ to $10E_g$) occur; this internal process would be akin to free-carrier, or intra-band, absorption. The material would therefore act as a one-way optical diode, only absorbing light into the multiplicity levels, but then emitting it from the bandgap alone. This issue is problematic for both dc and CM systems.

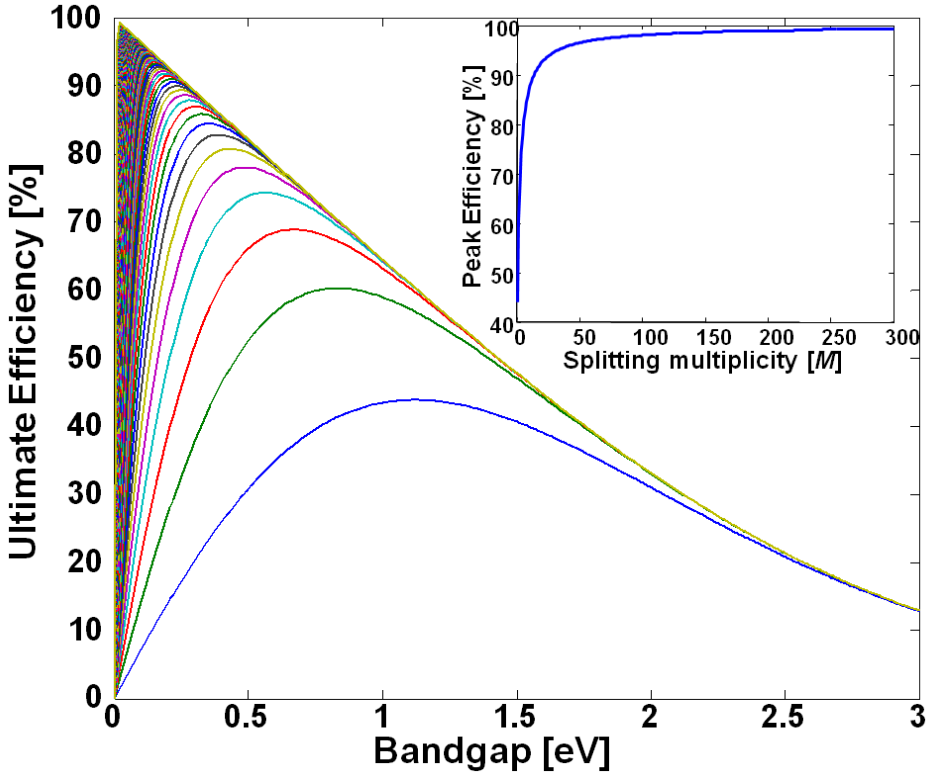

IV-7 Ultimate Efficiency with Near-Infinite Multiplicity. Plotted is the UE of a dc or CM system (which are equivalent for the UE model) with up to 300 levels of multiplicity. The peak UE reaches 99.26% for a bandgap of 0.02 eV (or 99.64% at ≈0.01 eV for *M*=1000) Inset: peak efficiency as a function of multiplicity, showing the approach to unity efficiency at higher multiplicity.

The concept of a diode-like material has been considered for the CM process, and has been thought to be possible using the process of *singlet fission* **[70,86]**. In this process, the diode-like function is provided by the absorption of photons into the 'singlet' state of a molecule, which is a quantum-mechanics-defined isolated energy state, and this energy state then decays into two 'triplet' states. This transition cannot occur optically, since the singlet and triplet state transition is quantum-mechanically forbidden. The use of the singlet fission process to provide a CM improvement has been analyzed before **[70]**, providing the same enhancement to the efficiency. However, it could be argued based on the analysis above that the singlet fission material would be useful as a dc material, as ohpposed to an actual cell material, with the eventual emission from the triplet states providing the two lower energy photons.

4. Comparison of Heat Generation

Comparing the two methods, dc and CM, from a generalized perspective of heat generation in the cell itself also provides a qualitative description for why the dc method has some advantages

over the CM method. Using the same terminology from Chapter **II**, and Fig. **II-2**, we can associate a heat loss due to the excess energy of the absorbed photons, as measured in relation to the bandgap, $E_{ph}=E_{ex}+E_g$. Since at open-circuit equilibrium, photons with approximately E_g worth of energy are also emitted from the solar cell, that excess energy can be said to have been transformed into heat via thermalization losses.

The situation for a dc or CM system however is different, since the amount of thermalization losses is reduced. Fig. **IV-8** displays the sequence of absorption, heat loss, and re-emission for a single photon event in each system. In either the dc or CM system, high energy photons with $E>2E_g$ are absorbed at either the dc layer or above the internal threshold level (step 1), and then create two dc photons or two immediate electrons (step 2). The two generated electrons can radiatively recombine and create to re-emission photons at the bandgap (step 3). The total amount of heat loss amounts to the excess energy: $Q_{lost}^{1}=E_{ex}$, and the 'thermal entropy' produced amounts to $Q_{lost}^{1}=E_{ex}/T_c$ in this first stage. In addition to the dc or CM process, photons with energy below the threshold, meaning with energies: $E_g<E<2E_g$, will be absorbed regularly in the solar cell (step 4), and generate the usual amount of thermalization loss, Q_{lost}^{2}.

The major difference between the two systems is that the first loss factor, Q_{lost}^{1} occurs in a material system *external* to the cell in the dc system, whereas it occurs *internally* in the CM system (see dotted lines in Fig. **IV-8**). Since we know from broad thermodynamic arguments that the generation of heat (and entropy, according to the classical view of the 2nd law of thermodynamics) is associated with a reduction in the amount of free energy utilizable in the system, the dc design is advantageous since this heat loss does not directly affect the free energy (and thus the V_{oc}). While the temperature of the dc layer and the cell will be the same if they are thermally coupled, with heat transferred from the dc layer to the cell is not the factor that reduces the free energy, rather it is the generation of heat in the solar cell that can reduce the free energy. The CM system is still advantageous in comparison to a regular cell from the heat generation perspective, since the current is increased, without generating a linear increase in thermalization losses. For every photons with $E>2E_g$, a total of Q_{lost}^{1} is generated, and creates two electrons, whereas a regular solar cell would only create a single electron, and $Q_{lost}^{1}+Q_{lost}^{2}$ amount of heat.

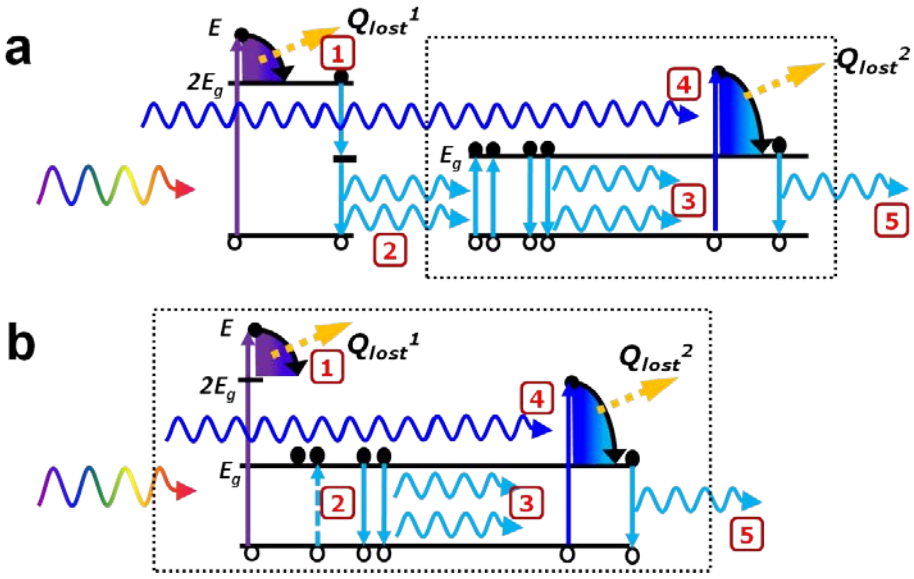

IV-8 Heat loss in the Down-Conversion and Carrier Multiplication Systems. (a) A dc system, and (b) a CM system. Photons with energy exceeding $2E_g$ are absorbed in the dc layer in (a), or above the CM threshold in (b), and generate a small amount of heat loss, Q_{lost}^1 (step 1, violet). The dc system creates two bandgap-energy photons (cyan), whereas the CM system directly produces two electrons via a non-radiative energy transfer mechanism (step 2, cyan). These 'cooler' photons can then be emitted at the bandgap (step 3, cyan). Photons with energies between the bandgap and the threshold of $2E_g$ are absorbed directly within the solar cell (step 4, blue), producing a concomitant amount of heat loss due to thermalization, Q_{lost}^2. These electrons will also be able to be re-emitted as a single photon from the bandgap (step 5, cyan). Dotted lines represent the boundaries of the solar cell, with the dc layer in (a) being external to the cell itself.

5. The Entropy Difference

The major difference between the two models for dc and CM described in this chapter related to the entropy term in the V_{oc}. The dc model was shown to have a 'gain' term due to the spectrum splitting of the dc layer, which better matched the incoming spectrum to the single bandgap of the underlying cell. However, we began this chapter by describing the original models for CM **[78]**, which we demonstrated was identical to the dc model, yet said that it was shown that this model violates the 2nd law of thermodynamics! This problem must be reconciled, since there is seemingly no reason why the 2nd law should be violated in the dc system, which was derived 'from scratch' in the previous chapter, and had fewer assumptions associated with it than the CM model. It is therefore surprising that there is an entropic issue with the original CM model, which was developed 8 years before the first dc model (which is different from the model described in the previous chapter, since the original dc model did not assume a regular semiconductor as the solar cell **[54]**).

The violation of the 2nd law was shown to occur at maximal concentration, producing a *net negative* amount of entropy **[45,82]**. The case of maximal concentration, itself a somewhat precarious physical notion questioned later in Chapter **VIII**, assumes that the light is concentrated to the maximal ≈90° angle that is comparable to stretching the incoming beam from the small angular radius to a full hemisphere above the cell. For a regular solar cell, or for a CM cell, this is the maximal concentration possible. However, for a dc solar cell, the flux absorbed by the cell is *not* the same as that absorbed by the regular cell, since the spectrum is different, *as well as* the angular distribution of the dc converted photons. Since the photons emitted from the dc layer are emitted isotropically (in fact, with Ω_{dc} up to 4π, instead of just 2π), the segment of spectrum above $2E_g$ should not be included into the maximal concentration ratio.

From the perspective of the formulas for V_{oc}, we showed that the gain term for the dc layer was proportionate to the segment of converted photons in the spectrum:

$$\boldsymbol{qV_{oc}^{gain} = kT_c \ln\left[\sum_{m=1}^{M} f_m \theta_m\right] \cong|_{M=2}\ kT_c \ln[1+\theta]} \qquad \textbf{IV.18}$$

For the maximal concentration case, $C=C^{max}\approx$46,000, this term (which will be negative for entropy, and positive for voltage) can surpass the amount of positive entropy produced by the cell, if no losses are included, amounting to a net negative entropy generation.

The issue can be resolved if we look at the total étendue of the light actually absorbed by the cell as being the combined étendue of the solar beam, sans the spectrum of energy above $2E_g$, in addition to the isotropically emitted dc beam. This dc beam therefore 'expands' the beam emitted onto the cell, even at maximal concentration, such that the total étendue of beam absorbed can actually *surpass* the full hemisphere above the cell. This situation is demonstrated in Fig. **IV-9** for both a regular flat cell, and a dc cell, at full concentration. The dc layer will emit extra photons into the initial étendue of the beam, in an isotropic manner (B_{dc}). These extra 'rays' in the incoming beam can be expanded beyond the initial distribution of rays, since the spectrum had been changed by the dc layer. The maximal concentration term should therefore be modified to include this contribution. This can easily be done by combining the gain term of Eq. **IV.18** into the term for the concentration, since the logarithmic terms can be combined, producing an *effective concentration* for the dc system:

$$\boldsymbol{C_{new} = C_0 \times \sum_{m=1}^{M} f_m \theta_m} \qquad \textbf{IV.19}$$

The effective concentration term for the dc system described the entopic gain for dc in terms of the modification of the étendue. This description is different from the one used in the previous chapter, which explained the entropy difference in terms of the spectrum and distribution of energy of the incoming beam, but is in no means contradictory. The information theory approach to entropy, which describes it as a measure of missing information or uncertainty, is objective to the exact quality of the information measured. The gain term in the voltage (loss term for entropy) of Eq. **IV.18** is completely compatible with the descriptions given in Eqs. **III.8** and **III.11**, and is an objective measure of information change in the dc system. The violation of the 2nd law found for the "old" CM model **[78,45,82]**, was not valid for the dc system since it

assumed that the maximal concentration was limited to $C^{max}=\pi/\Omega_S$, whereas here we showed that the étendue is increased in the dc layer. The argument *is* however valid for a CM system, since the multiplication occurs internally, and does not modify the beam's étendue properties (recall that the thermodynamic boundary is at the cell's surface). This once again highlights the difference between the dc and CM systems, with the spectral splitting occurring *externally* in the dc system, which provides it with an entropic benefit. Essentially the fact that the dc layer is "doing work" to split the spectrum first can be used informatively by the solar cell to increase its utilization of free energy. This, of course, assumes that the systems are lossless ($\kappa_{nr}=0$), and that the geometric factor is optimal ($B_{dc}\rightarrow 1$). This distinction between *external* and *internal* conversion will be again emphasized in the next chapter.

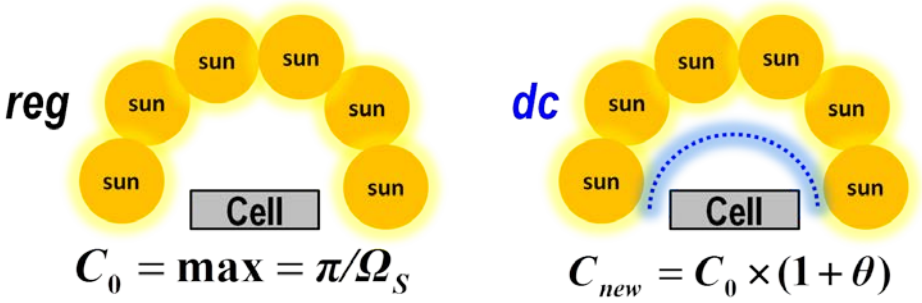

IV-9 Expansion of the Incoming Beam for a Down-Conversion Cell. (a) The maximal concentration for a regular solar cell is made possible when the full hemisphere above the cell is filled with suns, effectively creating an incoming étendue at an angle of 90°. (b) For a dc cell, the solar spectrum is first filtered through the dc layer, which produces more photons, in an isotropic manner.

V. Transfer Function Comparison between 3rd Generation Methods

**Publication note*[4]

The previous two chapters provided a detailed look at two of the processes to improve the efficiency of a cell beyond the SQ limit, while only changing a few basic assumptions used in the DB model. The principal rules for deriving the maximal thermodynamic efficiency were to concentrate on the flux into the surface of the solar cell, as well as focus on the emission emanating from that same surface at open-circuit equilibrium. These concepts were directly manifested in the TF method of Chapter **II**, for a regular solar cell. This chapter will generalize the method for other 3rd generation techniques, and provide a simple, graphical way of comparing them using circuit and signal diagrams. Since the previous chapters provided an ample introduction to the concepts of 3rd generation ideas, the formulas and derivations of this chapter will be truncated. In the interest of simplicity, only a single splitting layer will be added for each method.

1. TFs for Down-Conversion and Carrier Multiplication

Using the notations and descriptions of the dc and CM systems of the previous two chapters, we can easily devise a diagram for the dc system. The dc solar cell is a regular solar cell, with an added layer "on top" of it that affects the incoming spectrum. The actual location of the dc layer is not as important in the sense that it affects the *incoming* spectrum. Since signal diagrams are read from left to right, the dc layer should therefore be placed *before* the solar cell itself, in a *serial* process: first the dc occurs, and then the new spectrum is inputted into the solar cell. The TF of the regular solar cell, as described in Chapters **II** was a pseudo-linear system, and was a function of the input spectrum. Since the TF is indifferent to the exact spectrum, we can externally modify the spectrum as much as we want, and the TF of the dc system will remain the same. This situation is similar to the effect of adding concentration, which we have described in Chapter **I** to be adequately described as multiplying the number of suns in the sky by a factor of C. This is portrayed in the most basic signal diagram of Fig. **V-1a**. If the concentration is increased, we expect the TF of the regular sun to internally change only via the internal shift of the μ factor within the numerator of Eq. **II.23**. Specifically, under increased concentration, the chemical potential shifts closer to the bandgap, so that the factor $E-\mu_{oc}$ is reduced making the linewidth of the emission spectrum sharper. The effect of modifying the spectrum therefore indirectly changes the TF of the regular solar cell, $H_{reg}(\mu)$ by changing the internal parameter, μ. The only important thing for the solar cell itself is the *actual* input flux entering the dashed line of H_{reg}, which in this case is N_{in}^{C} in Fig. **V-1a**.

[4] The following chapter is a continuation of the conference proceedings paper in Ref. **[40]**. This chapter also includes material that was not included within that reference, as well as new TFs for the techniques described.

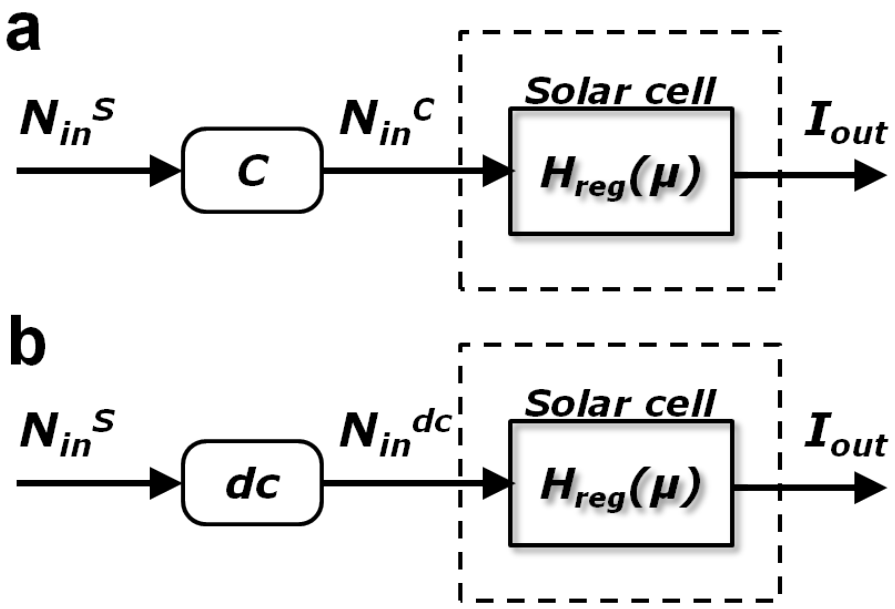

V-1 Transfer Function of a Concentrator Solar Cell and a Simplified Down-Conversion Cell. (a) The effect of adding concentration to a regular solar cell can be thought of as adding a multiplicative term, *C*, at the input side of the solar spectrum. The new spectrum that the cell effectively "sees" has been changed from $N_{in}^{C}=C\times N_{in}^{S}$. (b) A simplified version of the TF for a dc system. The dc layer modifies the input spectrum, producing a spectrum N_{in}^{dc} for the underlying cell. The internal working of the dc system is not important, and is itself a "black box".

The dc layer can be thought of in the same way, since as far as the solar cell is concerned, the important aspect is the spectrum that it can utilize for PV conversion, which is the final spectrum incident on the solar cell. We can imagine the dc layer to be another "black box", with an internal TF that is unknown, which produces a final spectrum N_{in}^{dc} that the solar cell then absorbs, in a similar fashion to the concentrating system, and as presented in Fig. **V-1b**. While this description of the dc system is useful in its simplicity, it does not help us analyze the efficiency of a dc system since we do not know the workings of the dc layer. This description would be useful only if we were given the output spectrum of a 'mystery' dc layer material, and asked what its affect would be when placed on a solar cell. However, it does not provide any analytical information that can be used for theoretical analysis.

Instead of simplifying the internals of the dc layer's TF, we can write out the internal functions of the dc layer as a function of energy filters: Low Pass Filters (LPFs) that allow photons with energy *up to* E_{LPF} to pass; High Pass Filters (HPFs) that allow photons with energies *above* E_{HPF} to pass; and Band Pass Filters (BPFs) that allow photons with energies between an upper and lower threshold to pass. Note that using this description we are discussing the photons that *pass through* the filter, as opposed to those that are absorbed or reflected away (This appear in the opposite form as that appearing in Ref. **[40]**). Effectively, the filters affect the limits of integration: the step-function absorptivity of Eq. **I.8**, where the solar cell only absorbed

from E_g and up, can be described as multiplying the solar spectrum by a HPF with a lower threshold of E_g. The rest of the spectrum is then "passed" to the cell, and then absorbed.

Using these concepts, we can re-write the TF of the dc system as portrayed in Fig. **V-2a**. The dc segment of the circuit is split into an upper branch that deals with all the photons below $2E_g$ to pass through, being the unconverted photons. The lower branch first removes all the photons below the dc threshold of $2E_g$ via a HPF, which effectively provides the numerator of the term θ from the previous chapter (Eq. **IV.4**); it then uses the internal TF described in Chapter **II**, H_{int}, which effectively transforms this cut-off spectrum into an LED-like emission, which it then transmits via a multiplier of 2 to consider the doubling of photons, and adds a conversion efficiency factor, f_m, as in the previous chapters to account for inefficiencies. The transformation of the solar spectrum to LED spectrum occurs at a chemical potential of μ_{oc}^{dc}, which is a constant formed by the flux equilibrium of Eq. **III.2**. The signal diagram of Fig. **V-2**a is thus more of an exercise in spectrum slicing, to understand which parts goes where, and then to recombine them into the input spectrum to the cell itself, N_{in}^{dc}.

The TF for a CM system is more complex, since the process is internal. Recall from the previous chapter that the original model for CM (the modified one, that was supposed to correct the 'entropy problem'), in Eq. **IV.3**, assumed that there were two separate chemical potentials (for M=2), in order for the photon flux to be matched. In fact, another model for CM that was derived using first-principals of Gibbs free energy, G, **[41]** conceived of the CM process as being akin to two separate voltage supplies in parallel, each with a voltage defined by the chemical potential. However, the problem with such a description (which was used for modeling an IB cell as well, see below), is that two separate voltage supplies cannot be connected in parallel *unless* they have identical voltages. If they have different voltages, the voltage out of the circuit will be limited by the *lower* of the two supplies (assuming one of them doesn't explode first). This type of process, which is limited by the lowest of the parallel processes is quite common in circuit theory. The authors of this first-principles model claimed that the supplies will become equal at maximal concentration conditions, when the entropic voltage loss in each branch (supply) is equivalent. This does not provide a solution for more realistic cases when the concentration is smaller than maximal. Moreover, the other model described for CM in the previous chapter **[79]** required setting the second voltage as equal to twice the first, namely that $\mu_1=\mu_2/2$, using the inverse-Auger model. In our newer model of the previous chapter, we set a requirement that the voltage (chemical potential) across the entire solar cell be constant and consistent, as per the original assumptions of the DB model.

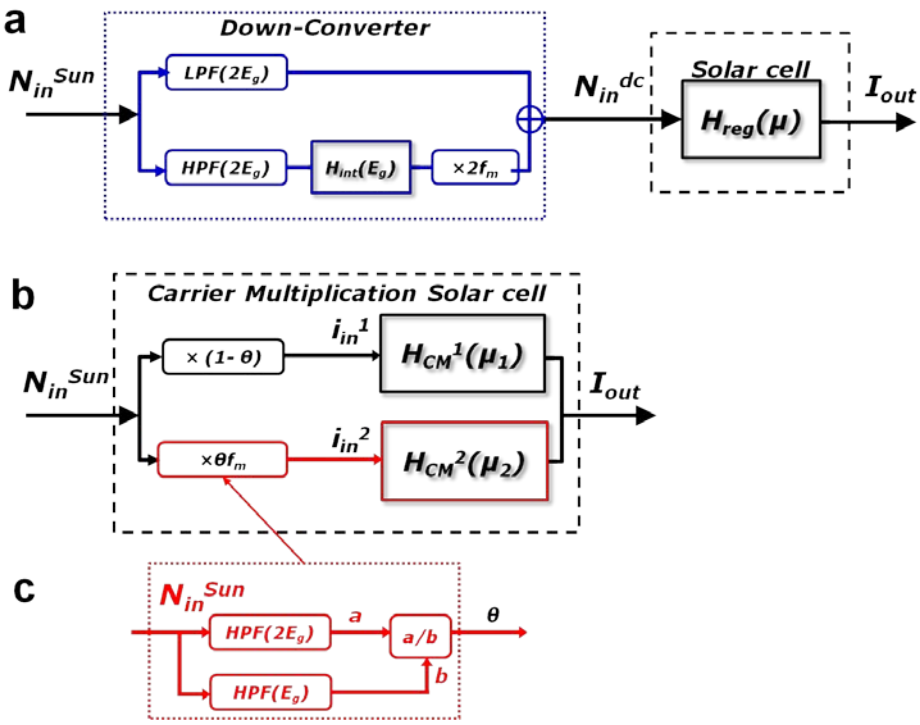

V-2 Transfer Functions for dc and CM. (a) The Internal TF for the dc layer includes an upper branch that is unaffected, and is cut-off from above at $2E_g$ using a LPF. The lower branch includes the segment above $2E_g$, which is converted into two 'cool' photons at the bandgap using the internal TF, H_{int}, and then multiplied by two (and the conversion efficiency factor, f_m). These branches are then added together to create the new spectrum irradiating the cell, N_{in}^{dc}. (b) A CM cell internally creates the two branches, which are theoretically fed into two parallel processes, with two TFs at μ_1 and μ_2. The upper branch is similar to the upper dc branch in (a). The lower branch only includes the fraction of photons above $2E_g$: θ, and multiplied by a similar factor of f_m. The fraction θ can itself be described in (c) as a devisor of the two relevant segments of the input spectrum.

Fig. **V-2b** displays the internal TF for a CM system, with two internal separate branches that can be compared to the internal branches within the dc system of Fig. **V-2a**. The upper branch acts like the upper branch of the internal dc system, and accounts for the photons that are unaffected by the existence of the CM process, between E_g and $2E_g$. This is described here as multiplied by the factor $(1-\theta)$, with θ given previously in Eq. **IV.4**, instead of using the LPF, and accounts for the first of the electrons generated in the CM process (and not the *multiplied* carrier). The other difference is that this segment of spectrum immediately feeds into an internal TF for the CM, $H_{CM}^{1}(\mu_1)$, since these photons create a voltage by themselves, as regulated by the vRS relation. $H_{CM}^{1}(\mu_1)$ is thus equivalent in action to the regular $H_{reg}(\mu)$, other than the index of the branch for the chemical potential. This branch of the CM system acts in a *linear* mode, with input equaling output fluxes at open-circuit equilibrium. The lower branch could have been taken directly from the lower branch of the dc internal system, since the CM process effectively creates another 'cool' electron at the bandgap. However, it is more accurately modeled as another, parallel, circuit where the input current/signal is the fraction of photons undergoing CM, given

previously by the fraction θ from Eq. **IV.4**, and multiplied by a conversion efficiency factor f_m for consistency. The factor θ itself can be described using signal diagrams, as is shown in Fig. **V-2c**, with θ being the division of the original spectrum after a HPF with threshold at $2E_g$, by the original spectrum with an HPF threshold at E_g (this threshold occurs due to the bandgap, which acts as a HPF). The output of this branch also feeds into an internal TF, which can theoretically be held at a different voltage, with $H_{CM}^{2}(\mu_2)$. The total re-emission from the cell is the combined output of $H_{CM}^{1}+H_{CM}^{2}$. Since these occur internally, we are interested in the *total* TF of the system, as delineated by the dashed line in Fig. **V-2b**. This can be found by adding the two internal TFs together. If we further argue that the chemical potential must be uniform, then $\mu_1=\mu_2$, resulting in a total TF of:

$$\boldsymbol{H_{CM}^{total} = H_{CM}^{1}(\mu_1) + H_{CM}^{2}(\mu_2) =|_{\mu_1=\mu_2} (1+ f_m\theta)H_{reg}(\mu)} \qquad \textbf{V.1}$$

Using this formalism, we can see why the CM process with this model provides no gain for the V_{oc}, since the V_{oc} is derived and defined at $H_{reg}(\mu_{oc})=0$; the added factor, $(1+f_m\theta)$, cancels out.

The advantage of the TF method for these 3rd generation concepts is that they allow one to easily recognize where the losses that can occur in the system will affect the overall characteristics of the PV conversion. Each branch of the diagrams can be considered as a separate impedance, or voltage/current supply, and dismantling one of them will directly affect the circuit. In the case of dc, an inefficiency in the dc conversion branch will result in a less favorable spectrum irradiating the cell; however it will not directly create losses in the cell, other than a slight drop in current and voltage if $f_m=0$. In contrast, in the CM system this branch is internal, and will affect the V_{oc} directly. This can be seen if the bottom branch is 'ruined' (open-circuited, or short-circuited): we required that $\mu_1=\mu_2$, but this can no longer be maintained if the CM process (the multiplication process itself) is cut off. From a material perspective, it becomes clear that anything affecting the internal CM process will detrimentally affect the entire crystal structure of the solar cell, whereas in the dc system, this loss is outside the solar cell itself. Once again, we emphasize that the losses in the CM process are internalized, whereas in the dc process, they are externalized, essentially outsourcing the losses to a spate material system.

2. Transfer Functions of Up-Conversion and Intermediate Band Cells

Until now, we have only described dc and CM as methods of improving the efficiency of solar cells beyond the SQ limit. Those methods address the problem of the higher energy photons whose excess energy is "wasted" through thermalization. An alternative approach is to make use of the lower energy photons, whose energy is below the bandgap of the semiconductor and are therefore transparent. There are two popular concepts to improve the efficiency using these photons: Up-Conversion (uc) and IB cells, whose simplified band diagrams are depicted in Fig. **V-3**.

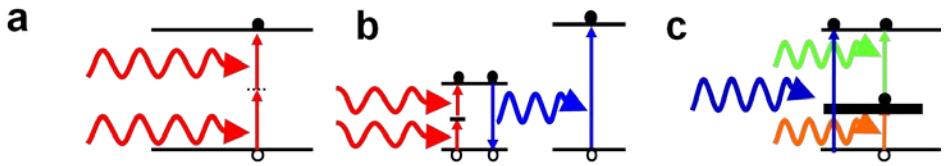

V-3 Band Diagrams of the Up-Conversion and Intermediate Band Cell. (a) The uc cell accepts two lower energy photons (with energies below the bandgap), and excite an electron to the conduction band via a trap or virtual state. The two photons must be absorbed nearly simultaneously by the same electron for this to occur. (b) The uc system with an intermediate layer, whereby the lower energy photons are first absorbed in a layer with a midlevel trap, and then converted to a single, bandgap energy photon that is absorbed by the cell. (c) The IB cell has an isolated band within the bandgap, that can absorb photons both directly (blue) at the bandgap, or into the intermediate bands (orange and green), with the cumulative effect of absorbing the lower energy photons.

The uc cell **[87-89]** makes use of lower energy photons by having two lower energy photons absorbed simultaneously at the bandgap, such that an electron is excited via a trap, or virtual state in the middle of the bandgap. This process can immediately produce an electron for the cell (Fig **V-3a**), or be used to produce another photon at the bandgap (Fig. **V-3b**). This process does not violate the conservation of energy, since (in its most simplified form), the energy of the two photons together adds up to the energy of the bandgap. However, the uc process is an *intensity dependent* process, since there is a very low probability that the second photon will come along at the same time and place as the first photon to help excite the electron to above the bandgap. For the process to occur, there should be a large number of photons within the cell, with the correct energies for the process to occur, and is therefore a function of the intensity of the incoming radiation. It should be noted that the uc process is *not* the mirror image of the dc process: the dc process is not an intensity related effect, and is a matter of the material parameters. Furthermore, the uc process relies on an increased lifetime of the electron within the trap/virtual state so that the second photons can be absorbed in a reasonable (finite) amount of time; the dc process merely requires that the trap state allow the electron to recombine in a radiative manner.

The IB cell **[65]** employs a unique form of material that has a ‘trap’ state that has coalesced into a single band lying within the bandgap **[64]**. This band is essentially a non-zero density of states within the bandgap of the semiconductor, which is a ‘paradox’ considering the meaning of the term ‘bandgap’. Nevertheless, there have been multiple theories for how to create such a band, and what its characteristics would need to be for it to be useful as a solar cell material **[90-92]**. In fact, there has recently been work showing that such a material is possible, using specially designed structures **[93]**. The band structure of an IB device appears in Fig. **V-3c**. The IB cell can absorb all the photons above the bandgap, just as a regular cell can, but can also utilize the lower energy photons by having them first be absorbed by the lower band, and then have another set of photons excite them further to the bandgap. The electrons are connected to a circuit *only* via the larger bandgap, with the internal band isolated from the circuit (a technically challenging feat). The IB cell is therefore designed to work at the larger potentials of bandgap, while increasing the current via the internal band. This band must be filled with electrons at all times in order for the effect to work **[92]**, and it also must have internal absorption coefficients

that only allow absorption of light to occur for the correct set of bands **[91]**. These and other limitations make the concept of IB bands quite difficult to achieve, however the feasibility of the IB technique will not be related here.

The uc and IB devices ostensibly vie for the same goal: to utilize the lower energy photons more effectively. Since the band structures in momentum-space are relatively symmetric (as in Fig. **I-5**), the first-second/upper-lower photons in the uc/IB models should also be symmetric in energies. This simplification is used to both shorten the derivation below, but also to point out that the uc/IB techniques are also *process limited* to the *lower* of the two photon rates: if there are 1000 photons at hv_1 and 2000 photons at $hv_2>hv_1$, then the number of electrons at the conduction band will be limited by the *smaller* of these two numbers. Since the photon rate follows the Planck spectrum and is non-uniform, we expect the photon rates to be different for each energy segment, and the maximal rate of electron excitation generation (for photons below the bandgap) will be maximized when the two rates of photons (first-second/upper-lower) are equal, meaning that the trap state (intermediate band) is in the *center* of the bandgap. This ignores the 'thickness' in energy of the trap state itself, which is assumed to be negligible.

The TF of the uc and IB systems will be here taken as nearly identical, since they only affect a portion of the incoming spectrum that would otherwise not have been utilized. The TF is displayed in Fig. **V-4**, with the IB cell contained within the dashed lines, including both internal branches, and the uc section isolated by the dotted lines, which emphasize the fact that the uc layer has a separate thermodynamic boundary than the solar cell itself. The upper branch of the TF contains the photons above E_g, which are unaffected. This is shown as passing through a HPF at E_g but this is not strictly necessary, since the solar cell itself will limit the absorption to above E_g via the absorption coefficient, α_{abs}, as in Eq. **I.8**. The lower branch only utilizes the photons with energies from half the bandgap up to the bandgap, as characterized by the BPF from $½E_g \rightarrow E_g$. It is then passed through an internal TF, which is similar to the internal TF from above, and which is characterized at open-circuit equilibrium (since the uc layer, or the internal band carry no current) by the equation:

$$H_{\text{int}}^{uc} : \frac{1}{2}\Omega_S \int_{E_g/2}^{E_g} \frac{E^2 dE}{\exp[E/kT_S]-1} = \Omega_o \int_{E_g}^{\infty} \frac{E^2 dE}{\exp[(E-\mu_{uc})/kT_{uc}]-1} \qquad \textbf{V.2}$$

This equation is quite similar to the dc layer's equilibrium from Eq. **III.2**, however, the factor of ½ is placed on the left hand side since every outgoing photon at E_g is supplied by 2 photons from the sun in the range $½E_g \rightarrow E_g$. Eq. **V.2** thus defines the internal production of the outgoing uc emission, without needing to understand how it occurs (whether by a trap or virtual state), as long as it follows the vRS emission on the output end. Finally, we add a conversion efficiency factor, f_m, for possible inefficiencies. These two branches are recombined, to create the new spectrum irradiating the solar cell, with TF H_{reg}.

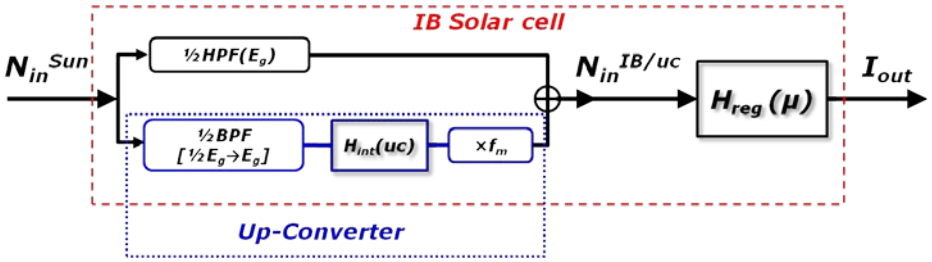

V-4 Transfer Function of the uc and IB Cells. The upper branch controls the photons above the bandgap, and the lower branch transforms some of the lower energy photons into higher energy ones, at a rate of half the incoming rate. The difference between the two techniques is demonstrated by the dashed/dotted lines, which encompass the boundaries of the IB/uc segments.

An additional perspective of viewing the uc/IB cells is to only focus on the absorption coefficient of the semiconductor alone. Instead of viewing the uc/IB cell as a linear material following Kirchhoff's law of radiation, with $\alpha_{abs}=\varepsilon_{emit}$, we can say that the uc/IB system emits at the bandgap, such that:

$$\varepsilon_{emit}^{uc/IB}(E)=u(E_g)=\begin{Bmatrix}0 & E<E_g\\ 1 & E>E_g\end{Bmatrix} \qquad \textbf{V.3}$$

with u being the Heaviside/step function, but in contrast the absorption is:

$$\alpha_{abs}^{uc/IB}=\frac{1}{2}\times\left[u(E_g/2)+u(E_g)\right] \qquad \textbf{V.4}$$

Note that the contribution from $u(E_g/2)$ adds up with the contribution from $u(E_g)$ after the step at E_g.

The formulas and TF above allow us to calculate the efficiencies of the uc/IB system, as well as isolate the contribution of the extra charge density to the V_{oc}. Following the procedure used to derive the dc and CM systems, the V_{oc} can be found using the approximations of the previous chapters ($E>>kT_S$ and $E-\mu>>kT_c$), to obtain:

$$qV_{oc}^{uc/IB}=qV_{oc}^{reg}+kT_c\ln\left(1-\frac{f_m}{2}+\frac{f_m}{8}\frac{\alpha_{uc1}}{\alpha_{S1}}\exp[E_g/2kT_S]\right) \qquad \textbf{V.5}$$

with V_{oc}^{reg} as defined in Eq. **II.6**, α_{S1} as defined in Eq. **II.7**, and a new small correction term:

$$\alpha_{uc1}=1+4\frac{kT_S}{E_g}+8\left(\frac{kT_S}{E_g}\right)^2 \qquad \textbf{V.6}$$

Eq. **V.5** contains a 'gain' term, similar to the dc system, which is a function of the bandgap. However, since the exponent contains a fraction of $2kT_S\approx1$ eV, for most values of bandgap, this contribution is quite small, and almost entirely negligible. Furthermore, for values of $f_m<1$, this

contribution will be even more negligible. While the entropy change has the same meaning as the dc case, as being the change in ration between the new and original spectra, this change is nearly meaningless since the number of photons in the blackbody spectrum below E_g is not that large. This is particularly true after being multiplied by a factor of ½ due to the conversion process of two photons in, and one photon out.

The efficiency can be calculated for the uc/IB processes for different values of concentration, as well as f_m, the uc/IB conversion efficiency. The plot in Fig. **V-5** displays the efficiency values for a regular solar cell for comparison (black), as well as the efficiency for an ideal uc/IB system (f_m=1, blue) and a system with some inefficiencies (f_m=0.5, red), under different concentration conditions. The efficiency of the uc/IB system improves the efficiency to 46.57% at an optimal bandgap of 1.95 eV (up from 30.4% at 1.32 eV), under no concentration (solid blue curve), and up to 55.61% at a maximal concentration of C^{max}=46,000 and an optimal bandgap of 1.69 eV (dashed blue curve). From this simple model, it is nearly as efficient to have a uc/IB layer with an internal conversion efficiency of f_m=0.5 with no concentration (solid red curve) as having maximal concentration for a regular cell (dashed black curve, and which will be claimed in Chapter **VIII** to be nearly impossible to achieve). However, this maximum will occur at a slightly higher bandgap.

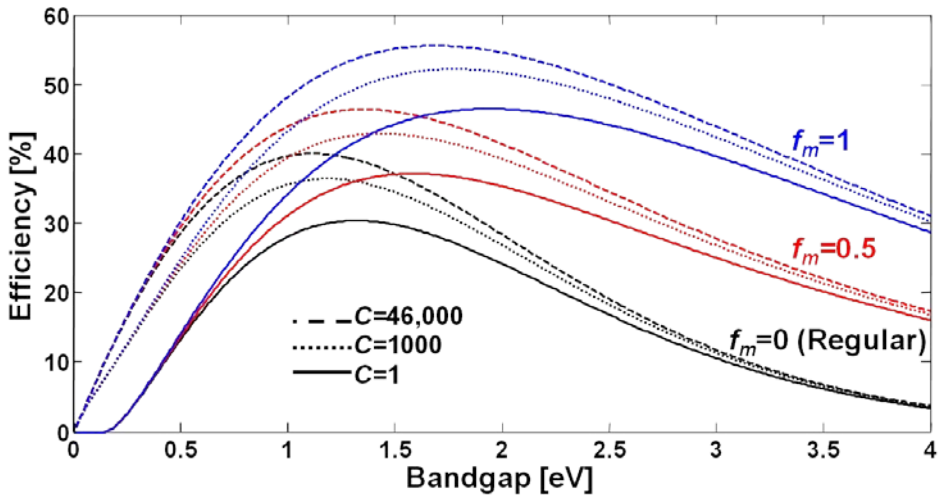

V-5 Efficiency of the uc/IB Systems. Plotted is the efficiency of the uc/IB system under different ranges of concentration: *C*=1, solid line; *C*=1000, dotted line; *C*=46,000, dashed line. The black curves represent the regular solar cell efficiency, with f_m=0. The blue curves represent the idea uc/IB performance, with f_m=1. The red curve represents the non-ideal performance, with f_m=0.5.

The high efficiencies reported as possible using uc or IB (which are slightly different from those given here, since the uc/IB model here is a near ideal model) include a logical fault, in that they assume that all the photons between $½E_g \rightarrow E_g$ are absorbed within the uc or IB system, yet no description of the momentum matching is used. For example, for the IB band diagram of Fig. **V-3b** only displays the *x-space* component of the intermediate band and is completely straight, however, it does not include the *k-space* component, which may be curved (as in Fig. **I-5b**). This curvature will prevent photons from being absorbed in a uniform fashion

throughout the semiconductor, and will cause the system to be process limited by the number of absorbed photons on the *top* layer alone. Likewise for the uc system, single trap states interspersed within the bandgap will require a highly momentum matched second photon to be absorbed to excite the electron up to the conduction band. Moreover, both systems will require a long lifetime of the electrons in the mid-level state. Note that these considerations are not relevant for the dc and CM systems. Finally, the difference between the uc and IB methods in terms of losses is the same as in the difference between the dc and CM methods: by combining all the spectral splitting within the boundaries of the solar cell in the IB system, any internal losses to one of the branches will immediately effect the entire solar cell, as opposed to having a separate layer do the spectral combination.

3. General Comparison between 3rd Generation Methods

The four concepts described until now for improving the efficiency beyond the SQ limit were described in pairs. This distinction emphasizes the two segments of the solar spectrum that are either un-utilized or not utilized as effectively as possible. The single-junction paradigm for a solar cell assumes an optimal bandgap that is best suited for both absorbing the spectrum, and producing enough voltage to create maximal power. The 3rd generation methods described until now have retained that paradigm of a single junction, which is why a single, optimal bandgap was found for each method. The choice of the bandgap immediately splits the solar spectrum into two (unequal) parts: transparent photons and excess-energy photons, or thermalized photons and unused photons. Furthermore, of the four techniques described until now, they were either a separate layer (dc and uc), or a new form of semiconductor that made use of a physical phenomenon that better utilized the spectrum internally. We can split these into an optical category, which spectrally modifies the incoming spectrum, and a solid-state category, which creates internal bands and multiplications. These categories are described in Fig. **V-6**, in a "square" matrix.

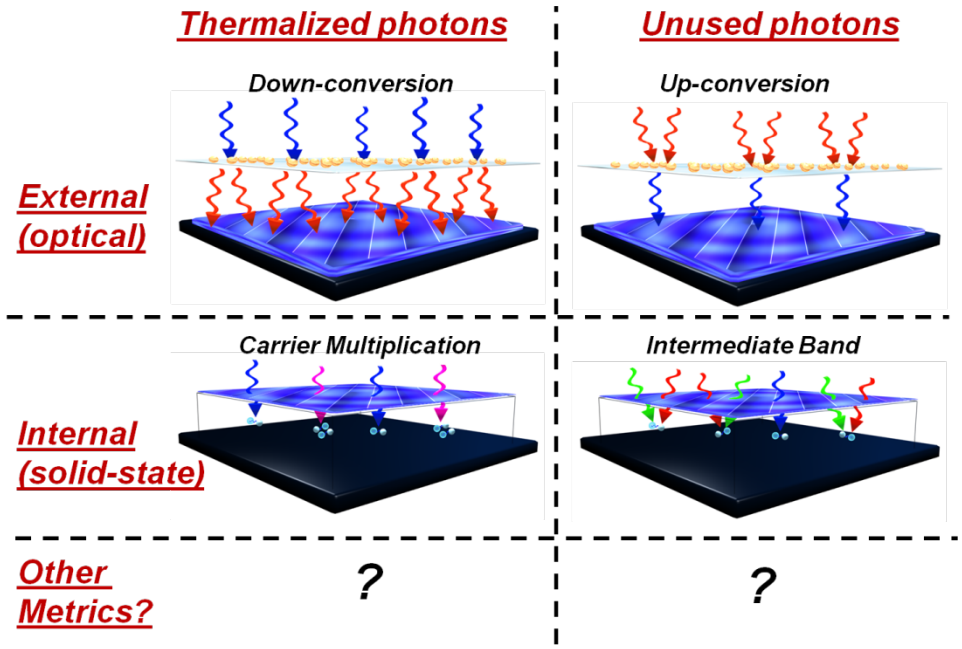

V-6 Categorizing 3rd Generation Methods. The columns depict the segment of the solar spectrum that can be improved, and the rows depict the method of improving, either external or internal. Other metrics can be added to these rows, whereas adding another column can be done by using a multi-junction cell.

The arguments made in this chapter – that the external methods of producing an efficiency improvement are better than internal ones – is in general the opposite trend of current research in PV, where the bulk of research is attempting to find all-in-one solutions to beating the SQ limit. While there is an advantage to having a single material do both the splitting/combining as well as the PV conversion itself, it creates many complexities that can create losses. These losses were contended to reduce the efficiency of the entire solar cell directly, as opposed to the external, multi-material/layer methods, which outsourced the possible losses to a different material system. Since solar cells today are quickly approaching the SQ limit, pushing the efficiency beyond that by using an added layer (as in dc and uc) seems to be more economically viable than building a new form of solar cell from scratch, using exotic materials.

The multi-junction solar cell is an obvious solution to many of these issues, since it replaces the single-junction paradigm, and allows better usage of the solar spectrum, while electronically coupling the cells together to have better voltage control. The multi-junction cells theoretically use more traditional materials, as opposed to the exotic CM and IB materials, but typically require extreme precision and high costs to produce good cells. Further examination of the multi-junction system will be done in Chapter **VII**.

There are other methods of 3rd generation that were not described so far. Chief amongst these is the method of hot-carrier solar cells **[94]**. These cells also attempt to solve the thermalized photon issues using the *internal*, all-in-one approach. The method attempts to slow the thermalization of photons, and particularly, to produce a bandgap of *phonons* so that the excited (hot-carrier) electrons generated by high energy photons cannot transfer their excess energy to a

phonon in the crystal. This method also has many internal requirements, some of which are in contrast of the typically characteristics of an ideal solar cell **[95]**. For hot-carrier devices, special electrodes must be used to extract the higher energy electrons from high within the conduction band, without extracting the electrons from the bandgap itself. A second set of electrodes can be used to extract those (regular) electrons, resulting in a device that uses a *single* junction material, but produces *multiple* voltages and current. This technique therefore retains the single-junction paradigm, while encroaching onto the territory of multi-junction cells. It should be noted that the internal structure of the hot-carrier cell results in a *different* internal TF, H_{int}, than the one described until now. Specifically, it may not rely on the simple vRS relation as its output emission (just as the original CM model did not). Consequently, it can be generally stated in this chapter that methods attempting to change the internal functions of the regular TF of a solar cell, H_{int} or H_{reg}, are more complicated than ones which leave the basic physics of the solar cell intact (such as the dc, uc or multi-junction cell systems).

Other methods may be found that tackle these two columns of categories (in Fig. **V-6**), while retaining the single-junction paradigm. In particular, other physical mechanisms can be found that modify the internal TF in a simple way, such that it changes one of the basic assumptions for the SQ DB model. The more assumptions that are broken, the more difficult the solar cell is to be made, but small changes to the assumptions can sometimes provide enough of an efficiency change to be worthwhile. For example, instead of increasing the étendue of the incoming beam via concentration, we can limit the outgoing étendue using optical means.

The next chapter addresses such a modification, by using *feedback* to modify the internal TF of a solar cell, such that the SQ DB limit does not strictly apply.

VI. Feedback Method of Shifting the Optimal Bandgap

**Publication note*[5]

The internal TF, H_{int}, presented in Chapter **II** assumed that the semiconductor was a "black box" that would emit LED-like radiation (following the vRS relation), as a function of the input. This TF was essentially a description of all of the assumptions made in the DB model, with the amount of outgoing flux equal to the incoming flux for a perfect cell. While it was less useful for developing models for other 3rd generation techniques, for which we used the TF H_{reg}, there are nevertheless still changes that can be made to this TF to adjust the characteristics of the SQ DB limit. The uc and dc methods involved a shift of the optimal bandgap of the underlying semiconductor caused by a shift in the input spectrum onto the solar cell. This also involved an efficiency gain due to breaking one of the assumptions used in the DB model: that the input spectrum is that of the sun (the CM and IB methods break other assumptions). The assumptions in the DB model did not even include the possibility of concentration, which utilizes optical means to modify the spectrum, and can increase the efficiency; however it easily can include it. In this chapter, another optical method is used, that similarly changes the optimal bandgap of the solar cell, and doesn't require any exotic materials to be used.

1. Optical Feedback Theory

The input and output spectrum in H_{int} from Fig. **II-3a** were assumed to be unchanged. A simple technique that is obvious to use when drawing system/signal diagrams is the *feedback* technique, where the output is fed back into the input. This is typically done by reducing the input by the output, in what is known as a *negative feedback loop*, and which prevents a system from losing its equilibrium. Feedback techniques are generally used to increase the stability of an electronic or mechanical system. The system will reach a new equilibrium point when the output is fed back into the system, and a new steady state will be reached. This feedback loop can be seen in Fig. **VI-1**, with the output added to the input in a *positive feedback loop* signified by the "+" sign. Usually, a positive feedback loop is unstable, since the system will continuously build up a current or voltage that will exceed the material (or system) limits allowed. For the solar cell, in open-circuit equilibrium, the semiconductor relieves the "pressure" of the incoming flux by emitting photons at the bandgap, as a function of $qV_{oc}=\mu_{oc}$. We saw that in the dc system, and in a concentrating system, the increase in photon flux was associated with a shift in the chemical

[5] The following is taken mostly from Ref. **[96]**. This chapter includes much that was not included in that paper; in particular, it includes the description of the selective reflector as a feedback system, and many new figures. The interpretation of the system as a feedback system was hinted at in the original paper, but this chapter has been re-written to fit with the preceding chapters in terms of transfer functions and input/output diagrams. Furthermore, since this dissertation only includes portions of the work done by myself, it does not include "Figure 3c" from that paper.

potential, to increase the linewidth of the outgoing emission. Therefore, we would expect such a shift to occur if we increase the illumination flux in any way.

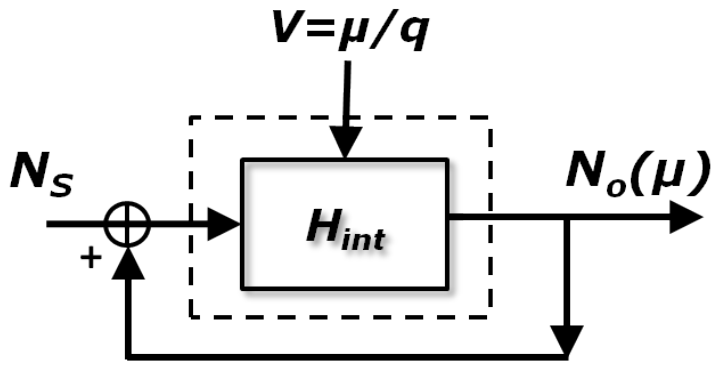

VI-1 Feedback Loop Design of a Solar Cell. The output flux is fed back into the input, in a positive feedback loop. The equilibrium voltage, V_{oc}, will change as a result of the different input.

The feedback loop design of Fig. **VI-1** is possible only if there is some method of optical feedback that can allow the outgoing emission to be diverted back into the cell. Optical confinement designs for solar cells have been thought of, particularly optical cavities **[32,97]**, but typically have the problem that if the output is completely confined by (e.g.) mirrors, then it will prevent the incoming light from being absorbed as well. However, we can make use of the disparity between the spectrum of the incoming and outgoing fluxes to block as much of the outgoing light as possible. It should be noted that the thermodynamic boundary of the cell remains the dashed line in Fig. **VI-1**, and it denotes that the properties of the emission must follow the vRS relation, unless some other exotic physical principal is used.

It can be recalled from Fig. **II-2** that the outgoing emission is tightly confined around the bandgap and chemical potential, so if we were to place an energy selective reflector around that emission bandwidth (the linewidth of the emission peak), we can block most of the outgoing light. By placing a *reflector* there the outgoing light is then reflected back into the cell. However, it will easily be noticed that if such a reflector is placed around the cell (or above it), it will also block some of the input light from being absorbed, which is detrimental to the current generation. Fig. **VI-2a** displays a conceptual cell with an optical feedback reflector design. The selective reflector allows higher energy photons to pass through it (blue and green, acting essentially a HPF or a BPF, as will be described below), and blocks lower energy photons (red). This includes the band-to-band recombination flux (red), which is confined within the cell-reflector system. Only higher energy photons (green) are allowed to exit the system.

The equilibrium condition is set when the incoming and outgoing fluxes are equal (assuming the material remains in the linear regime), just as with any other solar cell. Since the recombination photons are not allowed to escape, they will continuously be re-absorbed and emitted within the optical cavity, creating a build-up of electrons at the conduction band. This build up will shift the chemical potential slightly higher, by an amount $\mu_{oc}^{new}=\mu_{oc}+\delta$. Electrons at this slightly elevated energy level will also be emitted, but if the bandwidth of the selective

reflector is Δ, as shown in the band diagram of Fig. **VI-2b**, then they too will be reflected. Only when the population of electrons in the conduction band is elevated enough such that the Fermi level (chemical potential) is shifted to the height of the barrier, will photons be allowed to escape, and the build-up will stop. In Fig. **VI-2b**, this is portrayed as an absorption of all the photons with high energies down to the top of the selective reflector edge (violet-green), and then emitted once the Fermi level is shifted to the top of the reflector height (green).

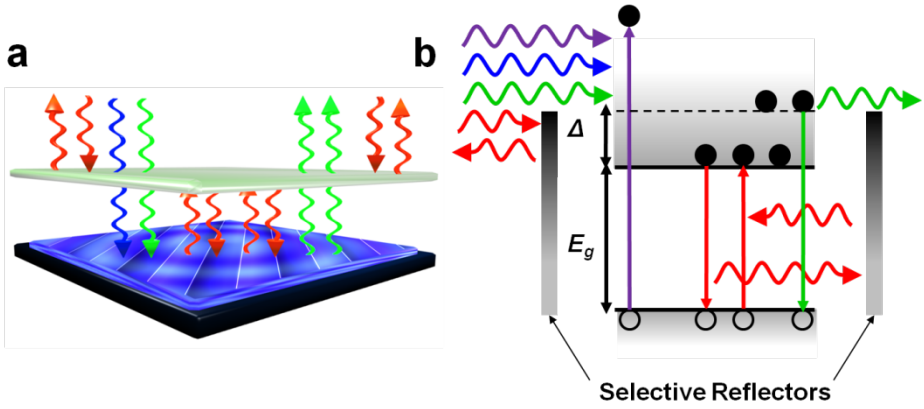

VI-2 Schematic of the Selective Reflector Design and Band Diagram. (a) Simplified drawing of the selective reflector design, with an energy selective reflector placed above a theoretical cell with a back reflector. High energy photons (blue, green) are transmitted, whereas lower energy photons (red), including the recombination photons, are reflected. The only light that can escape the cell-reflector system must be of higher energy (green). (b) Band diagram of the system, with the same color scheme as in (a). The recombination photons are fed back into the bandgap, such that there is a build-up of electrons at the band edge that are continuously emitted and re-absorbed. This build-up will induce an upward shift of the chemical potential, such that the photons emitted from the cell will be shifted to higher energies and escape.

The amount of light to be blocked by the reflector, Δ, is critical, since it both creates the feedback loop, but also reflects some of the incoming light. Blocking too much light will result in a drop in efficiency, since the current will drop to zero, despite the rise in chemical potential. Ideally, only light around the bandgap needs to be blocked, from E_g to $E_g+\Delta$, being a BPF; however, since the light below E_g is transparent to the semiconductor, using a HPF up to $E_g+\Delta$ would work as well. These combinations are shown in Fig. **VI-3**, including also the possibility of using a BPF whose lower threshold, E_L, lies somewhere within the bandgap. The advantage of using a HPF is that it blocks light that may create thermal phonons via absorption within the conduction band (free carrier absorption), however may be difficult to manufacture such a wide bandwidth HPF. The BPF option allows more freedom in the reflector design.

Note that although the term “filter” is used here in the HPF/BPF, it must be a *reflector* in order for the design to work. The reflectance of the photons constitutes the optical feedback design, and an absorptive material will simply result in less absorption current, since the thermodynamic boundary is at the surface of the *semiconductor*, as portrayed in the dashed line in Fig. **VI-1**, and not at the surface of the reflector/filter. Furthermore, the feedback design is what controls the stability of the cell-reflector system: If the reflectors are suddenly removed, the

entire systems will emit a large number of photons (in the range $E_g \rightarrow E_g+\Delta$), in a single burst, until the original equilibrium state is returned, with the incoming emission equaling the standard vRS re-emission. Furthermore, when current is extracted from the system, the feedback loop retains the elevated chemical potential, thus maintaining the stability of the system.

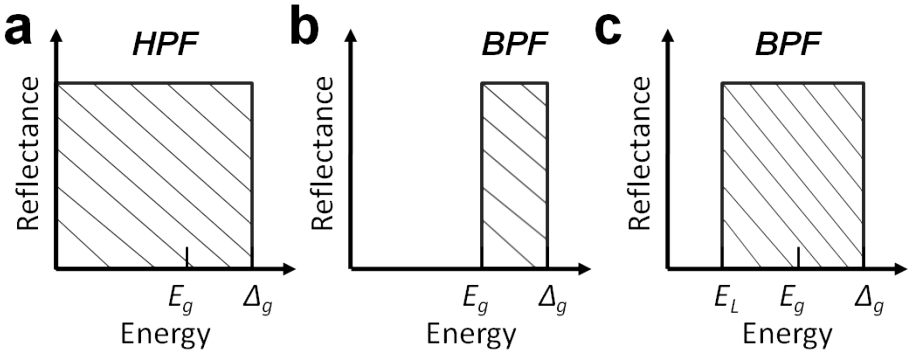

VI-3 Bandwidth Characteristics of the Selective Reflector. (a) HPF, reflecting all light below $E_g+\Delta$. (b) BPF blocking light from the bandgap up until Δ. (c) BPF with a lower threshold within the bandgap.

The elevated chemical potential can be found analytically by using the flux equilibrium method on the new system. The flux equilibrium condition is met when the incoming and outgoing emission rates are equal. Since the solar cell has remained unchanged (without any internal modifications, as in the CM system), its output characteristics are retained within the vRS relation. However, the input flux must now include the portion of the reflected light:

$$\Omega_S \int_{E_g+\Delta}^{\infty} \frac{E^2 dE}{\exp[E/kT_S]-1} + \Omega_o \int_{E_g}^{E_g+\Delta} \frac{E^2 dE}{\exp[(E-\mu_{oc})/kT_c]-1} = \Omega_o \int_{E_g}^{\infty} \frac{E^2 dE}{\exp[(E-\mu_{oc})/kT_c]-1} \quad \textbf{VI.1}$$

The incoming spectrum (leftmost term) is limited from below by the selective reflector edge, at $E_g+\Delta$, but now also includes the feedback re-emission from the semiconductor (using the vRS relation), from $E_g \rightarrow E_g+\Delta$. By rearranging Eq. **VI.1**, we can simplify the equation to:

$$\Omega_S \int_{E_g+\Delta}^{\infty} \frac{E^2 dE}{\exp[E/kT_S]-1} = \Omega_o \int_{E_g+\Delta}^{\infty} \frac{E^2 dE}{\exp[(E-\mu_{oc})/kT_c]-1} \quad \textbf{VI.2}$$

This equation is quite similar to the equilibrium condition for a regular cell, apart from the lower limits of integration. The similarity between the equations could lead one to assume that the only modification between the two systems is that the absorptivity and emissivity of the semiconductor have been changed from $\alpha_{abs}=\varepsilon_{emit}=u(E_g)$ to a new step function, $u(E_g+\Delta)$, however, this is only an effective shift in the absorptivity/emissivity as can be seen from Eq. **VI.1**, if the second term for the feedback re-emission is modified to include losses, or if the angular dependence of the re-emission is not the same as the emission from the solar cell: Ω_o.

The V_{oc} for the system can be isolated from Eq. **VI.2** using the regular assumptions ($E>>kT_S$ and $E-\mu>>kT_c$), to obtain the shift:

$$qV_{oc}^{SR} \cong \left(E_g + \Delta\right)\eta_C + kT_c \ln\left[\left(\Omega_S/\Omega_o\right)\left(T_S/T_c\right)\left(\alpha_{S\Delta}/\alpha_{c\Delta}\right)\right] \quad \textbf{VI.3}$$

with small correction terms α_{Δ} and $\alpha_{c\Delta}$ given by:

$$\alpha_{S\Delta} = a_{S1} + 2\frac{\Delta}{E_g} + \left(\frac{\Delta}{E_g}\right)^2 + 2\frac{kT_S\Delta}{E_g^2}$$
$$\alpha_{c\Delta} = a_{c1} + 2\frac{\Delta}{E_g} + \left(\frac{\Delta}{E_g}\right)^2 + 2\frac{kT_c\Delta}{E_g^2} \quad \textbf{VI.4}$$

with α_{c1} given in Eq. **II.8**, and α_{S1} given before in Eq. **II.7**. The shift in open-circuit voltage from that of a regular cell is therefore:

$$V_{oc}^{reg} \propto E_g$$
$$V_{oc}^{SR} \propto E_g + \Delta \quad \textbf{VI.5}$$

In contrast, the short-circuit current is *reduced* due to the reduced absorption, to:

$$I_{sc} \cong qg\Omega_S \int_{E_g+\Delta}^{\infty} \frac{E^2 dE}{\exp[E/kT_S]-1} \quad \textbf{VI.6}$$

The efficiency of the device with the selective reflector is found in the usual way, by maximizing the product $P=I\times V$, and is presented in Fig. **VI-4** for varying bandgaps, as well as varying bandwidths of the reflector. As is shown, for rising values of Δ, the optimal bandgap is shifted to lower energies on the left, in relation to the regular SQ DB curve given by Δ=0.

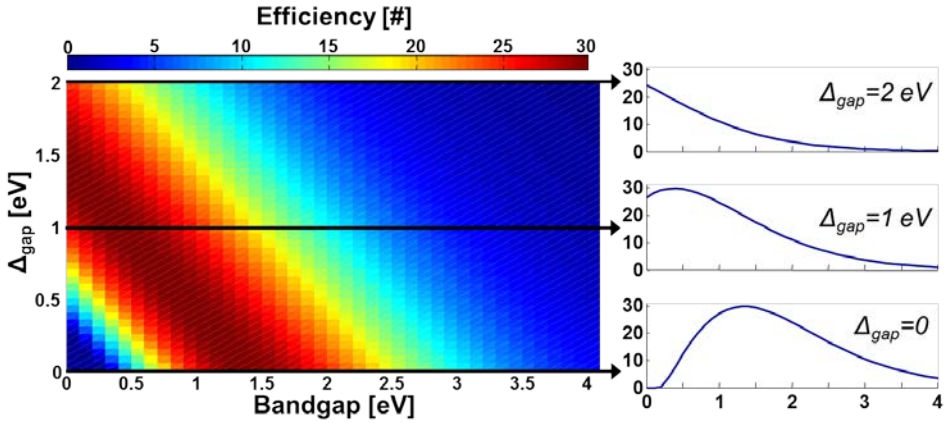

VI-4 Efficiency Calculation for a Selective Reflector System. The efficiency is calculated for various bandgaps and reflector bandwidths, Δ. To the right are the cross-section curves, beginning from the regular SQ DB curve on the bottom (Δ=0), and demonstrating the shift to the left for increasingly high bandwidths.

The concept of confining the outgoing photon flux was thought of by other authors, mainly as a way of improving the efficiency of a given system as close to the SQ limit as possible **[98,99]**. Particularly, as a means of reducing the thickness (amount) of the material needed for the solar cell, by using the light confinement technique to increase or optimize the absorption characteristics. In addition, this concept has been thought of for use in multi-junction systems **[100]**, and even IB cells **[101]**. However, it was generally assumed that the maximal voltage that this shift can achieve is limited to the bandgap, such that $V_{oc}^{max}=E_g$ **[102,7]**. Anything above this value was assumed to induce such a high concentration of carriers that the assumption in Eq. **I.14** that the spontaneous emission can be neglected is no longer valid **[103, 32]**. The stimulated emission will therefore probably become a limiting factor for this process, and may prevent the build-up of electrons to the height of the reflector barrier. Additional limiting factors may occur as well, due to the high concentration of light in the confined cell-reflector system. For example, this high intensity may induce a refractive index change in the solar cell, or induce other nonlinear effects **[104]**. Finally, Auger recombination will provide another limiting process **[102, 105]**, regardless of how high the chemical potential is shifted, as will be shown below.

2. High Carrier Concentration Limiting Factors

The shifting of the Fermi level in the material by a factor of Δ, as appearing in Eq. **VI.5**, is similar to another optical effect known as the Burstein-Moss (BM) shift **[104,106,107]**. This well-known effect causes the effective absorption coefficient of a semiconductor to "blue-shift", meaning to shift to higher energies, when the carrier concentration in the conduction band is increased. The carrier concentration increase can be created by heavily doping the semiconductor. The cause for this shift is that if the conduction band is full, photons with energies at the bandgap cannot excite electrons from the valence band to the conduction band, and require a slightly higher energy to be absorbed. More specifically, the *dynamic* BM shift **[108,109]** is the same effect, where the carrier concentration increase is induced by an external optical source (e.g. a laser pulse) that excites the carriers. The major difference between the two effects is that the dynamic BM effect can be implemented in a pristine (intrinsic) material. The dynamic BM effect has been shown to create large shifts in the effective bandgap of the material, even hundreds of meV, in various semiconductor materials **[109,110]**. The analogy between the dynamic BM effect and the effect described for the selective reflector design is clear, however it has yet to be shown that real semiconductor materials can handle the large shifts predicted.

The major advantage of the feedback design is that it allows the shift in the optimal bandgap of the cell to lower energies. The traditional materials used to make solar cells is typically limited to those that can achieve as close to the SQ limit as possible, and therefore lies in the range of ≈1-1.5 eV. These materials include Si, GaAs and CdTe, as shown superimposed on the SQ curve in Fig. **VI-5**. Using the optical feedback, this curve can be shifted to the left, and other materials, such as FeS_2 (Pyrite), GaSb and Ge can then be considered for use as optimal materials. While GaSb and Ge are used in multi-junction cells (bandgaps of 0.73 and 0.67 eV, respectively), a material like FeS_2 – which is an earth-abundant material **[111]** – and has a non-optimal bandgap (≈0.9-0.95 eV), can begin to be considered for use as solar cell materials. FeS_2, despite being an *indirect* bandgap material **[112]**, has an extremely high absorption coefficient,

making it an interesting possibility for a PV material. In contrast, Ge is also an indirect bandgap material, whose absorption coefficient is more similar to Si, and is therefore typically limited to inefficient PV conversion due to non-radiate trap states, known as Shockley-Read-Hall (SRH) recombination **[113]**.

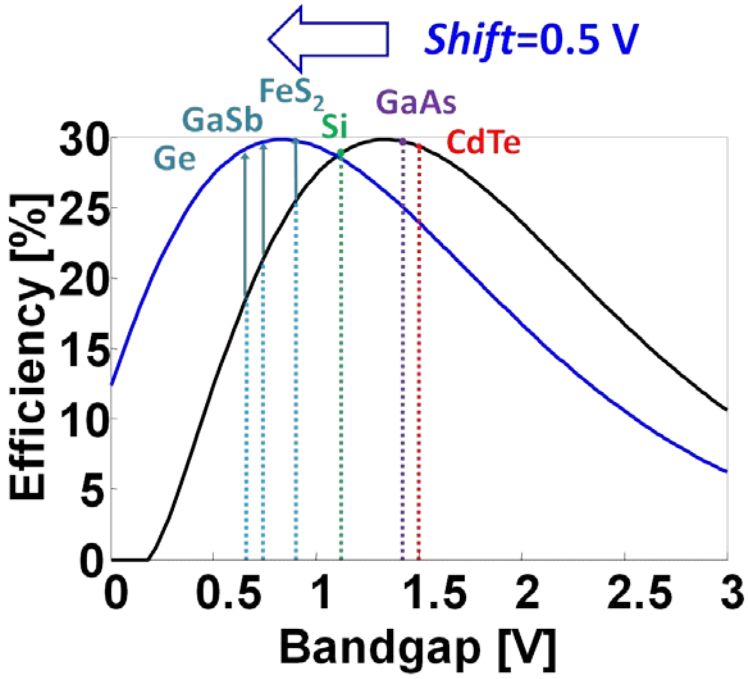

VI-5 Shifting of the Optimal Bandgap for Solar Cells. The SQ curve has a maximum at around 1.3 eV, limiting the number of materials that are near optimal for use as solar cells, such as Si, GaAs and CdTe. A shift of Δ=0.5 eV using a reflector can allow other materials to be considered, since their efficiencies could reach the optimum.

Other than stimulated emission limiting the shifting of the optimal bandgap, there is also the non-radiative Auger loss mechanism that typically reduces the possibility of ideal efficiency conversion, particularly under high carrier concentration densities such as those seen in concentrator systems **[114]**. Modeling the Auger, using the simplified thermodynamic relations, can be done by adding an additional "emission" term to the right hand side of Eq. **VI.2 [105]**. This term includes the intrinsic concentration of carriers, n_i, as well as a measured Auger recombination coefficient, C_{Aug}, as a function of voltage and thickness of the device:

$$N_{Auger} = LC_{Aug} n_i^3 \exp[3qV / 2kT_c] \qquad \textbf{VI.7}$$

The volume dependence of the Auger recombination is here only dependent upon the thickness, L, since the area (in m^2) is divided out in equations such as Eq. **VI.2**, which is a measure of flux per unit area. The third power of the intrinsic carrier concentration is due to the interaction between three types of carriers (e.g. two electrons and a hole), as was shown in Fig. **IV-2**. Direct bandgap materials such as GaAs and GaSb typically have much lower Auger coefficients than indirect bandgap materials, by a factor of 10^{-1} or more.

The Auger recombination was added to the calculation of the efficiencies, as a function of both thickness, L=0.1-10 µm, and bandwidth, Δ=0-0.3 eV, and displayed in Fig. **VI-6** for the materials described above. Ge was calculated with E_g=0.67 eV, C_{Aug}=10^{-31} cm^6/s, and n_i=2×10^{13} cm^{-3} **[113]**. Despite the fact that SRH recombination is the dominant recombination mechanism in Ge, we could expect a ≈2% increase if the SRH recombination is suppressed, leaving the Auger recombination alone. GaSb was calculated with E_g=0.73 eV, C_{Aug}=5×10^{-30} cm^6/s, and n_i=1.5×10^{12} cm^{-3} **[115]**. The efficiency increase does not quite reach the ≈31% optimum due to the strong Auger recombination even in thin devices, and is limited to 24.5%; however that still suggests an overall increase of over ≈4%. FeS_2 was calculated with E_g=0.9 eV, C_{Aug}=10^{-29} cm^6/s, and n_i=2.78×10^{12} cm^{-3} **[112]**. The strong Auger recombination effectively suppresses the effect described, regardless of the bandwidth shift. If the Auger recombination coefficient is improved (e.g. to C_{Aug}<10^{-31} cm^6/s **[112]**), the overall efficiency may increase. In all these calculations, the absorption was taken as unity to emulate the best-case scenario that can be achieved using various light trapping techniques.

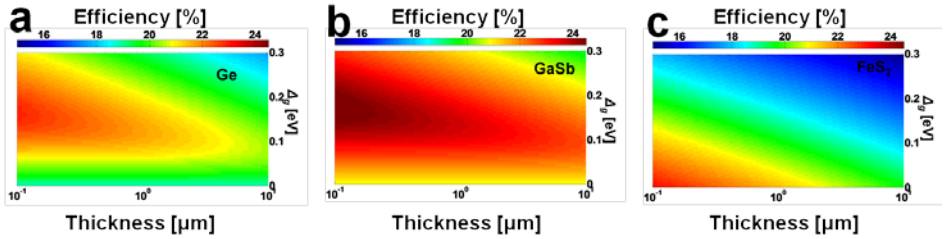

VI-6 Efficiency of Specific Materials Including Auger Recombination. (a) Ge, (b) GaSb and (c) FeS_2. The efficiency is plotted as a function of both thickness (in logarithmic scale from 0.1-10 µm) and bandwidth shifts (up to Δ=0.3 eV). All plots are on the same efficiency scale.

The Auger recombination effectively curtails most of the benefit of shifting the bandgap to lower bandgap materials. However, as was stated above, the inclusion of stimulated emission is a more fundamental loss process for this design. The Auger recombination rate can be suppressed using various techniques, and in fact the Auger recombination is typically known to be reduced in the BM effect **[116]**. The approximate Auger recombination rate of Eq. **VI.7** may therefore not be correct in this format at such high carrier concentrations.

The use of selective reflectors is not only limited to selectively reflecting the spectrum based on *energy*, but can also be used to reflect the angular dispersion of beams **[117-119]**. We noted in Chapter **II**, and in particular in Fig. **II-2**, that there is a mismatch between the small angular input beam and the isotropic output beam, which creates an entropic loss to the V_{oc}. Therefore, if one could restrict the outgoing emission back out of the solar cell at a smaller angle, this loss would be lowered. This concept of selective *angular* emission is quite similar to the concept of selective *spectral* emission, but would achieve a different goal: angular selectivity attempts to raise the efficiency of the cell above the DB limit to approach the UE limit, and is effectively the *inverse* of concentration **[120]**. The ability to selectively reflect the emission of light based on the angular emission has been attempted using various gratings, mirrors and Bragg reflectors, as well as photonic crystals **[118-120]**. It should be noted that there is a subtle difference between using a photonic crystal to selectively reflect the light *externally*, and using a photonic crystal to inhibit emission *internally*. The use of a photonic crystal *within* the lattice of the semiconducting solar

cell is designed to inhibit the spontaneous emission of the semiconductor, effectively reducing the vRS contribution. This can also be done by reducing the temperature of the cell to zero, which was described as the main difference between the UE and DB models. However, creating a photonic crystal within the semiconductor will also detrimentally affect many of the other parameters of the material (since there will be many recombination sites at the increased internal surface areas), and will generally ruin the material for use as a solar cell **[121]**. In contrast, using a photonic crystal outside the cell can reflect the light both angularly, and spectrally; however its properties must be tuned accordingly **[122]**.

The use of the optical feedback cavity in the design described here is also different from the mechanism of *photon recycling*. Photon recycling accounts for the recombination of photons within the cell, which can then be re-absorbed by the cell before escaping outside the (thermodynamic) boundaries of the cell **[123]**. The photon recycling model adds an additional layer of complexity to the analysis of semiconductor solar cells, since it does not simply assume that every photon absorbed is utilized, since every generated e-h pair has a lifetime before it recombines (radiatively). However, as stated in Chapter **I**, the ideal UE/DB models assumed no thickness of the cell, and therefore did not consider any internal processes or lifetimes, thus it provided an upper bound for PV conversion. The photon recycling model therefore was developed to close the distance between the traditional solid-state approach to modeling semiconductor solar cells, and the DB model **[124,125]**. After including the photon recycling in the equations for carrier concentrations, the divergence between the two sets of models has been properly solved.

The production of entropy in the photon recycling model is zero. That is because the re-emitted photons are "cool", and the absorption and emission of band-to-band photons have the same energy and chemical potential, thereby making the process completely reversible. However, for the selective reflector design, we only noted a small change in the derivation of the V_{oc} on the order of α_{Δ}. If we are more exact in the definition of entropy, we should be using the derivate of the chemical potential, as was done in Eq. **II.15**. We can therefore see an entropy difference, ΔS, between the two methods:

$$\frac{\Delta S}{k} \equiv \frac{S^{SR}}{k} - \frac{S^{reg}}{k} \cong \frac{\Delta}{kT_S} \qquad \textbf{VI.8}$$

The term "S/T" was described in Chapter **II** to be a heat loss entropy, and was E_g/kT_S for the regular cell. Here, we see that increasing the amount of photons circulating within the cell, by containing them within a reflector bandwidth of Δ, increases the heat loss by a proportionately similar amount. This heat loss, when coupled with the other fundamental limiting factors, will also contribute to preventing the feedback cell from improving the efficiency by a large amount. Note that the increase in entropy in the feedback system does not directly reduce the voltage since the internal energy, U, is increased by a similar amount, Δ, such that the two factors cancel out. Note however, that the increase in entropy, which typically lowers the overall efficiency of the cell due to its decrease of the open-circuit voltage, does not play the same role here, due to the effective increase in the bandgap. This reminds us that the overall efficiency is always a function of the *product* between the current and the voltage, and cannot be deduced directly from the formula for V_{oc} alone.

The *I-V* curve for the feedback design cell is shifted so that the I_{sc} is slightly reduced, whereas the V_{oc} is greatly increased. This is shown in Fig. **VI-7a**, comparing the cell before the addition of the reflector (black), and after (blue), using a bandwidth of Δ=0.5 eV. The cell before the reflector is added (here with E_g=0.73 eV) has a V_{oc}≈0.51 V (due to the constant entropy loss of 220 mV), and after has V_{oc}≈0.97 V. This improvement by approximately the bandwidth of the filter results in the total *area* underneath the *I-V* curve being increased relative to the case without the reflector. This is in spite of the reduction in short-circuit current. However, due to the arguments above concerning the voltage limited to the bandgap (V_{oc}<E_g) **[102,103]**, we can imagine that it is possible that the efficiency improvement described here might be curtailed at the bandgap. This is shown (graphically only) in the red curve in Fig. **VI-7a**, which has a V_{oc} cutoff at the bandgap. This cell will not have any efficiency gain since the reduction in I_{sc} is larger than the increase in V_{oc}, when taken as a product (this can be calculated manually). There would therefore be a maximal value of bandwidth beyond which the efficiency begins to drop. It should again be noted that this red curve is an assumption that the voltage cannot exceed the bandgap at all, which the BM effect was shown to contradict. Therefore, it is yet unknown whether the selective reflector design will have the required benefit. If this cutoff is real, then the maximal bandwidth would be the amount of entropic loss: Δ^{max}≈0.22 eV.

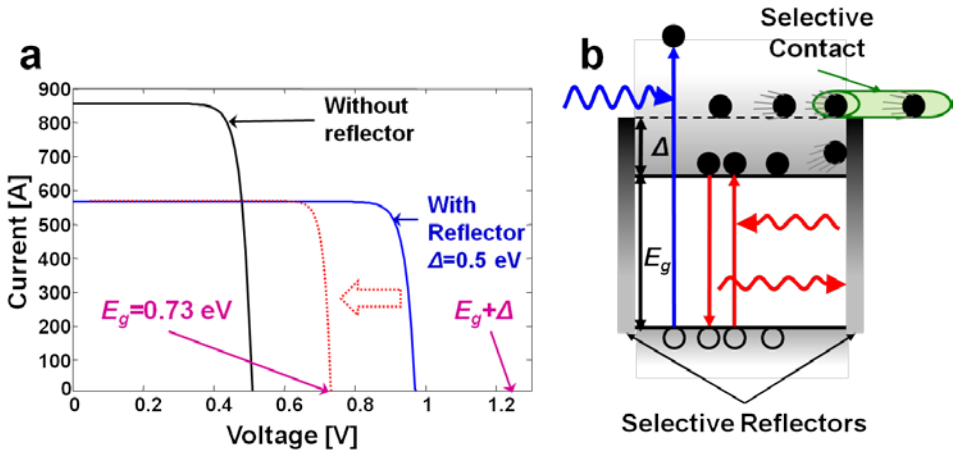

VI-7 I-V Curve for the Feedback Cell and Diagram Describing the Selective Contact. (a) The I-V curve for the cell shows an improvement in overall efficiency (area under the curve) for the cell with a filter (blue) compared to one without (black). Here E_g=0.73 eV and Δ=0.5 eV. Due to the possibility of a cutoff at the bandgap of the open-circuit voltage, the actual I-V curve may be shifted to the left (red), with a V_{oc} cutoff at the bandgap (this curve was hand-drawn). (b) A selective contact is needed at the shifted Fermi level in order to extract the electrons at the higher potential. Electrons at the bandgap would effectively see a barrier preventing them from reaching the energy height of the contact.

A final critical element in this design is the requirement of having selective contacts that can connect to the elevated Fermi level of the cell, to extract the excited electrons, as shown in Fig. **VI-7b**. A regular solar cell has an "Ohmic" contact at the edge of the bands so that there is no energy difference between the electrons at the band edge and within the metallic contact **[2]**.

However, the selective contacts here create a “Schottkey Barrier” so that the electrons at the conduction band cannot be extracted, and only the higher energy electrons can. These selective contacts are similar to the ones needed in hot-carrier devices **[4,94]**, and while making the design more complex, are not a fundamental limitation. It would, however, prevent the implementation of the feedback design on existing cells, which have existing, pre-matched, contacts.

VII. The "Sliver of Energy" Cell

**Publication note*[6]

1. Using Spectral Splitting to Maximize Efficiency

To fully utilize the solar spectrum, the central assumption of the original SQ model that can be broken is to use more than a *single* semiconductor junction. Since the choice of the bandgap for a single junction cell defines the ratio of absorbed, thermalized and unused photons, as described in Chapter **V**, changing the assumption regarding the single bandgap will fundamentally change the DB limit, on a per-bandgap basis. The use of a multi-junction cell was envisioned from the outset of solar cell research **[24]**, with higher photon absorption per junction for increasing number of bandgaps. Since adding a second junction to the cell would improve the overall efficiency, it was clear that continuing to add bandgaps to the cell would continue to improve the total efficiency. This calculation was done for a set of infinite bandgaps **[35,36]**, with and without concentration, and was shown to approach the theoretical thermodynamic limits for energy conversion **[37]**. Each junction in this stack would absorb a small "sliver" of energy from the solar spectrum, with a bandwidth of $dE=\Delta$, and each sliver would be maximally efficient for this small sliver of energy, since the amount of thermalization losses would be negligible in the conduction band from E_g to $E_g+\Delta$. The number of unused photons would also drop to zero, since the multi-junction array would be staggered from high to low energy bandgaps, such that each segment of the solar spectrum would be absorbed from 0 eV to infinity. In practice, since ~5 eV is the energy cutoff for the solar spectrum (AM0 or AM1.5) these junctions would only need to be spaced within this range. As we have shown in the Chapter **II**, there is a near constant entropy penalty for the open-circuit voltage of a cell due to étendue losses, so that the maximal efficiency limit can only be achieved at maximal concentration **[36,37]**.

For the infinite junction array analysis, it is assumed that each sliver of energy, represented by the absorption within a semiconductor with a bandwidth of $E_g \rightarrow E_g+\Delta$, will be independently isolated to maximize the power onto each sub-cell. However, a practical issue that must first be solved is how to geometrically stack this array. The most basic design consists of a multi-junction stack of cells, with the highest bandgap material on top, and the lowest on the bottom, such that each cell in the stack absorbs from above only those photons that are best tuned for the bandgap, with the photons for the segment below it being transparent (with energies below the bandgap). This is graphically shown in Fig. **VII-1a** for a simplified system with 3 bandgaps, such that each cell absorbs "a third" of the solar spectrum. In this figure, cell #3 has the largest bandgap, such that $E_{g3}>E_{g2}>E_{g1}$. This form of spectral splitting occurs "naturally" in the stacked multi-junction array, since it makes use of the same top aperture for absorbing the light.

[6] The following chapter is based on work that has yet to be published, and is currently in submission **[126]**.

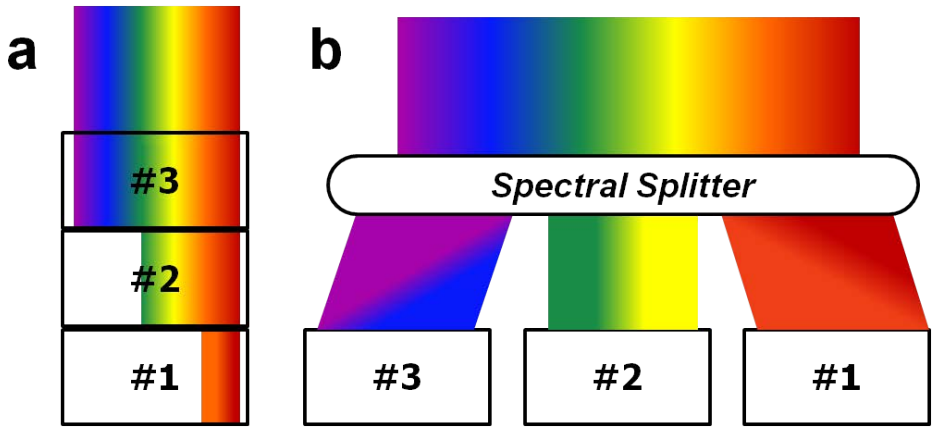

VII-1 Spectral Splitting Multi-Junction Arrays. (a) A Stacked combination, with each cell absorbing the segment of the spectrum matched to the bandgap, and transparently passing the lower energy photons. (b) A spectrum splitting array, with an external optical spectral splitter, segmenting the incoming spectrum to the appropriate bandgaps in the array.

In contrast, the light can be spectrally split *before* encountering the cells, as is shown graphically in Fig. **VII-1b**. The spectral splitter is any material system that can guide the light of the appropriate bandwidth ($E_{g\#}+\Delta_{\#}$) to the appropriate underlying cell. The idea of externally splitting the spectrum was devised early on **[127]**, but the ease at which the spectral splitting occurs in the multi-junction stack, as in Fig. **VII-1a**, pushed the research in the field to that simpler geometry.

For a multi-junction array, the other critical factor for designing the system is the circuit configuration of the cell. Since the cell is a power device, and can be roughly considered as a voltage supply or battery, it should produce a constant amount of either voltage or current. For this to occur in the stacked array, each cell must be connected in *series* as voltage supplies with different voltages (proportionate to the bandgap), and the current through each cell must be matched by having them absorb the same number of photons from the solar spectrum. This means that the bandgap spacing between each cell (the bandwidth $\Delta_{\#}$) must first account for the number of photons in the solar spectrum within that bandwidth, so that the number of e-h pairs produced in each will be the same. Since the solar spectrum changes throughout the day, particularly in terms of angular dispersion when no solar tracking is used **[13]**, the current through each cell will change throughout the day. This process limiting issue once again limits the overall current from the cell to the *lowest* current in the stack, such that the entire stack is extremely dependent upon the other layers. Furthermore, in a stacked array, each cell must be consecutively grown (e.g., epitaxially) on the underlying layer, with a thin *tunnel junction* between each stack. The tunnel junction allows the current to flow from one cell to the next, as they are connected in series. However, this produces an extreme materials limitation, as not all materials can grow on each other due to crystalline lattice mismatches. These mismatches will produce defects in the interfaces between each layer, and prevent the flow of current from one cell to the next. Due to these many technological difficulties, multi-junction cells are typically limited to 2-3 layers, with up to 5-6 layers currently being tested today. Furthermore, the high cost of these cells, and the current-carrying limitations primarily consign these types of cells to extraterrestrial and concentrated solar applications.

The adjacent spectral splitting design, such as the one in Fig **VII-1b**, would need to be connected in a more complex electronic circuit, since the current cannot easily be transferred from cell to cell. However, the major technological difficulty with this design is the spectral splitting layer itself. Over the past three decades, various techniques have been devised for creating such a layer **[128]**, including directional mirrors **[129]** filters **[130]**, and even holographic films **[131,132]**. Some of these designs have been reaching the same efficiencies as some of the best stacked cells **[133]**, in a more economical design.

A basic question that can be asked about the two different designs is whether there is any thermodynamic advantage to either? Moreover, is there a fundamental issue regarding the assumptions that have been made regarding the trend of these cells to continuously improve their efficiency as the bandwidths are made continuously smaller?

2. Geometry Dependent Photon Management

Each cell in the multi-junction structure absorbs the light from the bandgap and up to its bandwidth, $E_g \rightarrow E_g+\Delta$, but also emits light at its band-edge at open-circuit. Even when the cell is operated at its maximal potential, V_m, it still emits light out. This light can radiate isotropically, and for a flat cell this emission can be out of both the front and back sides, neglecting the emission from the side edges. The emission for the stacked cell geometry is obviously preferred in the direction of the cells below it, since these re-emitted photons can be re-used by the lower gap cells below. For a simple tandem cell (two junctions), as shown in Fig. **VII-2a**, the upper cell (#2) has a larger bandgap than the lower cell (#1), $E_{g1}>E_{g2}$, and the re-emitted photons are preferentially emitted towards the lower cell and are therefore not lost. We will denote this situation by a geometric emission parameter, B=1, which describes 100% of the re-emitted photons being recycled by the lower cell. This geometric factor is identical in concept to the one used in the dc layer in Chapter **III**, Eq. **III.5**.

While the preferential downward emission with B=1 is the ideal case, the most general case is where the cell emits isotropically, both above and below, such that only 50% of the photons are recycled by the cell below. In this case, depicted in Fig. **VII-2b**, B=½, since we are only interested in the cells emitted "downward". In the same vein, the cell may backscatter all the re-emitted photons away from the lower cell, such that B=0, as shown in Fig. **VII-2c**. [Note again the comparison with the description of the dc layer in Chapter **III** and Fig. **III-3**; in the dc system, we were not interested in the complete backscattering case]. The geometric factor B=0 can also be described for the adjacent cell system, as shown in Fig. **VII-2d**, since the re-emitted photons will not reach cell #1 (neglecting the edges), regardless of the direction of emission from cell #2. The parameter B thus provides a distinction between the two multi-junction designs, and can describe the full range of geometries for each cell pair, $0 \leq B \leq 1$, depending on the exact geometry.

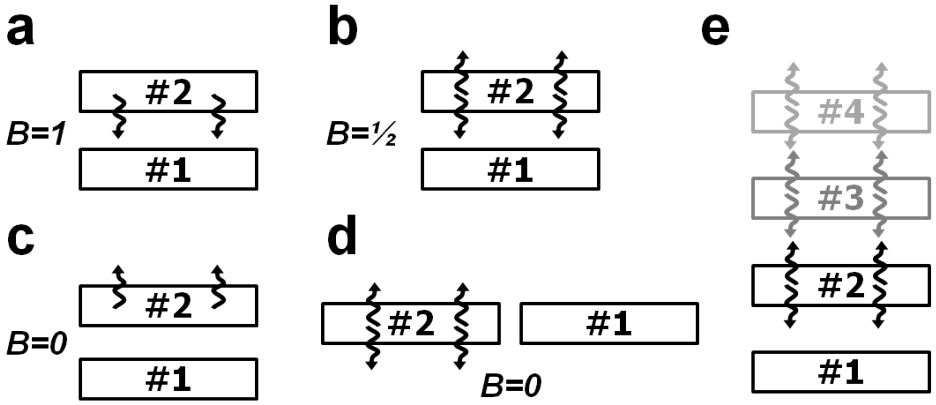

VII-2 Schematic of the Geometric Parameter, *B*, for a multi-junction cell. (a-c) A stacked tandem cell geometry, with cell #1 having a smaller bandgap than cell #2. The arrows denote the direction of band-to-band re-emission of photons from cell #2, which can be re-used by cell #1. The geometric parameter is shown for each configuration: (a) forward, *B*=1; (b) isotropic, *B*=½; and (c) backward, *B*=0, emission. (d) An adjacent tandem cell configuration has *B*=0, assuming that the edge emission is negligible, regardless of the emission direction from cell #2. (e) In a stacked multi-junction cell configuration, each underlying cell receives a contribution from the re-emission from the cells above it, as a fraction of the parameter *B* for each pair. In any emission characterized by *B*<1 per pair, the bottom cell will see less and less of the contribution from the cells above it.

The stacked multi-junction cell array will further amplify the geometric parameter's significance. This is shown for a 4-layer junction in Fig. **VII-2e**, assuming isotropic emission from each layer to the next. Since the geometric parameter *B* is typically less than unity, unless all the photons are completely emitted directionally towards the lower bandgap cell, the lowest cell in the stack (cell #1) will only receive half of the contribution from the cell above it, which had only received half of the contribution from the cell above it as well, *ad infinitum*. Effectively, in the isotropic emission case, a factor of half of the re-emission is lost between each pair of cells, resulting in the lower cells "seeing" less and less of the contributions from the cells above it. This analysis will be shown explicitly for a 3-junction (and more) cell below.

For the stacked cell, the directionality of emission can be controlled by index matching, or impedance matching, the cells to one another. This will require a careful balance of the indices of refraction, with the rule-of-thumb that lower bandgap materials have higher indices of refraction, which works in the opposite trend of what is desired (light is better matched to enter higher indices of refraction, as a function of Snell's law and the critical angle of total internal reflection).

The re-emission of the photons from each junction in the cell to the next was assumed to occur in all previous multi-junction analyses **[35-37]**, and directional emission was assumed as well, with *B*=1 between each layer. In fact, selective reflectors, such as the one described in the previous chapter, were described as well as a method to confine the re-emission to the correct bandgap cells **[38,134]**. The effect of the directional parameter on the cell's performance is one important factor added in the next sections on multi-junction cell analysis.

3. Tandem Cell Analysis

In addition to the geometric parameter contribution to the photon fluxes between cells, the effect of limiting the bandwidth of absorbed photons to each cell should be included as well. For a cell with bandgap E_g, sitting "below" (in a stacked configuration) a cell with bandgap $E_g+\Delta$, there will be fewer photons in the solar spectrum to absorb. This is shown in Fig. **VII-3**, for a cell with E_g=1 eV, and a bandwidth of Δ=1 eV as well. The lower the bandwidth of absorbed photons for this cell is, the lower the number of e-h pairs generated within it. Consequently, the electron density within the junction is lowered as well, which produces the voltage within the cell. We should therefore expect a dependence of the open-circuit voltage on the bandwidth, Δ. This dependence should also involve the geometric parameter, B, since at open-circuit, all the recombination photons are re-emitted (ideally), and for a tandem cell with B=1, we would expect the loss of incoming photons to be completely compensated by the re-emission from cell #2, such that the total *number* of photons reaching cell #1 would remain the same.

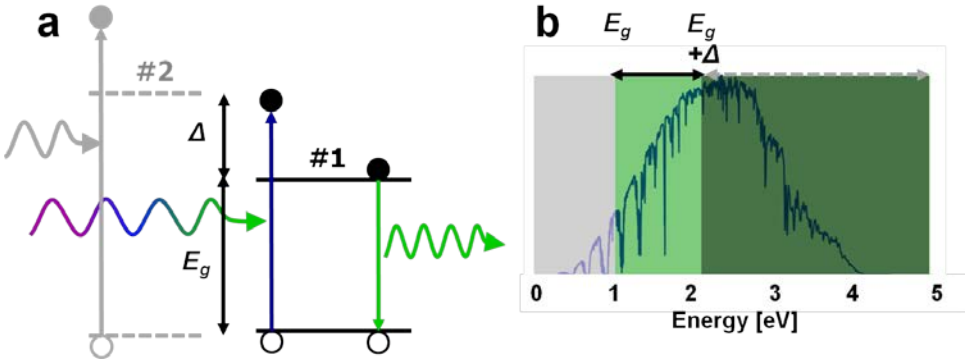

VII-3 Bandgap Diagram of a Tandem Cell Geometry. (a) A solar cell with bandgap E_g within a stack of tandem cells (cells #1 and #2, as in Fig. VII-2) will only absorb photons from the bandgap up to the lower level of the cell above it, signified by a difference of Δ. The cell "above" is shaded in grey. (b) The window of absorption of the solar spectrum, with Δ=1 eV, of a semiconductor with E_g=1 eV.

The analysis of this tandem cell at open-circuit is similar to that of the dc layer in Chapter **III**. We first use the flux equivalence methodology on the upper cell, #2, which itself is at open-circuit flux equilibrium. This can be written as:

$$\Omega_S \int_{E_g+\Delta}^{\infty} \frac{E^2 dE}{\exp[E/kT_S]-1} = \frac{\Omega_o}{\kappa_{nr2}} \int_{E_g+\Delta}^{\infty} \frac{E^2 dE}{\exp[(E-qV_{oc2})/kT_c]-1} \qquad \textbf{VII.1}$$

where we have included the possibility of non-idealities in the non-radiative term, κ_{nr2}, as well as taking the bandgap as $E_g+\Delta$. This flux equilibrium equation has no geometric parameter involved, since it absorbs light directly from the sun, and emits it at an étendue of $\Omega_{o2}=\Omega_o$, which we take here as a constant for generality.

Cell #1 lies "below" cell #2, and includes the absorption within the bandwidth of Δ, as well as the contribution of emission from cell #2 when under open-circuit conditions:

$$\Omega_S \int_{E_g}^{E_g+\Delta_g} \frac{E^2 dE}{\exp[E/kT_S]-1} + B\cdot\Omega_o \int_{E_g+\Delta}^{\infty} \frac{E^2 dE}{\exp[(E-qV_{oc2})/kT_c]-1} = \frac{\Omega_o}{\kappa_{nr1}} \int_{E_g}^{\infty} \frac{E^2 dE}{\exp[(E-qV_{oc1})/kT_c]-1} \quad \textbf{VII.2}$$

The emission from the cell above is multiplied by the geometric parameter, *B*, since we should only include the contribution from that cell. Note that this derivation is quite similar for that of the dc system in Chapter **III**, as well as the selective reflector from the previous chapter. The derivation continues in the same format, by first replacing the second term in Eq. **VII.2** with the right hand side of Eq. **VII.1**, as well as shifting the integration limits, to obtain:

$$\Omega_S \int_{E_g}^{\infty} \frac{E^2 dE}{\exp[E/kT_S]-1} + (B\cdot\kappa_{nr2}-1)\cdot\Omega_S \int_{E_g+\Delta}^{\infty} \frac{E^2 dE}{\exp[E/kT_S]-1} = \frac{\Omega_o}{\kappa_{nr1}} \int_{E_g}^{\infty} \frac{E^2 dE}{\exp[(E-qV_{oc})/kT_c]-1} \quad \textbf{VII.3}$$

Eq. **VII.3** is similar to the equation for a dc system, as well as bearing a relationship to the equation for the feedback selective reflector. The geometric parameter can be generalized to include the lossy contribution of the non-radiative term, to become: $B'=B\times\kappa_{nr2}$. This effective geometric parameter, *B'*, is almost certainly lower than unity, since nearly every material has some non-radiative losses. The equation above cannot be contracted any further; however using the same approximations as used in the previous chapters we can obtain a formula for V_{oc} as a function of the bandwidth, Δ:

$$qV_{oc}^{\Delta} = qV_{oc}^{reg} + kT_c \ln\left[1+(B\cdot\kappa_{nr2}-1)\left(\frac{\alpha_{\Delta}}{\alpha_{S1}}\right)\times\exp[-\Delta/kT_S]\right] \quad \textbf{VII.4}$$

Here, α_Δ is the same as in the previous chapter, Eq. **VI.4**, and the regular geometric parameter was used to explicitly show the dependence upon the upper junction's material properties. The non-radiative losses of the underlying cell (#1, κ_{nr1}) were already included in the term for V_{oc}^{reg} appearing in Eq. **II.6**. The term in the brackets is smaller than unity, for all values of *B*, due to the appearance of the exponential dependence on the bandwidth. Since $0\leq B\leq 1$ (as well as *B'*), the bracketed term will reduce the open-circuit voltage for all cases except when *all* photons are emitted preferentially towards the bottom cell, as well as the upper cell containing *no* non-radiative losses. As the bandwidth drops to zero, $\Delta\rightarrow 0$, which is the situation for an infinite junction cell, the exponent in the brackets will reduce the V_{oc} even further. Furthermore, as $B\rightarrow 0$, the bracketed term will reduce the voltage even more, as was shown to be the case for the lowermost cell in the stack of Fig. **VII-2e**. The existing theoretical calculations for infinite stacks therefore considered only cases where $B=1$ and $\kappa_{nr}=1$, which is the perfectly ideal case only.

The V_{oc} is plotted in Fig. **VII-4** for a GaAs cell with varying bandwidths blocking the incoming spectrum, as well as varying degrees of geometric parameters, assuming a pristine semiconductor ($\kappa_{nr2}=1$) placed above it. The exponential falloff at smaller bandwidth gaps, Δ, follows the natural logarithm in Eq. **VII.4**. The directional emission case, $B=1$ (red line), represents the case of constant V_{oc}^{reg}. Since each cell already begins with a ≈300 mV reduction of

the maximal open circuit voltage in comparison to the bandgap, this further reduction becomes more critical as the bandgap of the segment approaches zero. This is shown in the inset of Fig. **VII-4**, for a theoretical semiconductor with E_g=0.4 eV, with the V_{oc} approaching zero for smaller bandwidths. This loss will occur solely due to the bracketed bandwidth term in Eq. **VII.4**, and will be reduced even further for a lossy material. The reduction in maximal open circuit voltage will therefore reduce the efficiency of even the highest quality solar cell, since the power is proportional to V_{oc}.

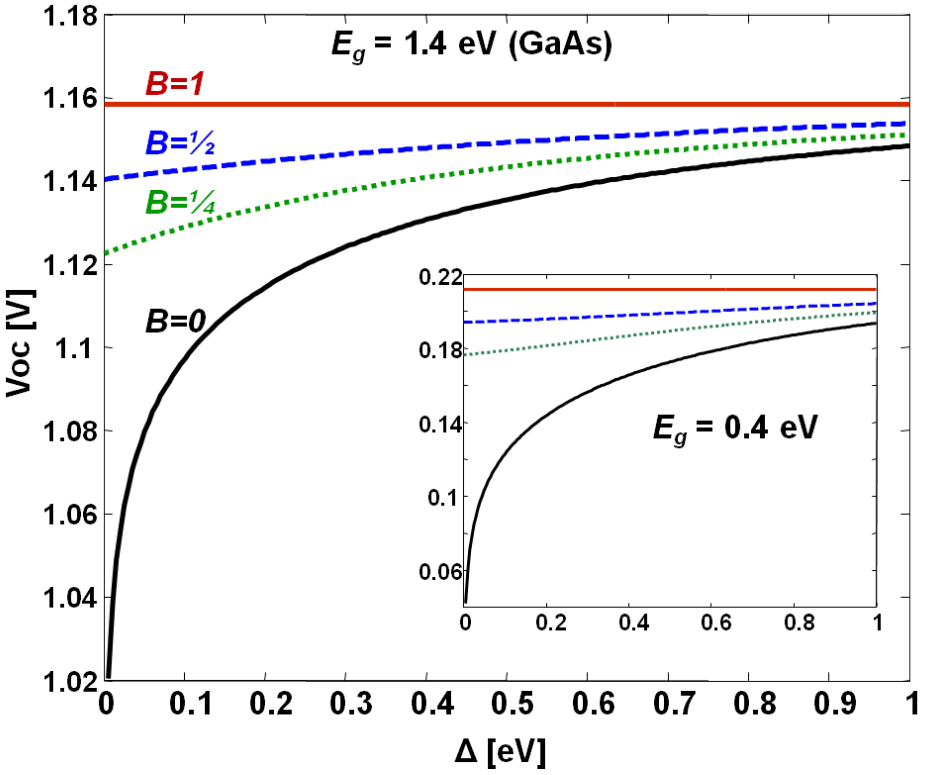

VII-4 Open-Circuit Voltage as a Function of Sliver Bandwidth. The graph is for a GaAs cell with E_g=1.4 eV, assuming no other non-radiative losses ($\kappa_{nr1,2}$=1). The geometric parameter, B, is varied over the possible ranges of directional emission, with B=1 being the traditional case where all photons are recycled. The voltage drops from its bulk value of ≈1.16 V to below 1 V with smaller slivers of bandwidth. Inset: For a smaller bandgap material of E_g=0.4 eV, the voltage drop can approaches zero, when no other losses are included.

The entropy term derived from Eq. **VII.4** can be described in nearly identical terms to that of the dc system. The physical meaning is best seen when B=0, showing the extreme of the backscattered loss case. The bracketed term is simply the ratio of the photons removed from the original spectrum to that of the original spectrum:

$$dS_{Sliver} = k \ln\left[\frac{N\{E_g \to \infty\} - N\{(E_g + \Delta) \to \infty\}}{N\{E_g \to \infty\}}\right] \qquad \textbf{VII.5}$$

The entropy (difference) increases for a smaller distribution of incoming photons, when compared to the original distribution. This term is simply the Kullback-Leibler divergence between the original and bandwidth-limited spectra. There is less free energy in the system when there are fewer photons absorbed.

4. Generalization to Multi-Junctions

The formulas above can be generalized to more than a tandem cell configuration, and include multiple junctions. For the case of multiple junctions in Fig. **VII-2e**, each pair of cells will have its own geometric parameter, B_i, as well as bandwidth spacing, Δ_i, and associated non-radiative loss terms, κ_{nri}. To simplify the derivation in order to obtain as close to a closed-form solution as possible, we will assume that the bandwidths are equal, $\Delta_i=\Delta$, and that the geometrical parameters are also identical: $B_i=B$. While the first assumption will not necessarily be true for current-matching stacked array configurations, it will approach this equality for increasing numbers of junctions within the array.

To obtain the open-circuit condition for cell #1, which is at the bottom of the array, we must first find the open-circuit conditions for the cells above it, in a recursive algorithm. The algorithm is identical to the tandem junction analysis, with the topmost cell solved first, and then inserted as an input term into the cell below it. This process is repeated until we find the open-circuit condition of the cell being analyzed (#1), which is:

$$\Omega_S \int_{E_g}^{\infty} \ldots + (B-1)\left[\int_{E_g+\Delta}^{\infty} \ldots + B \int_{E_g+2\Delta}^{\infty} \ldots \right] = \frac{\Omega_o}{\kappa_{nr1}} \int_{E_g}^{\infty} \frac{E^2 dE}{\exp[(E - qV_{oc1})/kT_c] - 1} \qquad \textbf{VII.6}$$

where the Planck blackbody integrands were truncated for clarity, and all non-radiative losses of the above cells were taken as unity, or similarly, included within the B term. The bracketed term supplies the number of reduced photons from the solar spectrum due to absorption by cells stacked above it, and inefficiently re-emitted towards the underlying cell; or for spectrum splitting cells, the reduction of the solar spectrum absorbed due to the spatial divergence of the spectrum.

Eq. **VII.6** is a recursive function, depending upon the number of cells lying above the one being analyzed (cell #1). A closed form for the V_{oc} will be meaningless in this context, and can only be compared with that of the tandem cell, which provides most of the important physical phenomenon encountered in this configuration. Nevertheless, it is instructive to examine the contribution of the bracketed term in Eq. **VII.6** for different values of B. As was stated above, an averaged value of B=½ can be assumed for each layer, given an isotropic emission from each layer. In comparison, B=¼ would provide the case of preferred back-scattering, and B=¾, the case of preferential forward-scattering. The leftmost term in Eq. **VII.6** consists of the absorption of the solar spectrum of a single-junction cell (at E_g), and the middle term provides the amount of photons to be removed from that spectrum. If we over-estimate the contribution of the integral from $N\{E_g+2\Delta \rightarrow \infty\}$ as being $N\{E_g+\Delta \rightarrow \infty\}$, we can then combine the two terms in the brackets, as a function of B. For B=¼, this will reduce -15/16 of the integral $N\{E_g+\Delta \rightarrow \infty\}$; For B=½, this

will reduce -12/16 of the integral; and for B=¾, this will reduce -7/16 of the integral. Therefore, for cell #1, lying below a stack of other cells, the combined re-emission spectrum of all the other cells will see a "total effective geometric parameter": B_{total}, which we see approaches the value of ½ from below, since what was calculated was (B-1). Therefore, for increasing layers of junctions within the stack, even with optimal photon re-emission, the value of V_{oc} will slowly transition from the blue to green to black curves in Fig. **VII-4**, as a function of the number of cells above it. This is what was meant by "seeing less" of the cells above it in Fig. **VII-2e**.

5. Experimental Verification

The verification of Eq. **VII.4** was done on a GaAs cell provided by Alta Devices, which produce the highest quality solar cells today **[135]**. GaAs has the lowest amount of non-radiative losses due to a high internal fluorescent yield [**136]**, which makes it an ideal solar cell material, as well as the material most closely following the equations described here.

Long Pass Filters (long *wavelength*, essentially a LPF) were placed above the cell within a solar simulator setup, such that light from $E_g \rightarrow \Delta$ was blocked off, for different values of Δ. Since the cell has some non-radiative losses, there is an offset of the V_{oc} from the pure theoretical value of 1.16 eV to 1.09 eV due to the non-radiative loss term, $k \times ln[\kappa_{nr}]$ (essentially, κ_{nr} ≈94.2%, meaning the radiative efficiency was 5.8%, which is high for a solar cell material). This creates an offset of the V_{oc}, regardless of the bandwidth measured. Fig. **VII-5** plots the theoretical curves, with and without the κ_{nr} offset, as well as the measured data points. As can be seen, the data points perfectly match the case where B=0, which is the case when the light is completely blocked off by the filter, and no re-emission occurs (since the filter is not a semiconductor). The error bars appearing include both possible errors in measuring the V_{oc} using the electronic setup (a two-point probe only), which was averaged over 3 experiments each in the y-axis, as well as adding a bandwidth uncertainty of the LPFs in the x-axis, which was added by measuring the bandwidth of transition of 10% transmission to 90% transmission.

A further set of experiments is currently being examined in order to emulate the effect of having $0<B<1$ (This set of experiments is currently being done in the lab of Prof. H. Atwater, and will appear in Ref. **[126]**). To do this, the emission profile of the radiative recombination from the slab sitting "above" the cell must be mimicked, and then added to the input spectrum illuminating the GaAs cell. Thus, if a slab with bandgap of 1.5 eV is placed above the GaAs cell in a tandem cell structure, a fraction of the spectrum from 1.5 eV to ∞ is re-emitted out towards the GaAs cell (and effectively creating Δ=1.5-1.43=0.07 eV). By changing the intensity of this reduced source, which must be added in the same light path as the direct source, data points for various different values of B can be simulated. This can also be produced by physically taking various slabs of semiconductor, with various bandgaps each, and placing them in the lightpath above the cell. However, that will add more variables to the equations, since we must then include the factors $\kappa_{nr,2}$ as well as the possibility of further reflections and deflections of the light away from the GaAs cell, which will reduce our knowledge of the effective geometric parameter, B'.

In addition, another set of experiments will be done to verify that this reduction in the V_{oc} caused by the lack of recycled photons can be improved upon by concentrating the light. In the original analysis of the infinite multi-junction cell **[36,37]**, the use of maximal concentration was used almost implicitly in order to prevent such differences between the bandgap and the V_{oc}. Therefore, we would expect that the exponential drop in voltage due to the lack of recycled photons will disappear at maximal concentration since the "impedence mismatch" between the incoming and outgoing light beams does not exist, and all photons are fully utilized. While theoretically, this is true, as can be seen by adding the concentration factor into these equations, a good question to ask is how it is possible to concentrate the light into each slab in such an effective manner. The next chapter addresses this issue, and asks whether the concept of "maximal concentration", which would be needed to achieve near-Carnot efficiencies, is thermodynamically valid.

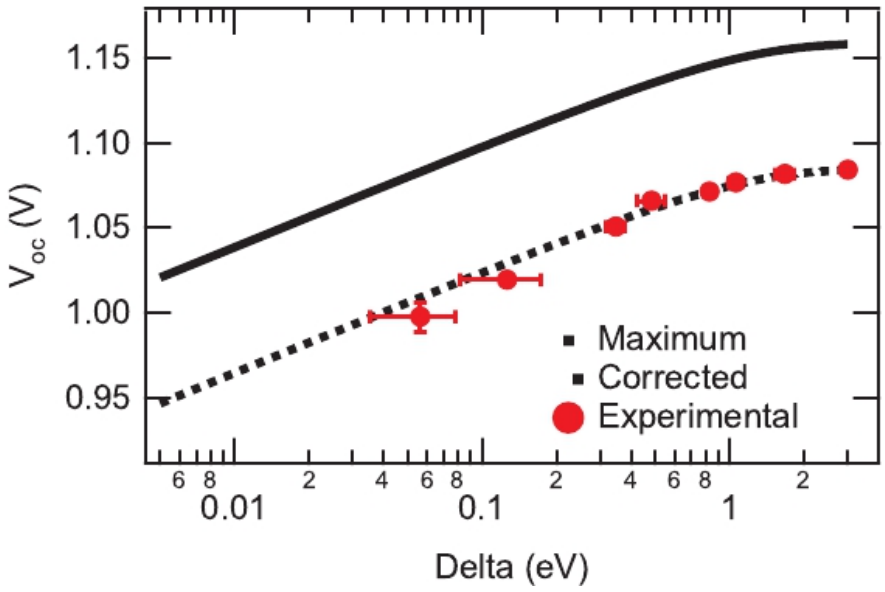

VII-5 Experimental Verification of the Sliver Cell Analysis for a GaAs Solar Cell. The V_{oc} is plotted for a high quality GaAs cell (E_g=1.43 eV), measured under the illumination of a solar simulator, with Long Pass Filters placed in the optical light path (red dots, semi-logarithmic x-axis). Also plotted is the theoretical curve of Eq. VII.4 (solid black), as well as the theoretical curve including non-radiative losses (dashed black), which is offset from the original curve by 25.8mV×$ln[\kappa_{nr}]$. [Graph courtesy of C. Eisler, Caltech].

The limitation on the open circuit voltage due to the decrease in photons absorbed within each segment of a stack of tandem cells provides an additional parameter which must be optimized for each stack. This will depend on the material parameters of each segment, as is represented by the κ_{nr} term, as well as the energetic distribution of the bandgaps, as represented in the Δ term.

While concentration can help improve the loss in V_{oc} due to the smaller bandwidth of absorption, it does not address the more fundamental issue of geometry and photon management, which provides an advantage to designs that best utilize the absorption and re-emission aspects of each sub-cell in the multi-junction system.

VIII. A New Limit to Concentration?

**Publication note*[7]

1. Maximum Concentration Overview

The maximal concentration, C^{max}, described in Chapter **I** was described as being a result of the application of the 2nd law of thermodynamics and the reciprocity relations, as well as described using the argument of the impossibility of bending light backwards. We will succinctly repeat that derivation here, following the derivation in Refs. **[13,28]**. The amount of radiation the sun emits is a function of the temperature, T_S, the Stefan-Boltzmann constant, σ: σT_S^4. The amount of radiation reaching the front aperture of a solar concentrator with an area A_{conc} is a fraction of the area of the sun's surface, given by the sun's radius: $4\pi r_s^2$, divided by the area of the total radiation at a distance of the sun-earth distance: $4\pi R_{S\text{-}E}^2$. This is shown in Fig. **VIII-1**.

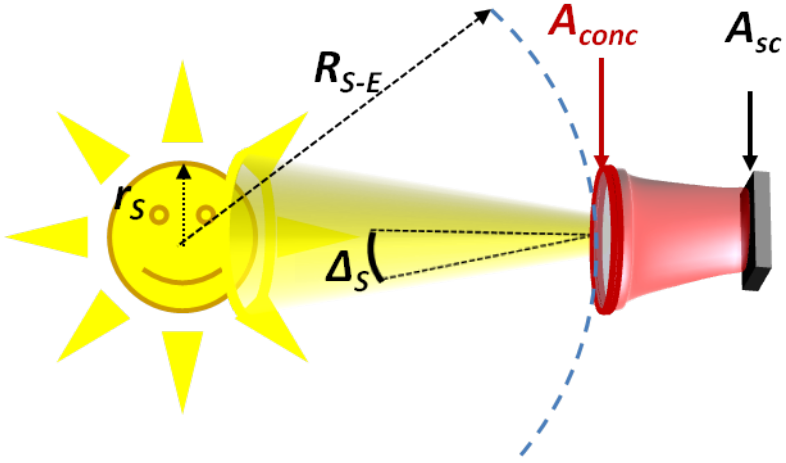

VIII-1 Diagram Describing the Transfer of Heat from the Sun to the Aperture of a Concentrating Solar Cell. All parameters are as defined in the text.

The amount of heat transferred between these surfaces is thus:

$$Q_{S-E} = A_{conc} \frac{r_S^2}{R_{S-E}^2} \sigma T_S^4 \qquad \textbf{VIII.1}$$

It is assumed that the aperture of the concentrator is flat, just like the differential surface area of the sphere with radius $R_{S\text{-}E}$. Note that the reciprocity relation is used to relate the area between the concentrator aperture, A_{conc}, and the source aperture.

The solar cell, with surface area A_{sc} and index of refraction, n_c, emits heat given by:

[7] This chapter is based on a paper that is currently in submission **[137]**.

$$Q_{sc} = A_{sc} n_c^2 \sigma T_c^4 \qquad \textbf{VIII.2}$$

where a material with any index of refraction emits more radiation by a factor of n_c^2.

The 2nd law of thermodynamics then states that the heat transfer between two objects *of equal temperature* must be zero (essentially zero entropy). This means that the two equations above must be equal.

$$\left.\begin{aligned} Q_{S-E} &= Q_{sc} \\ T_S &= T_c \end{aligned}\right\} A_{sc} n_c^2 = \frac{r_S^2}{R_{S-E}^2} A_{conc} \qquad \textbf{VIII.3}$$

Using the simple trigonometric identity relating the angular radius of the sun and the distances for small angles by $tan\Delta_S \approx sin\Delta_S = R_{S-E}/r_S$, and assuming that the transfer of heat can be *no larger* than the amount occurring at equal temperatures (due to the 2nd law), we can find the concentration maxima is the ratio of apertures:

$$C = \frac{A_{conc}}{A_{sc}} \le \frac{n_c^2}{\sin^2 \Delta_S} \qquad \textbf{VIII.4}$$

If we ignore the index of refraction, $n_c=1$, we re-obtain Eq. **I.19**. The application of the 2nd law of thermodynamics here was based on the Clausius definition of the 2nd law, where in the absence of external work, the flow of heat must be from hot to cold bodies. In mathematical form, using the concept of entropy, *S*, this is stated as $\Delta S = \Delta Q/T \ge 0$. Given that the flow of heat is from the concentrator to the cell, this defines $\Delta Q \equiv Q_{S-E} - Q_{sc}$. Clearly the minimum possible entropy generation is found for the case of equal temperatures, such that $Q_{S-E} - Q_{sc} = 0$ when $T_S = T_c \equiv T$.

For useful cases when the temperature of the solar cell does not reach that of the sun (which would be untenable), we can find the relation between the temperatures as a function of the efficiency of heat extraction, η_{ext}. Assuming no heat is lost to any other sources, the transmission of the heat/light is perfect, and that the absorptivity is equal to the emissivity ($\alpha_{abs} = \varepsilon_{emit}$), we can equate the heat into the cell with the heat out of the cell as:

$$Q_{S-E} = Q_{sc} + \eta_{ext} Q_{S-E} \qquad \textbf{VIII.5}$$

This relation holds since the total emission out of the cell (right hand side) must equal the thermal emission plus whatever heat extraction (including possible losses) occur in the system. By plugging into Eq. **VIII.5** the values for Q_{S-E} and Q_{sc} from above, and using the relation for the angle $sin\Delta_S$, we get:

$$A_{conc} \sin^2 \Delta_S \sigma T_S^4 \times (1 - \eta_{ext}) = A_{sc} \sigma T_c^4 \qquad \textbf{VIII.6}$$

Further, by using the maximal concentration of Eq. **I.19** (as well as Eq. **VIII.4** with $n_c=1$), we can find the temperature of the absorber, assuming some form of extraction efficiency:

$$T_c \cong T_S \left[(1 - \eta_{ext}) \frac{C}{C^{\max}} \right]^{1/4} \qquad \textbf{VIII.7}$$

Note that the extraction efficiency η_{ext} is not the same as the PV conversion efficiency, η_{eff}, and includes losses due to other processes, as well as being generalized for photo-thermal processes

as well. This relation states that the temperature of the cell will depend upon the concentration of the system, with temperatures being *equal* at maximal concentration.

The maximal concentration is therefore found to be *no higher* than C^{max} (assuming the geometries described above, and not for spherical systems), due to a simple application of the 2nd law of thermodynamics. However, this limit has no dependence upon the material parameters of the system (if $\alpha_{abs}=\varepsilon_{emit}$), particularly the limited absorption from the bandgap of a semiconductor. Nevertheless, it has been assumed that the maximal concentration, $C^{max}\approx$46,000 is an *invariant* parameter of any PV system.

2. Bandgap Dependence of the Maximal Concentration

Using the formalism of the generation of entropy in the PV conversion, we can apply a more general version of the 2nd law of thermodynamics to the process, and require that:

$$\Delta S_{PV} \geq 0 \qquad \textbf{VIII.8}$$

This is the most general form of the 2nd law, stating that the entropy must always increase (or remain zero) for any spontaneous process, such as the PV energy conversion process.

First, we will re-write the open-circuit equilibrium condition, for an input source that is concentration dependent, $N_{in}(C)$, being either the blackbody or AM (0 or 1.5) spectra:

$$N_{in}(C) = \Omega_o \int_{E_g}^{\infty} \frac{E^2 dE}{\exp[(E-\mu_{oc})/kT_c]-1} \qquad \textbf{VIII.9}$$

We then apply the regular approximation of the integral, which only assumes that $E\text{-}\mu_{oc}>>kT_c$:

$$\mu_{oc} = E_g - kT_c \cdot \ln\left[\frac{\Omega_o E_g^2 kT_c \alpha_{c1}}{N_{in}(C)}\right] \qquad \textbf{VIII.10}$$

We note that even in the case of maximal concentration, where $\mu_{oc}=E_g\times\eta_C\rightarrow E_g$, this approximation generally holds for most bandgaps above the thermal energy kT_c=25.8 meV **[138]**. We can then find the entropy, as was done for Eq. **II.15**, by finding: $S=-\partial\mu/\partial T_c$:

$$S = k\frac{\alpha_{c2}}{\alpha_{c1}} + k\ln\left[\frac{\Omega_o E_g^2 kT_c \alpha_{c1}}{N_{in}(C)}\right] \qquad \textbf{VIII.11}$$

where α_{c1} and α_{c2} were defined in Chapter **II**. The entropy in Eq. **VIII.11** is bandgap dependent, even when ignoring the α correction terms, as well as concentration dependent. If we now apply Eq. **VIII.8**, requiring that the entropy production always be *positive*, we can find a functional dependence of the concentration on the bandgap:

$$N_{in}(C) \leq \Omega_o E_g^2 kT_c \alpha_{c1} \exp[\alpha_{c2}/\alpha_{c1}] \qquad \textbf{VIII.12}$$

We do not ignore the α correction terms, which can be quite large at smaller bandgaps.

The entropy limitation can be simplified by only taking the bracketed term in Eq. **VIII.11**, which can be seen directly in the formula for μ_{oc} in Eq. **VIII.10**, which leads to:

$$S' \cong k \ln\left[\frac{\Omega_o E_g^2 k T_c \alpha_{c1}}{N_{in}(C)}\right] \qquad \textbf{VIII.13}$$

This approximation is imprecise, and leads to errors in the calculation of the entropy for other systems, such as what was shown in Chapter **VI**, in Eq. **VI.8**. Instead, a more compact formula for the maximal concentration can be found when plugging in the analytical formula for $N_{in}(C)$, neglecting the ambient radiation, as was done in Chapter **I**. This will result in the equation for the entropy found previously in Eq. **II.15**, and we can similarly require that the entropy production is positive, resulting in:

$$\frac{E_g}{kT_S} + \frac{\alpha_{c2}}{\alpha_{c1}} + \ln\left[\frac{\Omega_o T_c \alpha_{c1}}{\Omega_S T_S \alpha_{S1}}\right] - \ln[C] \geq 0 \qquad \textbf{VIII.14}$$

Eq**. VIII.14** is more simplified than Eq. **VIII.12**, and is differentiated by requiring that $E>>kT_S$ as well as $E-\mu>>kT_c$. This difference in approximations may appear to be great, however are shown in Fig. **VIII-2** to be relatively negligible. Fig. **VIII-2** shows the entropy production from Eqs. **VIII.12** (solid line) and **VIII.14** (dashed line) for no concentration, C=1,000 and C=46,000. The zero-entropy threshold is depicted by the dotted line, demonstrating that the entropy production can be negative for rising values of concentration, as a function of the bandgap.

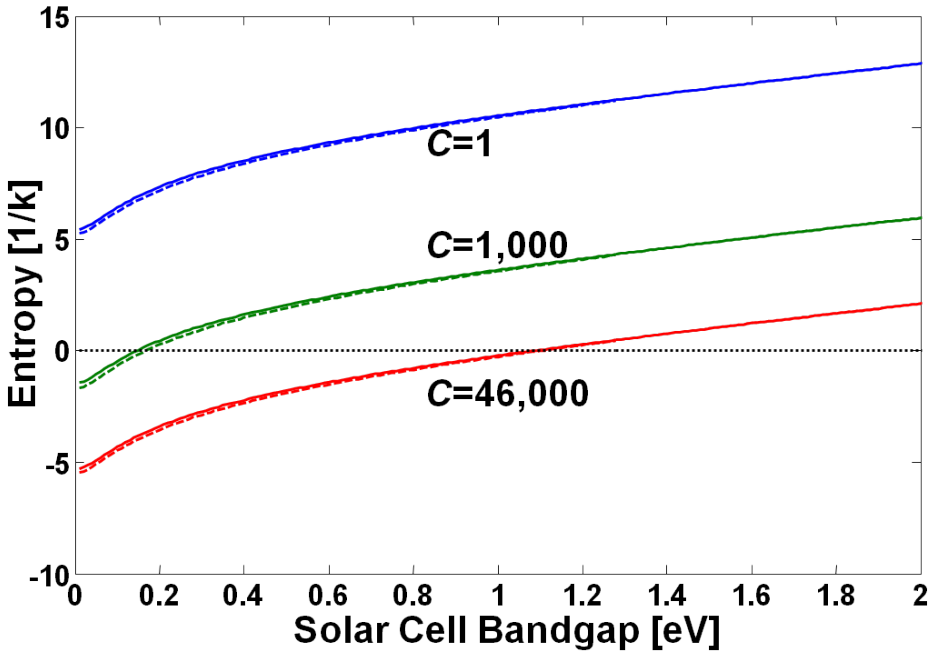

VIII-2 Entropy Production vs. Bandgap for Rising Concentration. The entropy is plotted using both Eq. VIII.12 and Eq. VIII.14, which is slightly more precise (dashed line). The entropy is plotted for three different values of concentration, as labeled, and the threshold for negative entropy production is demarcated by the dotted line at S=0.

We can then isolate the concentration, C, obtaining:

$$C^{\max} = \frac{\Omega_o T_c}{\Omega_S T_S}\left(\frac{\alpha_{c1}}{\alpha_{S1}}\right)\times \exp\left(\frac{E_g}{kT_S}\frac{\alpha_{c2}}{\alpha_{c1}}\right) \qquad \textbf{VIII.15}$$

This formula requires that $E>>kT_S$, which is a stronger requirement than that used to derive Eq. **VIII.12**. However, it provides a clearer physical view of the system, for larger bandgap materials (e.g. with E_g=1 eV), particularly if we ignore the α correction terms (which is not strictly correct). The maximal concentration was found above when the temperatures of the sun and cell were equal. Plugging this requirement into the above equation will result in the simplified formula:

$$C^{\max}\big|_{T_S=T_c} = \frac{\Omega_o}{\Omega_S}\times \exp\left(\frac{E_g}{kT_S}\right) \cong \frac{n_c^2}{\sin^2 \Delta_S}\times \exp\left(\frac{E_g}{kT_S}\right) = C_0^{\max}\times \exp\left(\frac{E_g}{kT_S}\right) \qquad \textbf{VIII.16}$$

Note that here we used the outgoing emission only from the top half of the surface, as was done in the original SQ paper for a flat plate cell **[7]**, such that $\Omega_o=\pi$.

The simplified functional dependence of the maximal concentration on the bandgap is explicit in Eq. **VIII.16**, and the original maximal concentration, C_0. Note that this definition of a modified maximal concentration is similar to that used in Eq. **IV.19** in Chapter **IV** regarding the description of the dc gain term. Eq. **VIII.16** reverts back to Eq. **VIII.4** for a material with *zero bandgap*, E_g=0, such that it absorbs *all* the incoming light. In a semiconductor, not all of the light is absorbed, as a function of the bandgap. Eq. **VIII.16** therefore states that the concentration that *is* absorbed in the smaller subset of energy levels (from E_g and up) us therefore more limited than the case when all the light is absorbed uniformly. Furthermore, **VIII.16** necessitated $T_c=T_S$, which is a situation that would be impractical.

The concentration dependence on the bandgap is plotted in Fig. **VIII-3**, for different values of outgoing emission (with/without a back reflector, which effectively acts as a concentration of C=2). The maximal concentration value of 46,000 is plotted in a dashed line for reference. The plot in Fig. **VIII-3** provides a maximal concentration function of the bandgap, which is in direct contrast to the accepted invariance of the concentration limit. The graph follows the more precise calculation of the entropy limit from Eq. **VIII.12**. In comparison, Eq. **VIII.13** is plotted in the inset of Fig. **VIII-3**, for $\Omega_o=2\pi$, and is quite similar to the main plot, other than at small bandgaps, where the approximation is less valid, regardless.

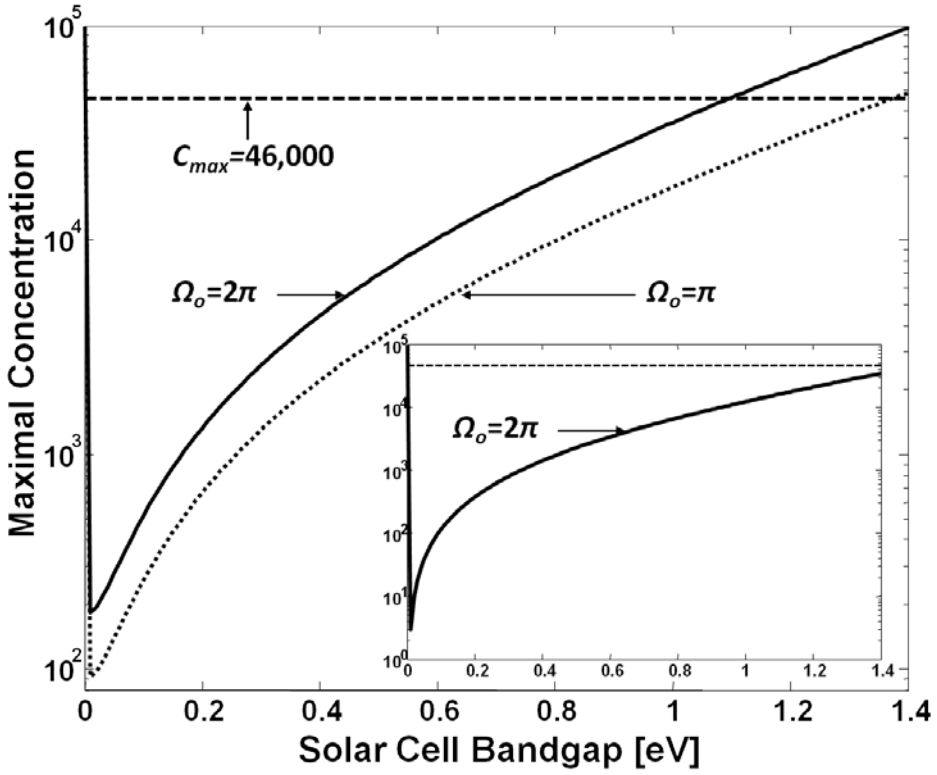

VIII-3 Maximal Concentration as a Function of the Solar Cell Bandgap. Plotted is the maximal concentration from the inequality in Eq. VIII.12, for two different values of outgoing emission étendue. Inset: The same relation when taking only the bracketed term in Eq. VIII.13.

Using the less-approximated version of the concentration limit in Eq. **VIII.12**, we can show that one of the flaws in the argument above is that the temperature of the cell remains constant. It was noted in Eq. **VIII.7** that the temperature of the cell must rise as a function of concentration, C, and extraction efficiency, η_{ext}. However, this was not taken into account, and the temperature was taken as a constant T_c=300 K. However, if we allow the temperature of the cell to rise, the entropy limitation of the maximal concentration is reduced. Cooling the cell using external power will be needed to maintain any form of PV efficiency. Moreover, the assumption that $T_c \neq T_o$, which was made earlier, will be more realistic.

Fig. **VIII-4** plots the maximal concentration from Eq. **VIII.12** using rising cell temperatures. As can be seen, the maximal concentration limitation is pushed upwards for higher temperatures. At these temperatures, the first application of the 2nd law of thermodynamics, which was applied in the beginning of this chapter to obtain C_0^{max} will become relevant, and as plotted in the dashed line. The allowance of a rise in temperature of the cell is therefore an obvious breakdown in the assumptions used in the SQ model, wherein T_c was held constant. However, once the temperatures are allowed to rise above ≈2,000 K, the bandgap dependent limitation of the maximal concentration disappears even for small bandgaps.

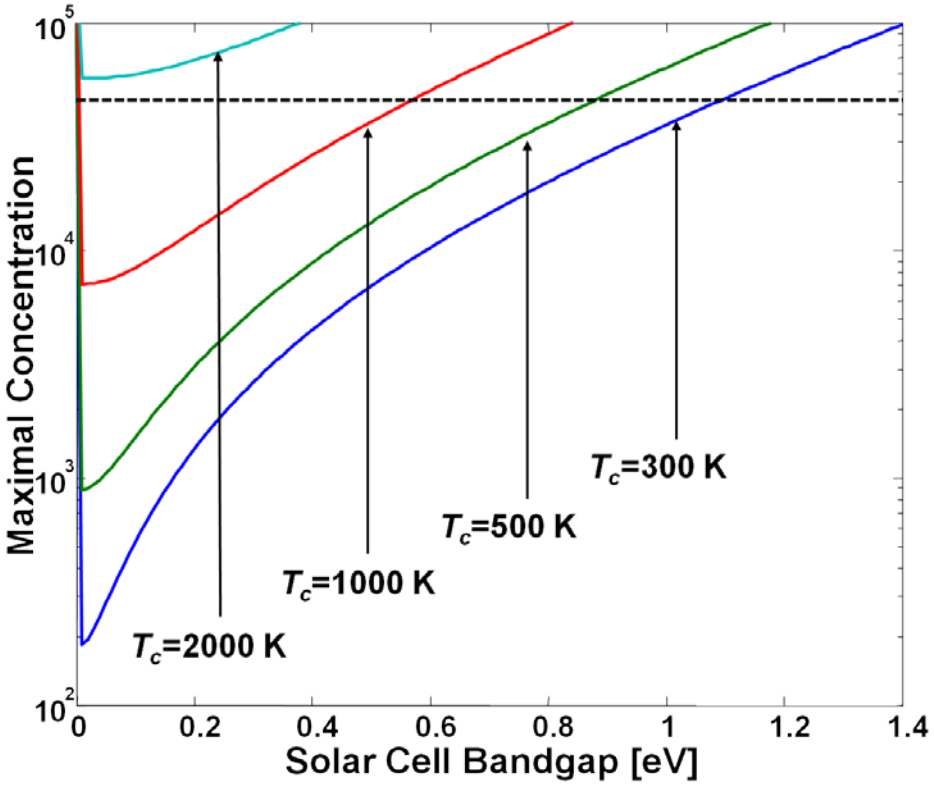

VIII-4 Maximal Concentration for Rising Cell Temperatures. The graph is plotted only for $\Omega_o=2\pi$, and shows the concentration dependent limit become less relevant at temperatures above 2,000 K.

The limits of concentration appearing here make the claim that the maximal concentration is not an invariant number, but rather is bandgap dependent. This results from a few simple applications of the 2nd law of thermodynamics to the equations of PV conversion. Whether this result is a consequence of the breakdown in the two-band model **[14,15]**, or an actual physical result is an interesting conundrum. However it would appear that the addition of the bandgap to the concentration maximum, as was simplified in Eq. **VIII.16**, would make sense in the sense that the étendues should not be the only factor limiting the concentration. In fact, similar concentration limits using an application of Eq. **VIII.8** were found for fluorescent (down-shifting) systems, where the energy is converted before reaching the solar cell **[139,140]**. The results for fluorescent systems were simpler, since they dealt with monochromatic light. Here, we have applied the 2nd law to the full solar spectrum, thereby obtaining a result that is dependent upon the average energy of the photons, E_g/kT_S.

The results of this chapter should be compared with the "maximal efficiency" curves for the 3rd generation techniques in Chapters **III** to **V**. Since we here have seen that the assumed maximal efficiency of 46,000 is not necessarily correct for a regular cell, it should not be used to analyze other 3rd generation techniques without taking into account the possible entropy violation.

IX. Summary & Future Work

The work presented in this thesis followed a set methodology: for every method described for PV conversion, isolate the thermodynamic boundaries, define the input and output fluxes, and find the equations for I_{sc} and V_{oc}. This algorithm can be simplified graphically using the TF approach. Whether the system is designed to match the SQ limit, or surpass it, using this methodology allows a clear and concise path for identifying the primary measureable parameters of interest, as well as the possible loss mechanisms that can detrimentally affect the PV conversion process.

The general perception in the PV field is that the power is mostly provided by the current. Although the simplest formula for the power is seemingly evenly split between the current and the voltage: $P=I\times V$, the current factor is typically thought of as being more important. In contrast, the voltage factor is generally estimated using a rule-of-thumb formula as a function of the bandgap, with $qV_{oc}\approx E_g$-300 meV. This formula is typically used in tandem with the formula for the FF (a derivative of Eq. **I.24**) to obtain the efficiency when using measurements from an actual cell. Focusing on the current requirements of the solar cell appears as a straightforward task of maximizing the absorption of all the photons from the solar spectrum. This must be implemented in parallel with devising a way of extracting the photo-generated electrons (and holes) from the cell. However, many methods of increasing the extraction of carriers, such as by shrinking the dimensions of the cell to nanometer sizes, will also reduce the voltage of the device due to loss mechanisms associated with non-radiative recombination at the surfaces of a semiconductor.

The reduction of the V_{oc} by 300 (or 400) mV is an implicit recognition of the entropic loss of information that was written in closed form in Eq. **II.6**. However, by assuming that this loss term is a constant (invariant), that cannot be directly modified, information is lost, in both the literal and figurative form. The use of Information Theory to describe the entropy in PV conversion has not been a recognized form of analysis for describing the reduction in voltages for a solar cell. In fact, there has been nearly no formal connection between the fields **[141]**, with only few authors recognizing the usefulness of isolating the entropic contribution to the reduction of voltage from an ideal solar cell **[22,41,43,122]**. Part of the reason for this may be the distancing of the "esoteric" concept of entropy from traditional intuitive thinking and teaching. There is nothing unintuitive about entropy, once one thinks in terms of distributions of parameters **[16,51]**. The basic form for the entropy is given by Eq. **II.11**: $S=k\times ln[W]$, and more appropriately for the issue of PV conversion is given by the Kullback-Leibler divergence, which compares the information distance or difference between two distributions. Eq. **II.15** provided a closed-form analytical formula for the entropy in the PV conversion process for a solar cell. This formula can be generalized for losses and can include the contribution for the case of a multi-junction cell, limited by a bandwidth of incoming light, Δ, as in Eq. **VII.4**. We can write this form of the total entropy of conversion in the "unit-less" units of S/k, and ignore all the correction factors α:

$$\frac{S}{k} \cong \frac{E_g}{kT_S} + 1 + \ln\left[\left(\frac{\Omega_o}{\Omega_S}\right)\left(\frac{T_c}{T_S}\right)\right] - \ln[C] - \ln[\kappa_{nr}] + \ln[f(\Delta)] \qquad \textbf{IX.1}$$

We here repeat the physical meaning of each contribution. The first bracketed term includes the ratio of distributions between outgoing and incoming étendues and average temperature of the photons. The next bracketed term is a negative term for concentration, *C*, which reduces the entropy since we are using optical means to "fight" against the natural tendency of the photons to expand their étendue, and we have shown in Chapter **VIII** that this factor can possibly lead to a violation of the 2nd law of thermodynamics. This term should technically be included as a multiplication of the factor for the incoming étendue, Ω_S, since the factor $C\Omega_S$ more correctly describes the incoming distribution of angles of the photons. The next term includes the non-radiative loss term, κ_{nr}, which can be considered as a ratio of distribution of photons contributing to the PV conversion, with those lost to thermalization. The final term includes the bandwidth dependent factor we had found for a multi-junction cell, with $f(\Delta)$ being the bracketed term in Eq. **VII.4**, and can be ignored for a regular single-junction cell. We could also add contributions of the dc process here, which was also shown to have an entropic loss (voltage gain) term in Eqs. **III.16** and **IV.15**. Both the dc and $f(\Delta)$ terms describe a ratio of photons compared to an initial distribution as we have described in detail in the previous chapters.

The only terms in Eq. **IX.1** that were not described directly as a ratio of distributions ($ln[W]$) are the constant of "1", which can be described as a baseline unit for converting the units of natural entropy (base "e", instead of base "2"), and the first term, with E_g/kT_S. This term should be describable using a ratio of distributions within a logarithm:

$$\frac{E_g}{kT_S} = \ln\left[\frac{W_{out}}{W_{in}}\right] \qquad \textbf{IX.2}$$
$$\Rightarrow \exp[E_g / kT_S] = W_{in} / W_{out}$$

While it would at first appear that the ratio in the equation above is simply a Boltzmann factor, which can describe the ratio of carriers in the conduction/valence bands with the intrinsic carrier concentration of a semiconductor **[1,2]**, it should be noted that the temperature appearing in Eq. **IX.2** is T_S and not T_c. Nevertheless, the similarity between this equation and that of the carrier concentrations in a semiconductor (intrinsic carrier concentration) can be interpreted as a description of the entropy produced by shifting the Fermi level of the semiconductor due to the generation of carriers (at temperature T_S) relative to the bandgap. Alternatively, we can say that the amount of excited carriers in the solar cell (in a semiconductor: $ln[n_i^2/n\times p]=E_g/kT_o$) is now proportionate to the ratio of energies between the bandgap and the solar temperature, in kT_S.

The most interesting aspect of the entropy term for the case of PV is that the value of the entropy is something directly quantified via the measurement of the open-circuit voltage, and its relation to the Gibbs free energy of the system. Therefore, we can invert the equation for V_{oc} that we have found, and ignoring the factor of S/k=1, and measure the entropy of the system nearly directly by measuring the bandgap of the cell as well as the V_{oc}. The agreement between the theoretical formula for V_{oc} and the measured value of the voltage from an actual cell demonstrates the validity of this indirect measurement of the entropy. Returning to Fig. **VII-5**, we can concentrate on the far right of the graphs, which describes the V_{oc} for a bulk material without the bandwidth dependence. There, we showed a constant offset of $kT_c ln[\kappa_{nr}]$ that appears between the theoretical value of the V_{oc} and the measured set of values (between the solid line and the dashed line). This allows us to directly infer the internal radiative fluorescence efficiency

of the GaAs to be >95%, as expected for this high-grade material. The theoretical value of V_{oc}=1.09 eV for the bulk cell when including the effects of the non-radiative losses matches the theory exactly, allowing the direct inference of the entropy from the difference between this value of V_{oc} and the bandgap (1.43 eV).

The measured value of the entropy from the open-circuit voltage of any given cell with a known bandgap provides an upper bound for the entropy of the conversion process. Since we have found an analytical expression for this entropy generation, which matches the measured value exactly, we know that there are no other contributions from other parameters of the system that we had perhaps forgotten to include. For example, we know that if we add a polarizer to the input of the cell, we will reduce the incoming spectrum by half (since the solar spectrum is un-polarized). This will reduce the I_{sc} by half, but only reduce the V_{oc} by a factor of $kT_c ln[2]$ (as described in Chapter **II**). There are no other "hidden parameters" of the system that we have not yet found, which means that the primary factors affecting the value of the open-circuit voltage (and the entropy) are the étendue factor of the incoming radiation, and the non-radiative loss term, which is a function of the choice of material. For a multi-junction cell, we must also add the component of the bandwidth of light, which reduces the voltage by another factor of $kT_c ln[f(\Delta)]$. Since the concentration factor can affect the incoming étendue term directly, we can control this loss factor externally by using optics. However, the other two terms, κ_{nr} and Δ, are based on the choice of material systems used to build the cell, and thus are extremely important factors for optimizing the efficiency of any type of solar cell system from the perspective of the open-circuit voltage. These parameters are different for each choice of semiconductor, and for a multi-junction cell, they must be optimized on a per-segment basis, in order to optimize the V_{oc} as well as the I_{sc}. Any algorithm for calculating the overall efficiency must take these parameters into account.

While it was just claimed that the measured value of the entropy is precise, based off of the measurement of the V_{oc} and E_g of the cell, there is an amount of error that was not included in this description. For example, the efficiency calculation was done for the direct component of the sunlight, and simulated experimentally using a solar simulator that mimics the AM1.5 spectrum. While this calculation is correct in laboratory settings, it should be recalled that the actual solar irradiation is broken into direct and diffuse components **[12]**, such that only 70% of the actual illumination spectrum is direct. Furthermore, the effects of Rayleigh scattering in the atmosphere, which "preferentially" scatters the higher energy (bluer) photons, should be included into this scattered spectrum. Therefore, the incoming étendue parameter should no longer be a constant, Ω_S, but rather should be a function of the photon's energy: $\Omega_S(E)$. This energy (frequency) dependence would mean that the étendue term will not be outside the integral for the incoming solar irradiation (Eq. **I.9**), but will be within the integrand. The outgoing étendue should follow a similar path, with the factor $\Omega_o=\Omega_o(E)$. Furthermore, the index of refraction, which was taken at near constant until now, particularly when an AR coating is used, should be placed within the integrand as well, as a function of the energy. The use of AR coatings greatly reduces the mismatch between indices of refraction, as well as the outgoing emission characteristics of the cell. Nevertheless, a precise description of the entropy losses in the PV conversion should account for all of these functional characteristics of the parameters if the solar cell is to be completely optimized. Such an inclusion of the parameters within the integrals will prevent a closed-form analytical formula for the entropy to be found, but can be

evaluated numerically. This numerical solution can also include the effects of the thickness and absorption coefficient of the material, as well as any optical elements attached to the cell (or cell segment in a multi-junction system). A full algorithm for finding the optimal distribution of bandgaps of the semiconductors while including optical methods, material properties would be an interesting next step of research in this field. This should include the choice of circuit that the solar cell utilizes, whether placing the cells in series or in parallel, as well as combinations of these two basic configurations.

The work described here therefore provides a first step in finding ways to optimize the conversion efficiency of any PV system in the most thorough way possible. All factors must be individually isolated, optimized, and not neglected if we are to extract as much power as we possibly can from the solar illumination. In addition, to surpass the SQ DB limit, we can attempt to find amongst the few parameters characterizing the PV process modifications that lie outside the set of assumptions listed in Chapter **I** and throughout this work. Methods of improving the voltage are just as important as methods of improving the current, and new paradigms of generating power from the solar spectrum might yet be found that have maximal absorption and minimal entropic losses.

References

1. M. Grundmann, *The Physics of Semiconductors* (Springer-Verlag, Berlin, 2nd ed. 2010).
2. S.M. Sze, *Physics of Semiconductor Devices* (Wiley, New York, 1981).
3. M.A. Green, *Solar Cells: Operating Principles, Technology and System Applications* (Prentice-Hall, Englewood-Cliffs, 1982).
4. M.A. Green, *Third Generation Photovoltaics* (Springer-Verlag, Berlin, 2003).
5. A. De Vos, *Endoreversible Thermodynamics of Solar Energy Conversion* (Oxford University Press, New York, 1992).
6. A. De Vos, *Thermodynamics of Solar Energy Conversion* (Wiley-VCH, Berlin, 2008).
7. W. Shockley and H.J. Queisser. Detailed Balance Limit of Efficiency of *p-n* Junction Solar Cells. *J. Appl. Phys.* **32**, 510 **(**1961).
8. ASTM G173-03 data taken from the NREL website for SMARTS: http://rredc.nrel.gov/solar/spectra/am1.5/ASTMG173/ASTMG173.html
9. G. Smestad, H. Ries, R. Winston and E. Yablonovitch, The thermodynamic limits of light concentrators. *Sol. Energ. Mater.* **21**, 99 (1990).
10. T. Markvart, The thermodynamics of optical étendue. *J. Opt. A*, 10, 015008 (2008).
11. M. Born and E. Wolf, *Principles of Optics* (Cambridge University Press, New York, 7th ed., 1999).
12. W.H. Press. Theoretical maximum for energy from direct and diffuse sunlight. *Nature* 264, 75 (1976).
13. A. Rabl, *Active Solar Collectors and Their Applications* (Oxford University Press, New York, 1985).
14. P. Baruch, A two-level system as a model for a photovoltaic solar cell. *J. Appl. Phys.* **57**, 1347 (1985).
15. W. Ruppel and P. Würfel, Upper Limit for the Conversion of Solar Energy. *IEEE T. Electron Dev.* **27**, 877 (1980).
16. A. Ben-Naim, *A farewell to entropy: statistical thermodynamics based on information: S=logW* (World Scientific Publishing, Singapore, 2008).
17. http://www.ioffe.ru/SVA/NSM/Semicond/GaAs/optic.html
18. J. Mattheis, J.H. Werner and U. Rau, Finite mobility effects on the radiative efficiency limit of pn-junction solar cells. *Phys. Rev. B* 77, 085203 (2008).
19. K.H. Böhm and B. Schlender, Tabelle von Integralen über die Kirchhoff-Planck Funktion. *Zeitschrift für Astrophysik* **43**, 95 (1957).
20. W. van Roosbroeck and W. Shockley, Photon-Radiative Recombination of Electrons and Holes in Germanium. *Phys. Rev.* **94**, 1558 (1954).
21. G. Lasher and F. Stern, Spontaneous and Stimulated Recombination Radiation in Semiconductors. *Phys. Rev.* **133**, A553 (1964).
22. R. T. Ross, Some Thermodynamics of Photochemical Systems. *J. Chem Phys*. **46**, 4590 (1967).
23. R.T. Ross and J.M. Collins, Efficiency of quantum-utilizing solar energy converters in the presence of recombination losses. *J. Appl. Phys.* **51**, 4054 (1980).
24. M. Wolf, Limitations and Possibilities for Improvement of Photovoltaic Solar Energy Converters, Part I: Considerations for Earth's Surface Operation. *Proceedings of the Institute of Radio Engineers* **48**, 1246 (1960).

25. M. Wolf, A New Look At Silicon Solar Cell Performance. *Energ. Conv.* **11**, 63 (1970).
26. A. Martí, J.L. Balenzategui and R.F. Reyna, Photon recycling and Shockley's diode equation. *J. Appl. Phys.* **82**, 4067 (1997).
27. T. Kirchartz and U. Rau, Detailed balance and reciprocity in solar cells, *Phys. Stat. Sol. A* **205**, 2737 (2008).
28. A. Rabl, Comparison of solar concentrators. *Sol. Energy* **18**, 93 (1976).
29. P. Baruch, P.T. Landsberg, A. De Vos, Thermodynamics limits to solar cell efficiencies under various illumination conditions, in *11th E. C. Photovoltaic Solar Energy Conference*, Montreal, Canada, October 1992, p. 283.
30. M. A. Green, Accuracy of analytical expressions for solar cell fill factors. *Solar Cells* **7**, 337 (1982).
31. A. Luque and V. Andreev, *Concentrator Photovoltaics* (Springer, Berlin, 2007).
32. A. Luque and G.L. Araújo, *Physical Limitations to Photovoltaic Energy Conversion* (Adam Hilger, Bristol 1990).
33. M.A. Green, Third Generation Photovoltaics: Ultra-High Conversion Efficiency at Low Cost. *Prog. Photovolt: Res. Appl.* **9**, 123 (2001).
34. J. Gordon, A simple derivation of work and efficiency limits for blackbody radiation converters. *Am. J. Phys.* **61**, 821 (1993).
35. C.H. Henry, Limiting efficiencies of ideal single and multiple energy gap terrestrial solar cells. *J. Appl. Phys.* **51**, 4494 (1980).
36. A. De Vos, Detailed balance limit of the efficiency of tandem solar cells. *J. Phys. D: Appl. Phys.* **13**, 839 (1980).
37. A. De Vos and H. Pauwels, On the Thermodynamic Limit of Photovoltaic Energy Conversion. *Appl. Phys.* **25**, 119 (1981).
38. A. Martí, G.L. Araújo, Limiting efficiencies for photovoltaic energy conversion in multigap systems. *Sol. Energ. Mat. Sol. C.* **43**, 203 (1996).
39. T. Markvart and P.T. Landsberg, Thermodynamics and reciprocity of solar energy conversion. *Physica E* **14**, 71 (2002).
40. Z.R. Abrams, A. Niv, M. Gharghi, C. Gladden and X. Zhang, A Comparison of 3rd Generation Solar Cell Efficiencies Using Thermodynamic Transfer Functions: Which Method is Best? In: *Proceedings of the 37th IEEE Photovoltaic Specialist Conference*, 19-24 June 2011, Seattle, WA, USA.
41. T. Markvart and P.T. Landsberg, Everyman's guide to third generation efficiencies. *Proceedings of the Third World Conference on Photovoltaic Solar Energy Conversion*, Osaka, Japan, 2003, p. 289.
42. T. Markvart, Thermodynamics of losses in photovoltaic conversion. *Appl. Phys. Lett.* **91**, 064102 (2007).
43. T. Markvart, Solar cell as a heat engine: energy–entropy analysis of photovoltaic conversion. *Phys. Stat. Sol. A* **205**, 2752 (2008).
44. G.D. Cody and T. Tiedje, Physical Limits to Solar Cell Efficiency, in *Energy and the Environment*, B. Abeles, A. Jacobson, P. Sheng, Eds. (World Scientific Publishing, Singapore, 1992) pp. 147-217.
45. A. Luque and A. Marti, Entropy production in photovoltaic conversion. *Phys. Rev. B* **55**, 6994 (1997).
46. H. Ries and A.J. McEvoy, Chemical potential and temperature of light. *J. Photochem. Photobiol. A: Chem.* **59**, 11 (1991).

47. P. Würfel, The chemical potential of radiation. *J. Phys. C: Solid State Phys.* **15**, 3967 (1982).
48. P.T. Landsberg and T. Markvart, The Carnot Factor in Solar-Cell Theory. *Solid State Electron.* **42**, 657 (1998).
49. P.T. Landsberg and V. Badescu, Carnot factor in solar-cell efficiencies. *J. Phys. D: Appl. Phys.* **33**, 3004 (2000).
50. E. Yablonovitch and G.D. Cody, Intensity Enhancement in Textured Optical Sheets for Solar Cells. *IEEE Trans. Electron. Dev.* **ED-29**, 300 (1982).
51. J.R. Pierce, *An Introduction to Information Theory: Symbols, Signals & Noise* (Dover Publications, New York, 2nd Ed. 1980).
52. T.M. Cover and J.A. Thomas, *Elements of Information Theory* (Wiley-Interscience Publications, New York, 1991).
53. Z.R. Abrams, A. Niv and X. Zhang, Solar energy enhancement using down-converting particles: A rigorous approach. *J. Appl. Phys.* **109** 114905 (2011).
54. T. Trupke, M.A. Green and P. Würfel, Improving solar cell efficiencies by down-conversion of high-energy photons. *J. Appl. Phys.* **92**, 1668 (2002).
55. V. Badescu, A. De Vos, A.M. Badescu and A. Szymanska, Improved model for solar cells with down-conversion and down-shifting of high-energy photons. *J. Phys. D: Appl. Phys.* **40**, 341 (2007).
56. V. Badescu and A. De Vos, Influence of some design parameters on the efficiency of solar cells with down-conversion and down shifting of high-energy photons. *J. Appl. Phys.* **102**, 073102 (2007).
57. R. T. Wegh, H. Donker, K. D. Oskam and A. Meijerink, Visible Quantum Cutting in LiGdF4:Eu3+ Through Downconversion. *Science* **283**, 663 (1999).
58. B. M. van der Ende, L. Aarts and A. Meijernik, Lanthanide ions as spectral converters for solar cells. *Phys. Chem. Chem. Phys.* **11**, 11081 (2009).
59. E. Yablonovitch, Thermodynamics of the fluorescent planar concentrator. *J. Opt. Soc. Am.* **70**, 1362 (1980).
60. H. Ries, Thermodynamic limitations of the concentration of electromagnetic radiation. *J. Opt. Soc. Am.* **72**, 380 (1982).
61. T. Markvart, Detailed balance method for ideal single-stage fluorescent collectors. *J. Appl. Phys.* **99**, 026101 (2006).
62. P. Kittidachachan, L. Danos, T.J.J. Meyer, N. Alderman and T. Markvart, Photon Collection Efficiency of Fluorescent Solar Collectors. *Chimia* **61**, 780 (2007).
63. E. Klampaftis, D. Ross, K.R. McIntosh and B.S. Richards, Enhancing the performance of solar cells via luminescent down-shifting of the incident spectrum: A review. *Sol. Energ. Mat. So. C.* **93**, 1182 (2009).
64. A. Luque, A. Martí, E. Antolín and C. Tablero, Intermediate bands versus levels in non-radiative recombination. *Physica B* **382**, 320 (2006).
65. A. Luque and A. Martí, Increasing the Efficiency of Ideal Solar Cells by Photon Induced Transitions at Intermediate Levels. *Phys. Rev. Lett.* **78**, 5014 (1997).
66. B. M. Kayes, H. A. Atwater and N. S. Lewis, Comparison of the device physics principles of planar and radial p-n junction nanorod solar cells. *J. Appl. Phys.* **97**, 114302 (2005).
67. E. Garnett and P. Yang, Light Trapping in Silicon Nanowire Solar Cells. *Nano Lett.* **10**, 1082 (2010).

68. Z.R. Abrams, M. Gharghi, C. Gladden and X. Zhang, Theoretical Efficiency of 3rd Generation Solar Cells: Comparison between Carrier Multiplication and Down-Conversion, *Sol. Energ. Mat. Sol. C.* **99**, 308 (2012).
69. V.I. Klimov, Detailed-balance power conversion limits of nanocrystal-quantum-dot solar cells in the presence of carrier multiplication. *Appl. Phys. Lett.* **89**, 123118 (2006).
70. M.C. Hanna and A.J. Nozik, Solar conversion efficiency of photovoltaic and photoelectrolysis cells with carrier multiplication absorbers. *J. Appl. Phys.* **100**, 074510 (2006).
71. J.A. Mcquire, J. Joo, J.M. Pietryga, R.D. Schaller, V.I. Klimov, New Aspects of Carrier Multiplication in Semiconductor Nanocrystals. *Acc. Chem. Res.* **41**, 1810 (2008).
72. A.J. Nozik, Multiple exciton generation in semiconductor quantum dots. *Chem. Phys. Lett.* **457**, 3 (2008).
73. M. Wolf, R. Brendel, J.H Werner and H.J. Queisser, Solar cell efficiency and carrier multiplication in $Si_{1-X}Ge_X$ alloys. *J. Appl. Phys.* **83**, 4213 (1998).
74. D. Gachet, A. Avidan, I. Pinkas and D. Oron, An Upper Bound to Carrier Multiplication Efficiency in Type II Colloidal Quantum Dots. *Nano Lett.* **10**, 164 (2009).
75. M.T. Trinh, A.J. Houtepen, J.M. Schins, T. Hanrath, J. Piris, W. Knulst, A.P.L.M. Goossens and L.D.A. Siebbeles, In Spite of Recent Doubts Carrier Multiplication Does Occur in PbSe Nanocrystals. *Nano Lett.* **8**, 1713 (2008).
76. Y. Takeda and T. Motohiro, Requisites to realize high conversion efficiency of solar cells utilizing carrier multiplication. *Sol. Energy Mater. Sol. Cells* **94**, 1399 (2010).
77. O.E. Semonin, J.M. Luther, S. Choi, H.Y. Chen, J. Gao, A.J. Nozik and M.C. Beard, Peak External Photocurrent Quantum Efficiency Exceeding 100% via MEG in Quantum Dot Solar Cell, *Science* **334**, 1530 (2011).
78. J.H. Werner, S. Kolodinski and H.J. Queisser, Novel Optimization Principles and Efficiency Limits for Semiconductor Solar Cells. *Phys. Rev. Lett.* **72**, 3851 (1994).
79. J.H. Werner, R. Brendel and H.J. Queisser, New upper efficiency limits for semiconductor solar cells, in: *Proceedings of the IEEE 1st World Conference on Photovoltaic Energy Conversion,* 1994, Waikoloa, HI, USA; pp. 1742-1745.
80. R. Brendel, J.H. Werner and H.J. Queisser, Thermodynamic efficiency limits for semiconductor solar cells with carrier multiplication. *Sol. Energy Mater. Sol. Cells* **41/42**, 419 (1996).
81. W. Spirkl and H. Ries, Luminescence and efficiency of an ideal photovoltaic cell with charge carrier multiplication. *Phys. Rev. B* **52**, 11319 (1995).
82. A. Luque, A. Martí and L. Cuadra, Thermodynamics of solar energy conversion in novel structures. *Physica E* **14**, 107 (2002).
83. A. De Vos and B. Desoete, On the ideal performance of solar cells with larger-than-unity quantum efficiency. *Sol Energy Mater. Sol. Cells* **51**, 413 (1998).
84. P.T. Landsberg and V. Badescu, Solar cell thermodynamics including multiple impact ionization and concentration of radiation. *J. Phys. D: Appl. Phys.* **35**, 1236 (2002).
85. H. Shpaisman, O. Niitsoo, I. Lubumirsky and D. Cahen, Can up- and down-conversion and multi-exciton generation improve photovoltaics? *Sol. Energy Mater. Sol. C.* **92**, 1541 (2008).
86. M.B. Smith and J. Michl, Singlet Fission. *Chem. Rev.* **110**, 6891 (2010).
87. T. Trupke, M.A. Green and P. Würfel, Improving solar cell efficiencies by up-conversion of sub-band-gap light. *J. Appl. Phys.* **92** (2002), pp. 4117-4122.

88. A. Shalav, B.S. Richards and M.A Green, Luminescent layers for enhanced silicon solar cell performance: Up conversion. *Sol. Energ. Mater. Sol. C.* **91**, 829 (2007).
89. C. Strümpel, M. McCann, G. Beaucarne, V. Arkhipov, A. Slaoui, V. Švrček, C. del Caññand I Tobias, Modifying the solar spectrum to enhance silicon solar cell efficiency-An overview of available materials. *Sol Energ. Mater. Sol. C.* **91**, 238 (2007).
90. A. Luque and A Martí, A Metallic Intermediate Band High Efficiency Solar Cell. *Prog. Photovolt: Res. Appl.* **9**, 73 (2001).
91. M.Y. Levy and C. Honsberg, Absorption coefficients of intermediate-band media. *J. Appl. Phys.* **106**, 073103 (2009).
92. R. Strandberg and T.W. Reenaas, Drift-diffusion model for intermediate band solar cells including photofilling effects. *Prog. Photovolt: Res. Appl.* **19**, 21 (2011).
93. N. López, L.A. Reichertz, K.M. Yu, K. Campman and W. Walukiewicz, Engineering the Electronic Band Structure for Multiband Solar Cells. *Phys. Rev. Lett.* **106**, 028701 (2011).
94. P. Würfel, Solar energy conversion with hot electrons from impact ionization. *Sol. Energy Mater. Sol. Cells* **46** (1997), pp. 43-52.
95. Y. Takeda, T. Ito, T. Motohiro, D. König, S. Shrestha and G. Conibeer, Hot carrier solar cells operating under practical conditions. *J. Appl. Phys.* **105**, 074905 (2009).
96. A. Niv, Z.R. Abrams, M. Gharghi, C. Gladden and X. Zhang, Overcoming the Bandgap Limitation on Solar Cell Materials. *Appl. Phys. Lett.* **100**, 083901 (2012).
97. R.A. Sinton and R.M. Swanson, Increased Photogeneration in Thin Silicon Concentrator Solar Cells. *IEEE T. Electron. Dev.* **8**, 547 (1987).
98. G.L. Araújo and A. Martí, Absolute limiting efficiencies for photovoltaic energy conversion. *Sol. Energ. Mat. Sol. C.* **33**, 213 (1994).
99. T. Markvart, Beyond the Yablonovitch limit: Trapping light by frequency shift. *Appl. Phys. Lett.* **98**, 071107 (2011).
100. A. Martí and G.L. Araújo, Limiting efficiencies for photovoltaic energy conversion in multigap systems. *Sol. Energ. Mat. Sol. C.* **43**, 203 (1996).
101. R. Strandberg and T. W. Reenaas, Limiting efficiency of intermediate band solar cells with spectrally selective reflectors. *Appl. Phys. Lett.* **97**, 031910 (2010).
102. M. A. Green, Limits on the Open-circuit Voltage and Efficiency of Silicon Solar Cells Imposed by Intrinsic Auger Processes. *IEEE Trans. Electron Devices* **31**, 671 (1984).
103. J. E. Parrott, Self-consistent detailed balance treatment of the solar cell. *IEE Proc.* 133 , 314 (1986).
104. T. S. Moss, Theory of Intensity Dependence of Refractive Index. *Phys. Stat. Sol. B* 101, 555 (1980).
105. T. Tiedje, E. Yablonovitch, G. D. Cody and B. G. Brooks, Limiting Efficiency of Silicon Solar Cells. *IEEE T. Electron. Dev.* **31**, 711 (1984).
106. E. Burstein, Anomolous Optical Absorption Limit in InSb. *Phys. Rev.* **93**, 632 (1954).
107. W. Kaiser and H.Y. Fan, Infrared Absorption of Indium Antimonide. *Phys. Rev.* **98**, 966 (1955).
108. P. D. Dapkus, N. Holonyak, R. D. Burnham and D. L. Keune, Direct Observation of a Dynamic Burstein Shift in a GaAs:Ge Platelet Laser. *Appl. Phys. Lett.* **16**, 93 (1970).
109. P. V. Kamat, N. M. Dimitrijevic and A. J. Nozik, Dynamic Burstein-Moss Shift in Semiconductor Colloids. *J. Phys. Chem.* **93**, 2873 (1989).

110. K. L. Litvinenko, L. Nikzad, C.R. Pidgeon, J. Allam, L.F. Cohen, T. Ashley, M. Emeny, W. Zawadzki and B.N. Murdin, Temperature dependence of the electron Landé g factor in InSb and GaAs . *Phys. Rev. B* **77**, 033204 (2008).
111. C. Wadia, A. P. Alivisatos and D. M. Kammen, Materials Availability Expands the Opportunity for Large-Scale Photovoltaics Deployment. *Environ. Sci. Tech.* **43**, 2072 (2009).
112. P. P. Altermatt, T. Kiesewetter, K. Ellmer and H. Tributsch, Specifying targets of future research in photovoltaic devices containing pyrite (FeS2) by numerical modeling. *Sol. Energ. Mat. Sol. C.* **71**, 181 (2002).
113. A. Vossier, B. Hirsch and J. M. Gordon, Is Auger recombination the ultimate performance limiter in concentrator solar cells? *Appl. Phys. Lett.* **97**, 193509 (2010).
114. P. Campbell and M.A. Green, The Limiting Efficiency of Silicon Solar Cells under Concentrated Sunlight. *IEEE T. Electron. Dev.* **33**, 234 (1986).
115. G. Stollwerck, O. V. Sulima and A. W. Bett, Characterization and Simulation of GaSb Device-Related Properties. *IEEE T. Electron. Dev.* **47**, 448 (2000).
116. P.C. Findlay, C.R. Pidgeon, H. Pellemans, R. Kotitschke, B.N. Murdin, T. Ashley, A.D. Johnson, A.M. White. And C.T. Elliott, Auger recombination dynamics of $In_xGa_{1-x}Sb$. *Semicond. Sci. Technol.* **14**, 1026 (1999).
117. V. Badescu, Spectrally and angularly selective photothermal and photovoltaic converters under one-sun illumination. *J. Phys. D: Appl. Phys.* **38**, 2166 (2005).
118. C. Ulbrich, S.Fahr, J. Üpping, M. Peters, T. Kirchartz, C. Rockstuhl, R. Wehrspohn, A. Gombert, F. Lederer and U. Rau, Directional selectivity and ultra-light-trapping in solar cells. *Phys. Stat. Sol. (a*) **205**, 2831 (2008).
119. M. Peters, C. Ulbrich, J.C. Goldschmidt, J. Fernandez, J. Siefer and B. Bläsi, Directionally selective light trapping in a germanium solar cell. *Opt. Express* **19**, 136 (2011).
120. M. Peters, J.C. Goldschmidt and B. Bläsi, Angular confinement and concentration in photovoltaic converters. *Sol. Energy. Mater. Sol. C.* **94**, 1393 (2010).
121. E. Yablonovitch, Inhibited Spontaneous Emission in Solid-State Physics and Electronics. *Phys. Rev. Lett.* **58**, 2059 (1987).
122. M. Peters, J.C. Goldschmidt and B. Bläsi, Efficiency limit and example of a photonic solar cell. *J. Appl. Phys.***110**, 043104 (2011).
123. O. von Roos, Influence of radiative recombination on the minority-carrier transport in direct band-gap semiconductors. *J. Appl. Phys.* **54**, 1390 (1983).
124. V. Badescu and P.T. Landsberg, Influence of photon recycling on solar cell efficiencies. *Semicond. Sci. Technol.* **12**, 1491 (1997).
125. A. Martí, J.L. Balenzategui and R.F. Reyna, Photon recycling and Shockley's diode equation. *J. Appl. Phys.* **82**, 4067 (1997).
126. C. Eisler, Z.R. Abrams, M. Sheldon, H. Atwater and X. Zhang *in submission* (2012).
127. W. Blocker, High-Efficiency Solar Energy Conversion Through Flux Concentration and Spectral Splitting. *Proc. IEEE* **66**, 104 (1978).
128. A.G. Imenes and R. Mills, Spectral beam splitting technology for increased conversion efficiency in solar concentrating systems: a review. *Sol. Energ. Mat. Sol. C.* **84**, 19 (2004).
129. J.D. McCambridge, M.A. Steiner, B.L. Unger, K.A. Emery, E.L. Christensen, M.W. Wanlass, A.L. Gray, L. Takacs, R. Buelow, T.A. McCollum, J.W. Ashmead, G.R.

Schmidt, A.W. Haas, J.R. Wilcox, J. Van Meter, J.L. Gray, D.T. Moore, A.M. Barnett and R.J. Schwartz, Compact spectrum splitting photovoltaic module with high efficiency. *Prog. Photovolt: Res. Appl.* **19**, 352 (2011).

130. B. Mitchell, G. Peharz, G. Siefer, M. Peters, T. Gandy, J.C. Goldschmidt, J. Benick, S.W. Glunz, A.W. Bett and F. Dimroth, Four-junction spectral beam-splitting photovoltaic receiver with high optical efficiency. *Prog. Photovolt: Res. Appl.* **19**, 61 (2011).
131. E.R. Torrey, J. Krohn, P.P. Ruden and P.I. Cohen, EFFICIENCY OF A LATERALLY ENGINEERED ARCHITECTURE FOR PHOTOVOLTAICS, in 35th *IEEE Photovoltaic Specialist Conference*, Honolulu, HI, USA, June 2010, p. 2978.
132. E.R. Torrey, P.P Ruden and P.I. Cohen, Performance of a split-spectrum photovoltaic device operating under time-varying spectral conditions. *J. Appl. Phys.* **109**, 074909 (2011).
133. M.A Green and A. Ho-Baillie, Forty three per cent composite split-spectrum concentrator solar cell efficiency. *Prog. Photovolt: Res. Appl.* **18**, 42 (2010).
134. A.S. Brown and M.A. Green, Detailed balance limit for the series constrained two terminal tandem solar cell. *Physica E* **14**, 96 (2002).
135. M.A. Green, Radiative efficiency of state-of-the-art photovoltaic cells. *Prog. Photovolt: Res. Appl.* DOI: 10.1002/pip.1147 (2011).
136. I. Schnitzer, E. Yablonovitch , C. Caneau, T. J. Gmitter, Ultrahigh spontaneous emission quantum efficiency, 99.7% internally and 72% externally, from AIGaAs/GaAs/ AlGaAs double heterostructures. *Appl. Phys. Lett.* **62**, 11 (1993).
137. Z.R. Abrams and X. Zhang, *in submission* (2012).
138. H. Kiess, W. Rehwald, On the ultimate efficiency of solar cells. *Sol. Energ. Mat. Sol. C.* **38**, 45 (1995).
139. E. Yablonovitch, Thermodynamics of the fluorescent planar concentrator. *J. Opt. Soc. Am.* **70**, 1362 (1980).
140. H. Ries, Thermodynamic limitations of the concentration of electromagnetic radiation. *J. Opt. Soc. Am.***72**, 380 (1982).
141. Y.M. Svirzhev and W.H. Steinborn, Exergy of solar radiation: information approach. *Eco. Model.* **145**, 101 (2001).

Appendix: List of Formulas:

$$E\,[\mathrm{eV}] = h\nu = \frac{hc}{\lambda} \cong \frac{1.24}{\lambda\,[\mu\mathrm{m}]} \qquad \text{I.1}$$

$$n_S = g \times \frac{E^2}{\exp[E/kT_S] - 1} \qquad \text{I.2}$$

$$g = \frac{2}{h^3 c^2} \qquad \text{I.3}$$

$$\delta\varepsilon = n^2 \cos\theta\, \delta\Omega\, \delta A \qquad \text{I.4}$$

$$\Omega_S = \pi \sin^2 \Delta_S \cong 6.85 \times 10^{-5}\, sr \qquad \text{I.5}$$

$$N_S = g \times \Omega_S \times \int_{E_{th}}^{\infty} \frac{E^2 dE}{\exp[E/kT_S] - 1} \qquad \text{I.6}$$

$$N_S = g \times \Omega_S \times \int_{0}^{\infty} \frac{\alpha_{abs}(E) \times E^2 dE}{\exp[E/kT_S] - 1} \qquad \text{I.7}$$

$$\alpha_{abs}(E) = u(E_g) = \begin{Bmatrix} 0 \mid & E < E_g \\ 1 \mid & E > E_g \end{Bmatrix} \qquad \text{I.8}$$

$$N_S = g \times \Omega_S \times \int_{E_g}^{\infty} \frac{E^2 dE}{\exp[E/kT_S] - 1} \qquad \text{I.9}$$

$$\eta_{UE} = g_2 \times E_g \times \int_{E_g}^{\infty} \frac{E^2 dE}{\exp[E/kT_S] - 1} \qquad \text{I.10}$$

$$g_2 = 15/(\pi k T_S)^4 \qquad \text{I.11}$$

$$\int_{E'}^{\infty} \frac{E^2 dE}{\exp[E/kT] - 1} \cong kTe^{E'/kT} E'^2 [1 + 2kT/E' + 2(kT/E')^2] \qquad \text{I.12}$$

$$r_{abs} = r_{spon} + r_{stim} \qquad \text{I.13}$$

$$r_{abs} \cong r_{spon} \qquad \text{I.14}$$

$$N_{out} = g \times \Omega_o \times n_c^2 \times \int_{E_g}^{\infty} \frac{E^2 dE}{\exp[(E-\mu)/kT_c] - 1} \qquad \text{I.15}$$

$$V = \mu / q \qquad \text{I.16}$$

$$N_{out} = \frac{g \times \Omega_o \times n_c^2}{\kappa_{nr}} \times \int_{E_g}^{\infty} \frac{E^2 dE}{\exp[(E-\mu)/kT_c] - 1} \qquad \text{I.17}$$

$$f_\Omega \equiv \frac{\Omega_o}{\Omega_S} \le 1 \qquad \text{I.18}$$

$$C^{\max} = \frac{1}{\sin^2 \Delta_S} \cong 46{,}000 \qquad \text{I.19}$$

$$N_{BB} = g(1 - Cf_{\Omega})\Omega_o \int_{E_g}^{\infty} \frac{E^2 dE}{\exp[E/kT_o] - 1} \qquad \text{I.20}$$

$$N_{Total} = gC\Omega_S \int_{E_g}^{\infty} \frac{E^2 dE}{\exp[E/kT_S] - 1} + g(1 - Cf_{\Omega})\Omega_o \int_{E_g}^{\infty} \frac{E^2 dE}{\exp[E/kT_o] - 1} \qquad \text{I.21}$$

$$\eta_{DB}(E_g, C) = g_2 \times V \times \left[\int_{E_g}^{\infty} \frac{E^2 dE}{\exp[E/kT_S] - 1} - \frac{1}{C\Omega_S} \int_{E_g}^{\infty} \frac{E^2 dE}{\exp[(E - qV)/kT_c] - 1} \right] \qquad \text{I.22}$$

$$FF \equiv \frac{I_m V_m}{I_{sc} V_{sc}} \leq 1 \qquad \text{I.23}$$

$$FF = \frac{v_{oc} - \ln[v_{oc} + 1 - \ln(v_{oc})]}{v_{oc} - \ln[v_{oc} + 1 - \ln(v_{oc})] + 1} \times \frac{v_{oc} - \ln\{v_{oc} - \ln[v_{oc} + 1 - \ln(v_{oc})] + 1\}}{v_{oc}\left[1 - \exp(-v_{oc})\right]} \qquad \text{I.24}$$

$$\eta_{eff} = FF \times I_{sc} \times V_{oc} \qquad \text{I.25}$$

$$I_{sc}^{reg} = qgC\Omega_S \int_{E_g}^{\infty} \frac{E^2 dE}{\exp[E/kT_S] - 1} - qg\Omega_o \int_{E_g}^{\infty} \frac{E^2 dE}{\exp[(E - 0)/kT_c] - 1}$$

$$\approx qgC\Omega_S \int_{E_g}^{\infty} \frac{E^2 dE}{\exp[E/kT_S] - 1} \qquad \text{II.1}$$

$$\alpha_{abs} = \varepsilon_{emit} = u(E_g) \qquad \text{II.2}$$

$$C\Omega_S \int_{E_g}^{\infty} \frac{E^2 dE}{\exp[E/kT_S] - 1} = \Omega_o \int_{E_g}^{\infty} \frac{E^2 dE}{\exp[(E - qV_{oc})/kT_c] - 1} \qquad \text{II.3}$$

$$\frac{E}{kT_S} = \frac{E - \mu_{oc}}{kT_c} \qquad \text{II.4}$$

$$qV_{oc}^{\max} = \mu_{oc}\Big|_{C=C^{\max}} = E_g\left(1 - \frac{T_c}{T_S}\right) \equiv E_g \eta_C \qquad \text{II.5}$$

$$qV_{oc}^{reg} = E_g\left(1 - \frac{T_c}{T_S}\right) + kT_c \times \ln\left[\left(\frac{C\Omega_S}{\Omega_o}\right)\left(\frac{T_S}{T_c}\right)\left(\frac{\alpha_{S1}}{\alpha_{c1}}\right)\right] + kT_c \times \ln(\kappa_{nr}) \qquad \text{II.6}$$

$$\alpha_{S1} = 1 + 2kT_S/E_g + 2(kT_S/E_g)^2 \qquad \text{II.7}$$

$$\alpha_{c1} = 1 + 2kT_c/E_g + 2(kT_c/E_g)^2 \approx 1 \qquad \text{II.8}$$

$$qV_{oc}^{reg} = E_g\left(1 - \frac{T_c}{T_S}\right) + kT_c \times \ln\left[\left(\frac{C\Omega_S}{\Omega_o}\right)\left(\frac{T_S}{T_c}\right)\right] \qquad \text{II.9}$$

$$G = U - T \times S = \mu \qquad \text{II.10}$$

$$S = k \times \ln(W) \qquad \text{II.11}$$

$$S_{\Omega} = k \ln(\Omega_o / C\Omega_S) \quad \text{II.12}$$

$$S_T = k \ln(T_c / T_S) \quad \text{II.13}$$

$$S = -\frac{\partial G}{\partial T_c} = -\frac{\partial \mu}{\partial T_c} \quad \text{II.14}$$

$$S = \frac{E_g}{T_S} + k\left(\frac{\alpha_{c2}}{\alpha_{c1}}\right) + k \times \ln\left[\left(\frac{\Omega_o}{C\Omega_S}\right)\left(\frac{T_c}{T_S}\right)\left(\frac{\alpha_{c1}}{\alpha_{S1}}\right)\right] \quad \text{II.15}$$

$$\alpha_{c2} = \frac{\partial(T_c \alpha_{c1})}{\partial T_c} = 1 + \frac{4kT_c}{E_g} + 6\left(\frac{kT_c}{E_g}\right)^2 \quad \text{II.16}$$

$$\frac{S}{k} \cong \frac{E_g}{kT_S} + 1 + \ln\left[\left(\frac{\Omega_o}{C\Omega_S}\right)\left(\frac{T_c}{T_S}\right)\right] \quad \text{II.17}$$

$$N_{Total} = gC\Omega_S \int_{E_g}^{\infty} \frac{E^2 dE}{\exp[E/kT_S]-1} \times \left[1 + \Omega_o \int_{E_g}^{\infty} \frac{E^2 dE}{\exp[E/kT_o]-1} \Big/ \Omega_S \int_{E_g}^{\infty} \frac{E^2 dE}{\exp[E/kT_S]-1}\right] \quad \text{II.18}$$

$$N_{Total} = gC\Omega_S \int_{E_g}^{\infty} \frac{E^2 dE}{\exp[E/kT_S]-1} \times [1 + \beta_o] \quad \text{II.19}$$

$$\beta_o = \frac{\Omega_o}{\Omega_S}\frac{\alpha_o}{\alpha_{S1}} \times \exp[-E_g \times \eta_C / kT_o] \quad \text{II.20}$$

$$\alpha_o = 1 + 2kT_o / E_g + 2(kT_o / E_g)^2 \cong \alpha_{c1} \cong 1 \quad \text{II.21}$$

$$V_{oc}^{reg}(\text{with ambient}) = V_{oc}^{reg} + kT_c \times \ln[1+\beta_o] \cong V_{oc}^{reg} \quad \text{II.22}$$

$$H_{reg}(\mu)/q = 1 - \frac{g\Omega_o \int_{E_g}^{\infty} \frac{E^2 dE}{\exp[(E-\mu)/kT_c]-1}}{N_{in}} \quad \text{II.23}$$

$$I_{out} = N_{in} \times H_{reg}(qV) \quad \text{II.24}$$

$$L(a \times x + b \times y) = a \times L(x) + b \times L(y) \quad \text{II.25}$$

$$N_S(x) = N_S \times \exp(-a_{abs} x) \quad \text{III.1}$$

$$f_{abs}\Omega_S \int_{2E_g}^{\infty} \frac{E^2 dE}{\exp[E/kT_S]-1} = \frac{1}{2} f_{dc}\Omega_{dc} \int_{E_g}^{\infty} \frac{E^2 dE}{\exp[(E-\mu_{dc})/kT_{dc}]-1} \quad \text{III.2}$$

$$\Omega_S \int_{E_g}^{2E_g} \frac{E^2 dE}{\exp[E/kT_S]-1} + f_{NA}\Omega_S \int_{2E_g}^{\infty} \frac{E^2 dE}{\exp[E/kT_S]-1}$$
$$+ B_{dc} \times f_{dc}\Omega_{dc} \int_{E_g}^{\infty} \frac{E^2 dE}{\exp[(E-\mu_{dc})/kT_{dc}]-1} = \Omega_o \int_{E_g}^{\infty} \frac{E^2 dE}{\exp[(E-\mu_{oc})/kT_c]-1} \quad \text{III.3}$$

$$\int_a^b dx = \int_a^\infty dx - \int_b^\infty dx \qquad \text{III.4}$$

$$\Omega_S \int_{E_g}^{\infty} \frac{E^2 dE}{\exp(E/kT_S)-1} + f_{dc}(2B_{dc}-1)\Omega_S \int_{2E_g}^{\infty} \frac{E^2 dE}{\exp(E/kT_S)-1} = \Omega_o \int_{E_g}^{\infty} \frac{E^2 dx}{\exp(E-\mu_{oc}/kT_c)-1} \qquad \text{III.5}$$

$$N_S\{E_g \to \infty\} + f_{dc}(2B_{dc}-1)N\{2E_g \to \infty\} = N_o\{E_g, \mu_{oc}\} \qquad \text{III.6}$$

$$N_S\{E_g \to \infty\} \times \left[1 + f_{dc}(2B_{dc}-1)N\{2E_g \to \infty\}/N\{E_g \to \infty\}\right] = N_o\{E_g, \mu_{oc}\} \qquad \text{III.7}$$

$$qV_{oc}^{dc} = E_g\left(1 - \frac{T_c}{T_S}\right) + kT_c \ln\left[\left(\frac{\Omega_S}{\Omega_o}\right)\left(\frac{T_S}{T_o}\right)\left(\frac{\alpha_{S1}}{\alpha_{c1}}\right)\right] + kT_c \ln(1+\beta_1) \qquad \text{III.8}$$

$$\beta_1 = f_{dc}(2B_{dc}-1) \times 4\left(\frac{\alpha_{S2}}{\alpha_{S1}}\right)\exp(-E_g/kT_S) \qquad \text{III.9}$$

$$\alpha_2 = 1 + \frac{kT_S}{E_g} + \frac{(kT_S)^2}{2E_g^{\,2}} \qquad \text{III.10}$$

$$\beta_1 = f_{dc}(2B_{dc}-1) \times \frac{N_S\{2E_g \to \infty\}}{N_S\{E_g \to \infty\}} \qquad \text{III.11}$$

$$I_{sc} = qgN_S\{E_g \to \infty\} \times \left[1 + f_{dc}(2B_{dc}-1)\frac{N_S\{2E_g \to \infty\}}{N_S\{E_g \to \infty\}}\right] - qgN_o\{E_g, \mu = 0\} \qquad \text{III.12}$$

$$\eta_{dc} = g_2 V_m \times \left(N_S\{E_g \to \infty\} \times \left[1 + \beta_1\right] - qgN_o\{E_g, \mu = qV_m\}\right) \qquad \text{III.13}$$

$$\kappa_{dc} = \frac{f_{dc}}{f_{abs}} = \frac{f_{dc}}{f_{dc} + f_L} \qquad \text{III.14}$$

$$f_{abs}\Omega_S \int_{2E_g}^{\infty} \frac{E^2 dE}{\exp[E/kT_S]-1} = \frac{1}{2\kappa_{dc}}\Omega_{dc} \int_{E_g}^{\infty} \frac{E^2 dE}{\exp[(E-\mu_{dc})/kT_{dc}]-1} \qquad \text{III.15}$$

$$qV_{oc} = qV_{oc}^{reg} + kT_c \ln(1+\beta_2) \qquad \text{III.16}$$

$$I_{sc} = qgN_S\{E_g \to \infty\} \times \left[1 + \beta_2\right] - qgN_o\{E_g, \mu = 0\} \qquad \text{III.17}$$

$$\beta_2 = (f_{dc} + f_L) \times (2\kappa_{dc} B_{dc} - 1) \times 4\left(\frac{\alpha_{S2}}{\alpha_{S1}}\right) \exp[-E_g / kT_S] \qquad \text{III.18}$$

$$QE = \{\kappa_{dc} \mid f_{dc} + f_L = f_{abs} = 1\} \qquad \text{III.19}$$

$$I = g\Omega_S \left(\int_{E_g}^{2E_g} \frac{E^2 dE}{\exp[E/kT_S] - 1} + 2 \times \int_{2E_g}^{\infty} \frac{E^2 dE}{\exp[E/kT_S] - 1} - f_\Omega \int_{E_g}^{\infty} \frac{E^2 dE}{\exp[(E-\mu)/kT_c] - 1} \right) \qquad \text{IV.1}$$

$$I = qg\Omega_S N_S\{E_g \to \infty\} \times \left[1 + \frac{N_S\{2E_g \to \infty\}}{N_S\{E_g \to \infty\}} \right] - qg\Omega_o N_o\{E_g, \mu\} \qquad \text{IV.2}$$

$$\Omega_S \int_{E_g}^{\infty} \frac{E^2 dE}{\exp[E/kT_S] - 1} \times (1 + \theta) = \Omega_o \int_{E_g}^{\infty} \frac{E^2 dE}{\exp[(E-\mu)/kT_c] - 1} + \Omega_o \int_{2E_g}^{\infty} \frac{E^2 dE}{\exp[(E-2\mu)/kT_c] - 1} \qquad \text{IV.3}$$

$$\theta \equiv \frac{\displaystyle\int_{2E_g}^{\infty} \frac{E^2 dE}{\exp[E/kT_S] - 1}}{\displaystyle\int_{E_g}^{\infty} \frac{E^2 dE}{\exp[E/kT_S] - 1}} = \frac{N_S\{2E_g \to \infty\}}{N_S\{E_g \to \infty\}} \le 1 \qquad \text{IV.4}$$

$$\theta = \{\beta_1 \mid f_{dc} = B_{dc} = 1\} \qquad \text{IV.5}$$

$$qV_{oc}^{CM}(old) = qV_{oc}^{dc} - kT_c \ln\left\{1 + 4\exp[-E_g / kT_c] \times \left(\exp[qV_{oc}^{CM} / kT_c] - 1\right)\right\} \qquad \text{IV.6}$$

$$\Omega_S \int_{E_g}^{\infty} \frac{E^2 dE}{\exp[E/kT_S] - 1} \times (1 + \theta) = (1 + \theta) \times \Omega_o \int_{E_g}^{\infty} \frac{E^2 dE}{\exp[(E-\mu)/kT_c] - 1} \qquad \text{IV.7}$$

$$qV_{oc}^{CM} = qV_{oc}^{reg} + kT_c \ln[1 + \theta] - kT_c \ln[1 + \theta] = qV_{oc}^{reg} \qquad \text{IV.8}$$

$$N_{in}^{CM,dc}(M) = gC\Omega_S \left(\sum_{m=1}^{M} m \int_{m \times E_g}^{(m+1) \times E_g} \frac{E^2 dE}{\exp[E/kT_S] - 1} + f_m M \times \int_{M \times E_g}^{\infty} \frac{E^2 dE}{\exp[E/kT_S] - 1} \right) \qquad \text{IV.9}$$

$$N_{in}^{CM,dc}(M) = gC\Omega_S \sum_{m=1}^{M} f_m \int_{m \times E_g}^{\infty} \frac{E^2 dE}{\exp[E/kT_S] - 1} \qquad \text{IV.10}$$

$$N_{in}^{CM,dc}(M) = gC\Omega_S \times \left(\sum_{m=1}^{M} f_m \theta_m\right) \times \int_{E_g}^{\infty} \frac{E^2 dE}{\exp[E/kT_S]-1} \qquad \text{IV.11}$$

$$\theta_m \equiv \int_{m\times E_g}^{\infty} \frac{E^2 dE}{\exp[E/kT_S]-1} \Bigg/ \int_{E_g}^{\infty} \frac{E^2 dE}{\exp[E/kT_S]-1} \qquad \text{IV.12}$$

$$\eta_{eff}^{dc} = g_2 \times V_m \times \left[\int_{E_g}^{\infty} \frac{E^2 dE}{\exp[E/kT_S]-1} \times \sum_{m=1}^{M} f_m \theta_m - \frac{f_\Omega}{C} \int_{E_g}^{\infty} \frac{E^2 dE}{\exp[(E-qV_m)/kT_c]-1}\right] \qquad \text{IV.13}$$

$$\eta_{eff}^{CM} = g_2 \times V_m \times \sum_{m=1}^{M} f_m \theta_m \times \left[\int_{E_g}^{\infty} \frac{E^2 dE}{\exp[E/kT_S]-1} - \frac{f_\Omega}{C} \int_{E_g}^{\infty} \frac{E^2 dE}{\exp[(E-qV_m)/kT_c]-1}\right] \qquad \text{IV.14}$$

$$qV_{oc}^{dc} = qV_{oc}^{reg} + kT_c \ln\left[\sum_{m=1}^{M} f_m \theta_m\right] \qquad \text{IV.15}$$

$$qV_{oc}^{CM} = qV_{oc}^{reg}$$

$$\eta_{peak}(\mathrm{m}) = \eta_{\mathrm{m}\to\infty}\left[1-\exp(-m/X)\right] + \eta_{m=0} \qquad \text{IV.16}$$

$$e^{-m/X} = \sum_{M}^{\infty} \frac{E^4 m^3 dE}{\exp[E/kT_S]-1} \Bigg/ \sum_{1}^{\infty} \frac{E^4 m^3 dE}{\exp[E/kT_S]-1} \qquad \text{IV.17}$$

$$qV_{oc}^{gain} = kT_c \ln\left[\sum_{m=1}^{M} f_m \theta_m\right] \cong\Big|_{M=2}\ kT_c \ln[1+\theta] \qquad \text{IV.18}$$

$$C_{new} = C_0 \times \sum_{m=1}^{M} f_m \theta_m \qquad \text{IV.19}$$

$$H_{CM}^{total} = H_{CM}^{1}(\mu_1) + H_{CM}^{2}(\mu_2) =\Big|_{\mu_1=\mu_2}\ (1+f_m\theta) H_{reg}(\mu) \qquad \text{V.1}$$

$$H_{\mathrm{int}}^{uc} : \frac{1}{2}\Omega_S \int_{E_g/2}^{E_g} \frac{E^2 dE}{\exp[E/kT_S]-1} = \Omega_o \int_{E_g}^{\infty} \frac{E^2 dE}{\exp[(E-\mu_{uc})/kT_{uc}]-1} \qquad \text{V.2}$$

$$\varepsilon_{emit}^{uc/IB}(E) = u(E_g) = \begin{Bmatrix} 0 \,| & E < E_g \\ 1 \,| & E > E_g \end{Bmatrix} \qquad \text{V.3}$$

$$\alpha_{abs}^{uc/IB} = \frac{1}{2} \times \left[u(E_g/2) + u(E_g)\right] \qquad \text{V.4}$$

$$qV_{oc}^{\,uc/IB} = qV_{oc}^{\,reg} + kT_c \ln\left(1 - \frac{f_m}{2} + \frac{f_m}{8}\frac{\alpha_{uc1}}{\alpha_{S1}}\exp[E_g / 2kT_S]\right) \qquad \text{V.5}$$

$$\alpha_{uc1} = 1 + 4\frac{kT_S}{E_g} + 8\left(\frac{kT_S}{E_g}\right)^2 \qquad \text{V.6}$$

$$\Omega_S \int_{E_g+\Delta}^{\infty} \frac{E^2 dE}{\exp[E/kT_S]-1} + \Omega_o \int_{E_g}^{E_g+\Delta} \frac{E^2 dE}{\exp[(E-\mu_{oc})/kT_c]-1} = \Omega_o \int_{E_g}^{\infty} \frac{E^2 dE}{\exp[(E-\mu_{oc})/kT_c]-1} \qquad \text{VI.1}$$

$$\Omega_S \int_{E_g+\Delta}^{\infty} \frac{E^2 dE}{\exp[E/kT_S]-1} = \Omega_o \int_{E_g+\Delta}^{\infty} \frac{E^2 dE}{\exp[(E-\mu_{oc})/kT_c]-1} \qquad \text{VI.2}$$

$$qV_{oc}^{SR} \cong \left(E_g + \Delta\right)\eta_C + kT_c \ln\left[\left(\Omega_S/\Omega_o\right)\left(T_S/T_c\right)\left(\alpha_{S\Delta}/\alpha_{c\Delta}\right)\right] \qquad \text{VI.3}$$

$$\alpha_{S\Delta} = a_{S1} + 2\frac{\Delta}{E_g} + \left(\frac{\Delta}{E_g}\right)^2 + 2\frac{kT_S\Delta}{E_g^2}$$

$$\alpha_{c\Delta} = a_{c1} + 2\frac{\Delta}{E_g} + \left(\frac{\Delta}{E_g}\right)^2 + 2\frac{kT_c\Delta}{E_g^2} \qquad \text{VI.4}$$

$$V_{oc}^{reg} \propto E_g$$

$$V_{oc}^{SR} \propto E_g + \Delta \qquad \text{VI.5}$$

$$I_{sc} \cong qg\Omega_S \int_{E_g+\Delta}^{\infty} \frac{E^2 dE}{\exp[E/kT_S]-1} \qquad \text{VI.6}$$

$$N_{Auger} = LC_{Aug} n_i^3 \exp[3qV/2kT_c] \qquad \text{VI.7}$$

$$\frac{\Delta S}{k} \equiv \frac{S^{SR}}{k} - \frac{S^{reg}}{k} \cong \frac{\Delta}{kT_S} \qquad \text{VI.8}$$

$$\Omega_S \int_{E_g+\Delta}^{\infty} \frac{E^2 dE}{\exp[E/kT_S]-1} = \frac{\Omega_o}{\kappa_{nr2}} \int_{E_g+\Delta}^{\infty} \frac{E^2 dE}{\exp[(E-qV_{oc2})/kT_c]-1} \qquad \text{VII.1}$$

$$\Omega_S \int_{E_g}^{E_g+\Delta_g} \frac{E^2 dE}{\exp[E/kT_S]-1} + B\cdot\Omega_o \int_{E_g+\Delta}^{\infty} \frac{E^2 dE}{\exp[(E-qV_{oc2})/kT_c]-1} = \frac{\Omega_o}{\kappa_{nr1}} \int_{E_g}^{\infty} \frac{E^2 dE}{\exp[(E-qV_{oc1})/kT_c]-1} \qquad \text{VII.2}$$

$$\Omega_S \int_{E_g}^{\infty} \frac{E^2 dE}{\exp[E/kT_S]-1} + (B\cdot\kappa_{nr2}-1)\cdot\Omega_S \int_{E_g+\Delta}^{\infty} \frac{E^2 dE}{\exp[E/kT_S]-1} = \frac{\Omega_o}{\kappa_{nr1}} \int_{E_g}^{\infty} \frac{E^2 dE}{\exp[(E-qV_{oc})/kT_c]-1} \quad \text{VII.3}$$

$$qV_{oc}^{\Delta} = qV_{oc}^{reg} + kT_c \ln\left[1+(B\cdot\kappa_{nr2}-1)\left(\frac{\alpha_{\Delta}}{\alpha_{S1}}\right)\times\exp[-\Delta/kT_S]\right] \quad \text{VII.4}$$

$$dS_{Sliver} = k\ln\left[\frac{N\{E_g\to\infty\}-N\{(E_g+\Delta)\to\infty\}}{N\{E_g\to\infty\}}\right] \quad \text{VII.5}$$

$$\Omega_S \int_{E_g}^{\infty} \ldots + (B-1)\left[\int_{E_g+\Delta}^{\infty}\ldots + B\int_{E_g+2\Delta}^{\infty}\ldots\right] = \frac{\Omega_o}{\kappa_{nr1}}\int_{E_g}^{\infty}\frac{E^2dE}{\exp[(E-qV_{oc1})/kT_c]-1} \quad \text{VII.6}$$

$$Q_{S-E} = A_{conc}\frac{r_S^2}{R_{S-E}^2}\sigma T_S^4 \quad \text{VIII.1}$$

$$Q_{sc} = A_{sc}n_c^2\sigma T_c^4 \quad \text{VIII.2}$$

$$\left.\begin{matrix} Q_{S-E}=Q_{sc} \\ T_S=T_c \end{matrix}\right\} A_{sc}n_c^2 = \frac{r_S^2}{R_{S-E}^2}A_{conc} \quad \text{VIII.3}$$

$$C = \frac{A_{conc}}{A_{sc}} \le \frac{n_c^2}{\sin^2\Delta_S} \quad \text{VIII.4}$$

$$Q_{S-E} = Q_{sc} + \eta_{ext}Q_{S-E} \quad \text{VIII.5}$$

$$A_{conc}\sin^2\Delta_S\sigma T_S^4\times(1-\eta_{ext}) = A_{sc}\sigma T_c^4 \quad \text{VIII.6}$$

$$T_c \cong T_S\left[(1-\eta_{ext})\frac{C}{C^{\max}}\right]^{1/4} \quad \text{VIII.7}$$

$$\Delta S_{PV} \ge 0 \quad \text{VIII.8}$$

$$N_{in}(C) = \Omega_o\int_{E_g}^{\infty}\frac{E^2dE}{\exp[(E-\mu_{oc})/kT_c]-1} \quad \text{VIII.9}$$

$$\mu_{oc} = E_g - kT_c\cdot\ln\left[\frac{\Omega_o E_g^2 kT_c\alpha_{c1}}{N_{in}(C)}\right] \quad \text{VIII.10}$$

$$S = k\frac{\alpha_{c2}}{\alpha_{c1}} + k\ln\left[\frac{\Omega_o E_g^2 kT_c\alpha_{c1}}{N_{in}(C)}\right] \quad \text{VIII.11}$$

$$N_{in}(C) \le \Omega_o E_g^2 kT_c\alpha_{c1}\exp[\alpha_{c2}/\alpha_{c1}] \quad \text{VIII.12}$$

$$S' \cong k\ln\left[\frac{\Omega_o E_g^2 kT_c\alpha_{c1}}{N_{in}(C)}\right] \quad \text{VIII.13}$$

$$\frac{E_g}{kT_S}+\frac{\alpha_{c2}}{\alpha_{c1}}+\ln\left[\frac{\Omega_o T_c \alpha_{c1}}{\Omega_S T_S \alpha_{S1}}\right]-\ln[C]\geq 0 \qquad \text{VIII.14}$$

$$C^{\max}=\frac{\Omega_o T_c}{\Omega_S T_S}\left(\frac{\alpha_{c1}}{\alpha_{S1}}\right)\times\exp\left(\frac{E_g}{kT_S}\frac{\alpha_{c2}}{\alpha_{c1}}\right) \qquad \text{VIII.15}$$

$$C^{\max}\big|_{T_S=T_c}=\frac{\Omega_o}{\Omega_S}\times\exp\left(\frac{E_g}{kT_S}\right)\cong\frac{n_c^2}{\sin^2\Delta_S}\times\exp\left(\frac{E_g}{kT_S}\right)=C_0^{\max}\times\exp\left(\frac{E_g}{kT_S}\right) \qquad \text{VIII.16}$$

$$\frac{S}{k}\cong\frac{E_g}{kT_S}+1+\ln\left[\left(\frac{\Omega_o}{\Omega_S}\right)\left(\frac{T_c}{T_S}\right)\right]-\ln[C]-\ln[\kappa_{nr}]+\ln[f(\Delta)] \qquad \text{IX.1}$$

$$\frac{E_g}{kT_S}=\ln\left[\frac{W_{out}}{W_{in}}\right] \qquad \text{IX.2}$$

$$\Rightarrow \exp[E_g/kT_S]=W_{in}/W_{out}$$